Republic of Iraq
Ministry of Higher Education
and Scientific Research
University of Al-Qadisiyah
College of Science
Department of Chemistry

Evaluating the performance of titanium dioxide nanowires and nanotubes as a photoanodes in the dye sensitized solar cell

Thesis Submitted to The Council of the College of Science/ University of AL-Qadisiyah in Partial Fulfillment of the Requirements for The Degree of Master in Chemistry/physical chemistry

by

Noura Hussein Harran

B .SC .2011

Supervised by

Prof.Dr.Qahtan Adnan Yousif

2019 A.C 1440 A.H

بسم الله الرحمن الرحيم

﴿يَا أَيُّهَا الَّذِينَ آمَنُوا إِذَا قِيلَ لَكُمْ تَفَسَّحُوا فِي الْمَجَالِسِ
فَافْسَحُوا يَفْسَحِ اللَّهُ لَكُمْ ۖ وَإِذَا قِيلَ انْشُزُوا فَانْشُزُوا
يَرْفَعِ اللَّهُ الَّذِينَ آمَنُوا مِنْكُمْ وَالَّذِينَ أُوتُوا الْعِلْمَ دَرَجَاتٍ
ۚ وَاللَّهُ بِمَا تَعْمَلُونَ خَبِيرٌ ﴿١١﴾﴾

صدق الله العلي العظيم

سورة المجادلة الآية (11)

Supervisor's Certificate

I certify that thesis **"Evaluating the performance of titanium dioxide nanowires and nanotubes as a photoanodes in the dye- sensitized solar cell"** was prepared under my supervision at the University of Al-Qadisiyah, college of science as a requirement for the degree of Master degree in physical chemistry

Signature :

Name : Prof. Dr. Qahtan A. Yousif

Date : / / 2019

In view of the available recommendations I forward thesis for debate by the examining committee

Signature :

Name : Assistant Prof. Dr Muqdad E. Kadium

Date : / / 2019

Chairman of Department committee on graduate studies in chemistry

Date : / / 2019

Amendment Report

This is certify that I have read the thesis entitled **"Evaluating the performance of titanium dioxide nanowires and nanotubes as a photoanodes in the dye- sensitized solar cell"** and corrected the linguistic mistakes I found. The thesis is, therefore, qualified for debate.

Signature :

Name :

Title:

Date : / / 2019

Committee Certificate

We certify that we have read thesis entitled **(Evaluating the performance of titanium dioxide nanowires and nanotubes as a photoanodes in the dye-sensitized solar cell)** and as examining committee examined the student(Noura Hussein Harran) in its content at date 13/6/2019 and that in our opinion it meets the standard of a thesis for the degree of Master in science chemistry/ physical chemistry and the degree of (excellence) .

Signature :

Prof.Dr.Hamieda .E.Salman

(Chairman)

Title:college of education pure science

University of Kerbala

Date: / / 2019

Signature :

Asst.Prof.Oraas A.Hatem

(Member)

Title:college of science

University of AL-Qadisiyah

Date: / / 2019

Signature :

Asst. Prof.Dr.Abbas E.Kadhim

(Member)

Title: college of education

University of AL-Qadisiyah

Date: / / 2019

Signature :

Prof.Dr .Qahtan Adnan Yousif

(Member & Superviser)

Title: college of education

University of AL-Qadisiyah

Date / /2019

Approved by the college of science

Signature :

Prof.Dr.Nabeel.A.AL-Radha

Dean of the college of science , University of Al-Qadisiyah

Date: / / 2019

Dedication

To whom Allah has endowed with prestige and glory ... To those who taught me without giving gifts To whom I bear the name of all pride ... I ask God to extend in your age to see the fruit has come picking after a long time and will remain your words stars guided by today tomorrow and forever ... …… My father

To the one who was the invitation of my happiness secret and my success..... to the most expensive people .... My mother

To whom the light of the road shine

They support me and give up their rights

To satisfy me and live in bliss ..... My brothers

Acknowledgement

At first , thanks to Allah All-Mighty God for enabling me to complete this work .

I would like to express my gratefulness & appreciation to my supervisor **Prof. Dr Qahtan Adnan Yousif** for his supervision, suggestion on the topics of this dissertation, his invaluable advice and comments during the course of investigation and writing of this dissertation, his endless patience, generousness and kindness.

Deep thanks and appreciation to the Deanery of College of Science University of Al-Qadisiyah and to the head of chemistry Department **asst Prof. Dr. Muqdad E.Kadium**. I am deeply thankful to all members of chemistry Department and all my colleagues for their help and supporting me to accomplish my project and I would like to record my thanks to the college of Education/University of AL-Qadisiyah department of chemistry and College of Engineering /University of AL-Qadisiyah department of chemical engineering for their help during my achievement of this research work

I would like to express my sincere appreciations to my family for their continuous encouragement, especial thanks go to my father for his great support and patience.

Finally, my thanks all My Friends for their interest and support during this study.

NOURA

Abstract

Nanomaterials such as titanium dioxide nanowire and titanium dioxide nanotube were prepared in two ways (hydrothermal method and anodization method) from different precursors such as TiO_2 P25 was used as a precursors for the preparation of nanowire while titanium foil was used for the preparation of nanotube .Graphene nanoplates were deposited on the FTO glass in an electro deposition method using three electrodes technique as auxiliary electrode .Prepared material was identified using various techniques such as electron scanning spectroscopy ,transmission electron microscopy, x-ray diffraction, Raman spectroscopy, surface area, and the distribution of porous size of nanomaterials where used as photoanode electrodes in the dye sensitized solar cells.

Thus, N3 Ruthenium dye was used and electrolyte used included "0.5 M N-methyl-N-butyl-imidazolium iodide (BMII) + 0.1 M LiI + 0.05 M I_2 + 0.5 M 4-tert-butylpyridine" (TBP) in acetonitrile that used to improve dye sensitized solar cell conversion efficiency.

Ten fabrication of dye-sensitized solar cells were made as photoanode electrodes (6 electrodes were TiO_2 NTs and 4 TiO_2 NWs semiconductors). The efficiency of the solar cells were calculated by the current-voltage and current-power curves as well as the fill factors were calculated. The best conversion efficiency was 1.238 for titanium dioxide nanotube and 0.0089 for titanium dioxide nanowire.

Contents

List of Tables

List of Figures

List of Abbreviations

Abbreviation	The Meaning
AFM	Atomic Force Microscope
BET	Brunauer Emmett Teller
BJH	Barrett-Joyner-Halenda
D	Crystallite Size
DSSCs	Dye-sensitized solar cells
EDX-Mapping	Energy Dispersion X-Ray
E_g	Energy Gap
e^-	Photoelectron
FWHM	Full width at half maximum
FTO	Fluorine doped tin oxide
FF	Fill factor
HOMO	Highest Occupy Molecular Orbital
IPCE	Incident photon current efficiency
J_{sc}	Short-circuit current
LUMO	Lowest Unoccupy Molecular Orbital
N3	Cis-Bis(isothiocyanato)bis(2,2`-bipyridyl-4,4`-dicarboxylato ruthenium(II)
P25	Degussa TiO_2
Ra	Roughness Average
Rq	Root Mean Square
Ry	Distance between highest peak and lowest valley
SEM	Scanning electron spectroscopy
TEM	Transmission electron spectroscopy
UV-DRS	UV-Diffuse reflectance spectroscopy
V_{oc}	Open circuit voltage
XRD	X-Ray diffraction
0 D	Zero Dimensional
1 D	One Dimensional
2 D	Two Dimensional
3 D	Three Dimensional
CVD	Chemical Vapor Deposition
MBE	Molecular Beam Epitaxy
TCO	Transparent Conductors Oxide
AZO	Aluminum Zinc doped Tin Oxide
S.W.C.N.T	Single Walled Carbon Nanotube
M.W.C.N.T	Multi Walled Carbon Nanotube

Chapter One

Introduction

Introduction

1.1 Introduction to Nanotechnology

Nanotechnology is an advanced technology science that has the ability to revolutionize various fields. The origin of Nano is a Greek word for dwarf, and is combined with technology to indicate operations occurring on the scale of 10^{-9} meters. A nanometer is a billionth of a meter **[1, 2]** . The intensive research in the field of nanotechnology started in the 1980s, and has continued to be a modern astonish of scientific discovery , it is called the boundary between quantum and bulk effect " nanoscopic scale" **[3]** . Application of scientific information to manipulate and monitoring matter in the nanoscale in order that make use of size- and structure-dependent properties and phenomena, as distinct from related to individual atoms or molecules or those related to bulk materials **[4]** . Nanotechnology is a quickly developing field that is set to impact various areas of science and technology, essentially with applications in materials science, medicine, bioimaging and electronics **[5]**.

1.1.1 Background of Nanotechnology

The nanotechnology platform was developed by physicist Richard Feynman from the California Institute of Technology. At the 1959 winter meeting of the American physical Society, Feynman explained a speech entitled "There is Plenty of Room at the Bottom" **[6]**.The expression "nanotechnology" was not utilized until 1974, when Norio Taniguchi ,a researcher at the College of Tokyo, used it to allude to the capacity to engineer materials accurately at the nanometer level **[7]**.

1.1.2 Terminology

1-Nanotechnology: technology manipulation of matter on a very small scale in the scale of 1 and 100 nanometers., This technology exploits novel properties and functions that occur in matter in this scale **[8]**.

2- Nanoscience: The study of matter at the nanoscale , which is 1 to 100 nanometers (this means every one nanometer equal to 10^{-9} of a meter) in size **[9]**.

3- Nanomaterials: are materials with one or more component that possess at least one dimension in a range of 1 to 100 nanometers, and that include nanoparticles, nanotubes, and nanofibers **[10]**.

1.1.3 Nanomaterials

The term "nanomaterial" alludes to a wide range of substances have particles with at least one dimension in the nanometer range from 1-100 nm **[11].** Nanomaterials are the linked bridge between atoms and micro-structures, and the nanostructure are much near to dimensions that are near to atomic dimensions. By comparison, the bond length of between typical carbon atoms, or the spacing between these atoms in a molecule, is within the range of 0.15-0.12 nm **[12]**. Nanomaterials are diagnosed by using several techniques to determine the size of their particles or crystals, or to know their physical and chemical properties. The microscope, such as a transmission electron microscope (TEM), a high-resolution atomic force microscope Symbolized by the symbol (AFM) and a high resolution scanning electron microscope Symbolized by the symbol (SEM), are used to capture high – resolution images. Through these images, the external body of particle shapes and dimensions are recognized **[13]**. Spectroscopic techniques, such as Raman

spectroscopy and ultraviolet-visible spectroscopy, are used to determind some of the chemical and physical properties of nanoparticles. Raman spectroscopy is an important technique. In addition to its high precision in determining the nature of the bonds between atoms, especially in the fingerprint area, it is also used to denote certain crystalline properties of particles **[14]**. UV spectroscopy is also used to determine the maximum wavelength of nanomaterials, as well as the energy band gap, which depend on the shape and size of nanoparticles **[15]**. X-ray spectroscopies (XPS) are used to identify elements and calculate the proportions of elements in compounds, as well as to determine the chemical formula of nanoparticles **[16]**.Nanotechnology includes the production of a variety of nanomaterials (NM) , which include nano-objects and nanoparticles (NP). Nanomaterials having one dimension below 100 nanometers , while nanoscale objects have two dimensions less than 100 nanometers (such as carbon nanotubes) .Nanoparticles can be recognized as three-dimensional particles of less than 100 nanometers . The nanomaterials are sorted according to their dimensions : zero dimensional (0D) , one dimensional (1D) , two dimensional (2D) , and three- dimensional (3D) **[11, 17]**. The nanomaterials are usually in the form powders, fibers and soluble . There are numerous sorts of nanomaterials, such as, nanoporous structures, nanoclusters, and nanoparticles **[18]**.

1.1.4 Properties of Nanomaterials

The proportion of the surface area to the size and the improvement in the chemical properties is high when descending to the nanometer where the area is a characteristic of nanoparticles, and when the size of particles descends to less than 100 nm , The proportion of surface area to size becomes very high, as shown in Figure (1-1)

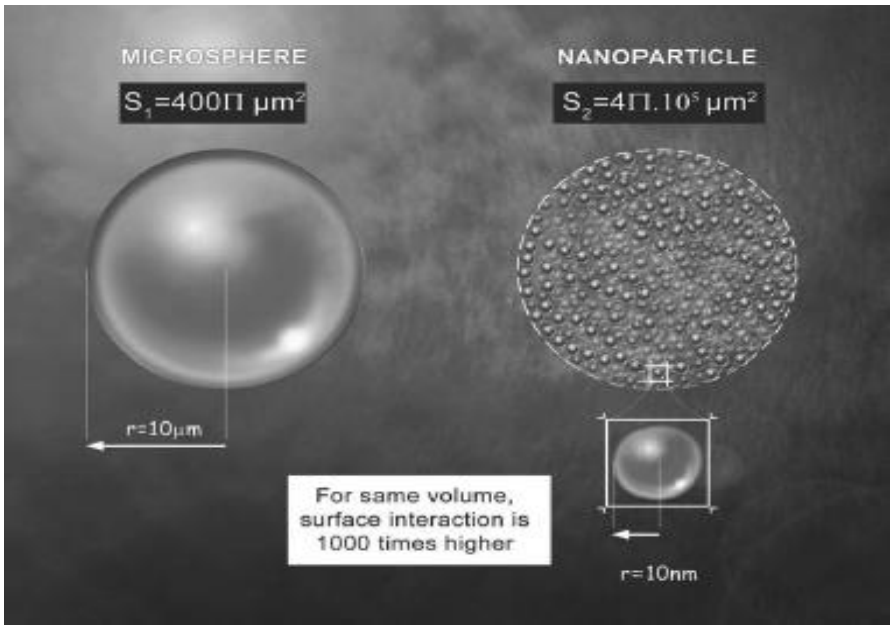

Figure (1-1): Effect of particle size on surface area [19]

There is a clear difference in the mechanical behavior of the materials at the nanoscale of the microscopic scale . Although continuous mechanics is observed when the sizes are higher than the 10 nm range , surface effects may control deformation properties .The micrometer structures where the elastic strain energy is controlled in the mechanical properties while nanometer length ranges , as a result of increasing surface – to- volume ratio , surface effects become predominating and can significantly alter the macroscopic properties **[20].**

1.1.5 Fabrication Techniques of Nanomaterials

Nanofabrication is the process of building functional structures with a minimum dimension of less than 100 nanometers. Nanofabricating incloude all building operation of nanoscale structures, devices and systems in 1D , 2D, and 3D dimintions **[18, 21]**.

The methods used to generate nanofabrication are (I) The top – down method and (II) Bottom – up method **[22].**

The current method from top to bottom is the transfer pattern on the nanometer scale **[23]**. The bottom – up nanofabrication process is done by assembling a molecule by a molecule of the nanostructure **[24]**as shown in Figure 1-2.

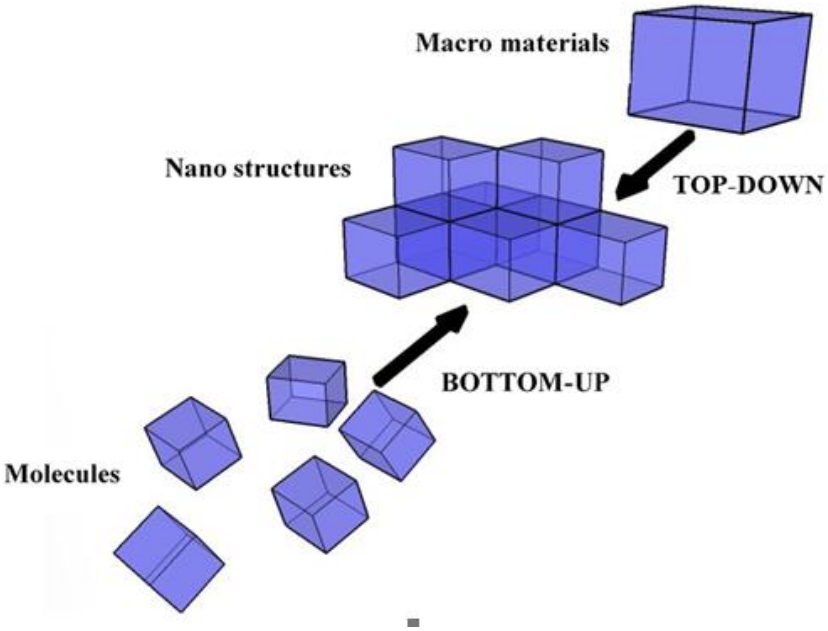

Figure 1-2: Scheme nanoscale manufacturing in both approaches top to down and bottom to up

1.1.5.1 Plasma Arcing

Plasma is an ionized gas and is carried out by making a gas conduct electricity , which gives a potential differance across two electrodes causing the gas to yield up its electrons and thus ionizes **[25]**.

1.1.5.2 Chemical Vapor Deposition

Chemical vapor deposition includes dissociation or chemical reactions of the gaseous reactants in activated environment such as (light ,heat ,plasma), followed by the formation of a stable solid produce **[26].**CVD is a widely used method for preparing two- dimensional nanomaterials on the solid substrates **[27]**. One or more of volatile precursors react or dissociation on the surface of the exposed material producing two –dimensional crystals in environmental conditions that be high temperatures and in a high vacuum **[28].** In a chemical vapor deposition that be a thin film of vaporous reactants deposition onto a substrate where the deposition is created by joining gas particles in a reaction chamber at a ambient temperature **[29]**.

1.1.5.3 Molecular Beam Epitaxy (MBE)

MBE is a technology that has evolved to an unprecedented extent with the growth of semiconductor heterostructures with a surface quality determined by single-monolayer precision **[30]**. The characteristics of MBE are monocrystallization with high purity and growth in an ultrahigh vacuum, as well as smooth and flawless surfaces of heteroepitaxy , and the formation of thin structures with unexpected changes at the surface relatively low growth temperatures forbidding interdiffusion**[31]**.

1.1.5.4 Solution Geleration (sol-gel) method

It is a chemical technique performed at the liquid phase, and has recently been used in many fields, including materials science and ceramics engineering. It has been used primarily in the manufacture of materials (usually metal oxide) that start with a chemical solution that acts as a precursor **[32]**.

1.1.5.5 Hydrothermal/Solvothermal Method

This technique is carried out in the autoclave , which is a steel pressure vessel with or without Teflon. It has temperature control or pressure, and the reaction takes place in the aqueous solution that was used in the preparation of TiO_2**[33]**.

1.1.6 Titanium Dioxide

Nanomaterials TiO_2 are non-toxic, stable and inexpensive. TiO_2 has a large energy gap (3-3.2 eV), and therefore appears to respond only to ultraviolet absorption, and it's transparent to the visible emission of solar energy**[19, 34]**In 1916, TiO_2 was widely used as a dye **[35].** Nanocrystalline titanium oxide (TiO_2,titana) has been broadly used for its singular characteristics that made it an quite attractive photocatalyst **[36]**. These days it is notable that TiO_2 is a standout amongst semiconductors for photocatalysis, and has been connected into different photocatalytic responses**[37]**. TiO_2 has three crystalline phases: Anatase, rutile, and brookite (Table 1-1), Anatase shows high photocatalysis efficiency, and rutile shows as a white dye because its high scattering effect , which protects it from ultraviolet radiation , Photocatalysis of TiO_2 includes three procedures: The excitation, the bulk diffusion, and the surface transport of photoinduced charge carriers **[38]**.

Titanium dioxide is an insoluble, thermally stable, non-combustible and non-silicate mineral oxide. The real wellspring of TiO_2 is ilmenite, though rutile and anatase polymorphs are primarily fabricated commercially **[39]** Titanium dioxide (TiO_2) is a cheap, nontoxic, and simple to deal with material, which makes of great interest. TiO_2 is a semiconductor material with a band gap of ~ 3.3 eV, corresponding to a wavelength of ~390 nm **[40]** . TiO_2 is already an n-type semiconductor because of its oxygen deficiency **[41]**.

Table 1-1 Three Phases of TiO_2

Phase	Crystal System
Rutile	Tetragonal
Anatase	Tetragonal
Brookite	Orthorombic

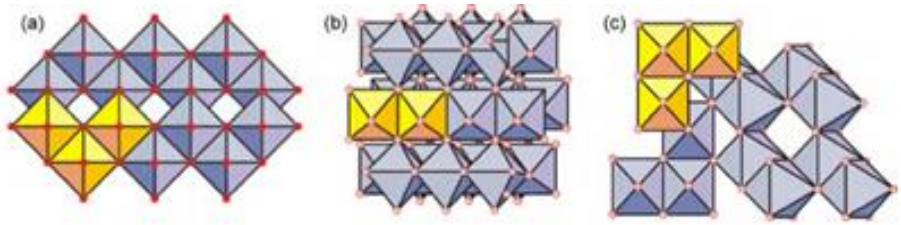

Figure.1-3 . Schame of crystalline structure of anatase (a) , brookite (b) , and rutile (c) [42]

1.1.6.1 Properties of TiO_2

The physical properties of the anatase and rutile phases for Titanium dioxide as shown in the table 1-2 **[41]**:

Properties	**Anatase**	**Rutile**
Molecular weight	79.88 (g/mol)	79.88 (g/mol)
Melting point	1825 (˚c)	1825 (˚c)
Boiling point	2500~3000 (˚c)	2500~3000 (˚c)
Density	3.79 (g/cm^3)	4.13 (g/cm^3)
Refractive index	2.55	2.75

1.2 Generations of solar cells

The solar cell is mainly divided into three generations .The first generation utterly depends on crystalline silicon (C-Si), while the second generation is based on thin film technologies involving vapor deposition of semiconductors **[43]** . The 3 rd generation of solar cells consists of solar cells that are sensitive to dye and solar cells of organic semiconductors , which surpasses the first and second generations of solar cells with numerous properties that are compatible with flexible substrates , inexpensive materials and manufacturing **[44]** .

1.2.1 Why 3rd generation of solar cells ?

Dye sensitize solar cells have the potential to be third- generation cells due to they are made from cheap and nontoxic components , and one of most photovoltaic technologies for renewable energy production . They are clean and affordable technology , and designed with an array of different colors and transparencies **[45]**. Both the 1st and 2ed generation solar cells are single junction apparatus. 31% of the thermodynamic efficiency of single junction solar cells assumes that a single-electron-hole pair is the result of the absorption of individual photons, and that photon energy in excess of the energy gap is considered a lost heat shape, which is called a Shockley-Queisser. This can be bypassed by different types of 3G solar cells devices **[46].**

1.2.2 The Dye- sensitized solar cell (DSSC)

Oregan and Grätzel In 1991, manufactured the first dye sensitive nanocrystalline solar cells, where the conversion speed of the photovoltaic power was 7.1%, and the efficiency to convert the incident photon into an electric current was 80% **[47]** .In 2014, there was a significant improvement in the photovoltaic conversion power of these cells from 7.1% to 13%, and this transformation was necessary for commercial use **[48]** .The use of TiO_2 nanocrystalline in dye-sensitive solar cells has attracted considerable attention in the industrial medium because of its high power conversion efficiency (PCE) **[49].** Conversion efficiency is affected by a combination of factors including the very tinny structure of the titanium dioxide photo-electrode and the physical properties of the sensitizer **[50].**

1.2.3 Major components of (DSSC

The main components of the DSSC are as the following **[51]**:-

I. Photoanode.

II. Sensitizer.

III. Counter electrode.

IV. Electrolyte .

both "fluorine doped tin oxide" and" indium doped tin oxide" act as transparent conductors oxide in Grätzel cells, and also used alternative low-cost TCO materials, such as graphene and AZO, electrolyte which is usually iodide and triiodide, which is undergoes redox reaction , Figure .5 shows a representative diagram of dye-sensitive solar cell **[52]**.

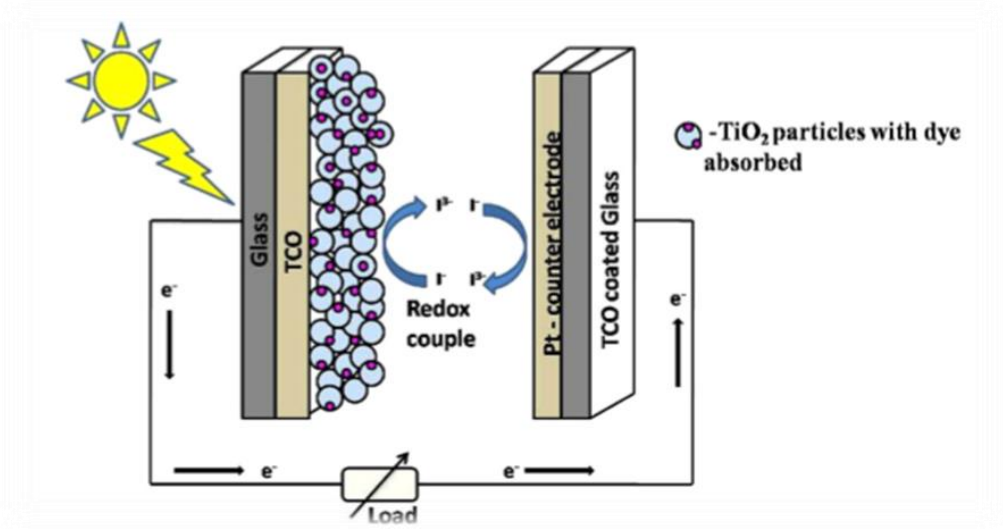

Fig .1-4 diagram of DSSC[52]

1.2.4 Operational principle of (DSSC)

Any solar cell sensitive to dyes acts on the basis of absorption, separation, and assembly of charge carriers. The efficiency of this type of cell depends on improving the parameters, whereas when the photon falls on the surface of dye sensitive solar cells, the dye molecules collect photons and produce excited electrons. Here, the role of the sensitizer is expressed, it injects this electron into nanostructure semiconductor, the injected electron then travels from the working electrode and reaches the counter electrode, the molecules dye after losing electrons get oxidized **[53]**. the speed of these electrons depends on the intensity incident and trapping- detrapping influence **[51]** .The performance of this cell depends on several factors, one of these factors is the transparent conductive oxide, which has two types of it ITO "indium doped ten oxide" and FTO "fluorine doped tin oxide", where it plays an important role in cell efficiency **[54]**.

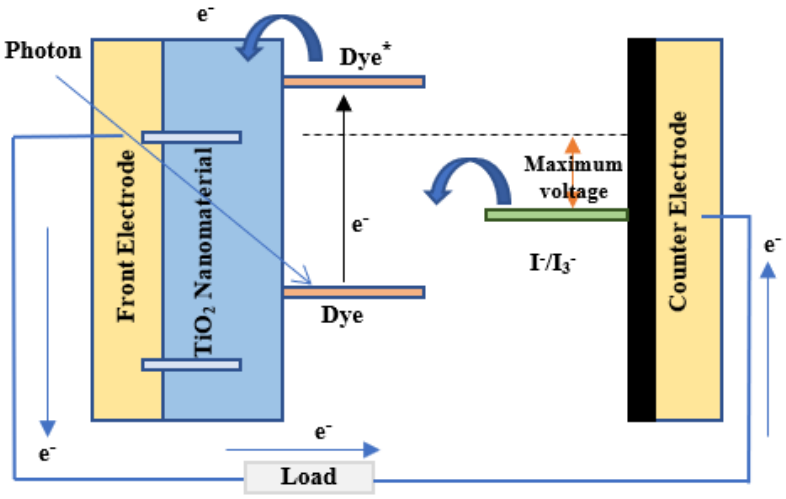

Fig 1-5 Diagram of dye sensitive solar cell[54].

The electrolytes role is emerged in reducing the recombination between the injected electrons in the semiconductor metal oxide bonding band and the oxidizing dye. The electrolyte contains the ion iodide, which in turn gives the electrons the oxidizing dye, thus preventing recombination. Preventing recombination requires the regeneration of the dye to occur at the speed of the ns. The electrons move to the counter electrode, which contains tri iodide, which then turns into oxidized iodide **[55]**. The kinetics of ultrafast electron injection kinetics occurs over a period of sub-picosecond time for the type of sensitive dyes, which is faster than the emission decay time. These kinetics lead to the separation of a very effective charge and high electron velocity dependent on the coupling of strong electrons of the LUMO orbitals dye with the metal oxide conduction band **[56,57]**.

Below are the relative kinetic equations of the charge transfer **[58]**.

$S + h\upsilon \rightarrow S^*$ Electron excitation (1)

$s^* \rightarrow s^+ + e^-_{CB}$ Electron injection into the CB (2)

$S^+ + \frac{3}{2} I^- \rightarrow \frac{1}{2} I_3^- + S$ Dye regeneration (3)

$I_3^- + 2e^-_{CB} \rightarrow 3I^-$ Elecrolyte regeneration at the CE (4)

$S^* \rightarrow S$ Fall to ground state (5)

$S^+ + e^-_{CB} \rightarrow s$ Regeneration of dye by injected electron (6)

1.2.5 DSSC construction

The dye sensitize solar cell is a complex system that converts light into electricity, and its installation is similar to the basic design of Grätzal It consists of the following parts **[59]** .

1.2.5.1 Substrates

Both the cathode and the anode are prepared on to a transparent conductor oxide, which in turn allows light to pass through the cell, which is characterized by its large transparency in the visible spectrum and is inexpensive and availability. The used transparent conductive materials are (FTO) and (ITO) **[60]**.

1.2.5.2 Semiconductor electrodes

The possession of titanium dioxide for high dielectric constant (ε=80 for anatase) has made it a good electrostatic shielding of the excited electrons that are injected on the surface of titanium dioxide, which comes from the oxidation of dye molecules and thus prevents the process of a union before the dye molecules are reduced by receiving the electrons produced from the oxidation process of the electrolyte **[61]**. It is also known that titanium dioxide has a high conversion efficiency of photoelectrics compared with other oxides such as ZnO, Fe_2O_3 and In_2O_3, as well as with composite oxides such as 15 Graphene-MOF and 14 AL-ZnO ,It also possesses photochemical stability and is non-toxic, and threfore has become one of the best materials for application in electronic devices **[62]** .

1.2.5.2.1 Nanotube

It is a nanostructured one-dimensional, and has a high surface area and a special geometric shape, which is characterized by the ease of migration of electrons during movement as compared to nanoparticles. This helps to reduce the time for electrons movement, making it suitable for using in DSSCs **[63]**. The high surface area and the particularly regular structure made the structure nanotubes a promising material for use as a photocatalyst **[64].**The charge is easily transported on the surface of the structure nanotube because it has a high vertical arrangement that travels along the structure nanotube from the solution to the conductive material. The easy access to the nanotube surface and better control of the interface makes it appropriate for dye-sensitize solar cell **[65]** . The structure of vertical nanotube on the transparent conductor oxides provides efficient collection of charge through rapid transport and slow recombination. it was attended by among other ways one of them the electrochemical oxidation of titanium element, which is a simple way to change morphological properties of the nanotube array such as the diameter of the hole, the thickness of the walls and the length of the tube **[66]**.

1.2.5.2.2 Nanowire

The lower surface area of the nanostructure such as nanowire reflects lower value performance of DSSC **[66]**. After an injection of the electron from the excited state of dye to the photo anode (such as the nanowire oxide) it will provide a direct path which in turn prevents the electron from recombination, high surface area and direct contact of the electron movement provided by the dense network nanowire **[67]**.

1.2.5.3 Electrolyte

The electrolyte is responsible for the conduction of electricity through the dissolution of the solution into the ions. It is usually a mixture of liquid solvent and inorganic salts, and has an important role in both the load and the transport of the charge in dye-sensitive solar cells , a solid –state and a quasi-solid-state are attempt to alternative for liquid electrolyte **[68]**. The electrolyte affects both the J_{sc} and the V_{oc} **[69]**.There are many requirements for electrolytes used in dye-sensitized solar cells after dye injection the electrons in the conduction band of a nanocrystalline semiconductor as shown below:

1- The electrolyte must have sufficient capacity to transfer the charge carriers between the photoanode and the auxiliary electrode where the oxidized dye must be reduced and returned to its fixed form. Therefore, the choice of electrolyte should take into account the possibility of dye reduction, and the renewal must have optical, chemical, and thermal long –term stability.

2- Electrochemical properties that do not cause the degradation of the dye from the surface of the oxide **[70]**.

Electrolytes in dye-sensitive solar cells are divided into three species: liquid electrolytes, solid state electrolytes, and quasi solid-state electrolytes.

1.2.5.3 .1 Liquid electrolyte

It is also known that iodide-tri iodide has good kinetic properties such as the speed of oxidation at the interface of semiconductor metals. It also helps the electrolyte to regenerate the dye effectively, and slows reduction at the interface of the electrode and electrolyte for the collection of a high load. It is easy to prepare, inexpensive, and has high stability.

It also has an absorption range in the visible area of 430 nm, and the corrosion elements of the auxiliary electrode as pt have contributed to the search for alternative electrolytes **[71]** .

1.2.5.3 .2 Solid state electrolyte

It is used as an alternative to liquid electrolyte because of its good mechanical stability, easy to manufacture and includes inorganic p-type semiconductors, where it replaces liquid electrolyte to avoid evaporation and leakage of liquid electrolyte **[47]**.

1.2.5.3 .3The Quasi Solid state electrolyte

It composites of the polymer and the liquid electrolyte, which is characterized from a liquid electrolyte with its long stability over time, high electrical conductivity and good interconnection due to the presence of polymers with a unique network structure. Polymer morphology and molecular weight have a role in quasi-solid electrolyte conductivity because the movement of charges is high in the non-crystallized form of the polymer when compared to the crystalline phase **[72]**.

1.2.5.4 The Counter electrode

It is one of the main components of the dye sensitize solar cells, its role appears in the reception of electrons from the outer circuit. It reduces the redox species in the electrolyte used to renewal the sensitizer after electron injection. It should also have low electrical resistance and high electrical catalytic activity in the face the iodide /triiodide redox reaction and be stable and transparent **[73]**.

1.2.5.4.1 Graphene

It is a two-dimensional sheet of carbon atoms associated by covalent bond, making it characterized by strong stimulation efficiency as well as possessing unique electronic properties. Several techniques have been used to prepare these sheets, including reduction of exfoliated graphite oxide and mechanical exfoliation of graphite **[74]**.

1.2.5.4.2 Polymers conductor

Polymer conductors are materials used as counter electrodes because of unique characteristics such as inexpensive, high conductivity, good stability, as well as the effectiveness of the catalyst to reduce $I_{3.}$ These polymers are polyanaline, which have become one of the most widely studied conductive polymers for their easy synthesis, good environmental stability, and exciting redox properties **[75]** .

1.2.5.4.3 Carbon nanotubes

Carbon nanotubes have advantages such as great surface area, chemical stability and high electrical conductivity. They are classified by chemical composition into S.W.C.N.T and M.W.C.N.T. where the S.W.C.N.T consists of a single graphene wrapped plate, while the M.W.C.N.T consists of several axially arranged graphene plates **[76]** .

1.2.5.5 Dyes sensitize

The sensitized dyes play a major role in the harvesting of sunlight as they convert solar energy into electrical energy, making the nanocrystalline oxide semiconductors sensitive, The ruthenium polypyridyl complex of the most efficient sensors possess the following :-

1- Terrible charge carrier absorbed in all visible ranges

2- Long excite lifetime

3- High efficiency in transporting the charge of metal to the ligand **[77]**.

In 1991, the conversion efficiency was 7.1% for the dye sensitize solar cell based on Ru. The most remarkable success of the Ru is that it has an octahedral geometrical structure that makes it possible to expand the specific ligands in a controlled manner. Ru (II) is controlled by photophysical, photochemical, and electrochemical properties. It possesses stable oxidation states from I to IV, and has perfect solubility in many solvents **[78]** . The following requirements are essential:

1 - It needs to be sensitive enough to show absorption in the visible areas and part of the vicinity of the IR.

2- In needs a high molar extinction coefficient (ε) that prevents multi-layer adsorption of the sensitizer on the surface of the semi-conductor metal.

3 - There needs to be anchoring groups, such as -COOH ,-SO3H, that make the bond of dye strong with semiconductor oxide.

4. The molecular structure of the sensitizer is important in preventing the formation aggregation of the dye on the surface of the semiconductor oxide **[79]** .

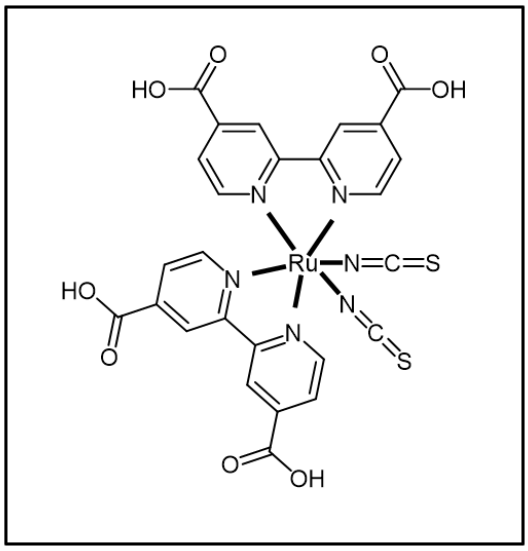

Figure1-6 Molecular structure of N3 dye cis bis(isothiocyanato)bis(4,4dicarboxlic acid-2,2-bipyridine) ruthenium(II)

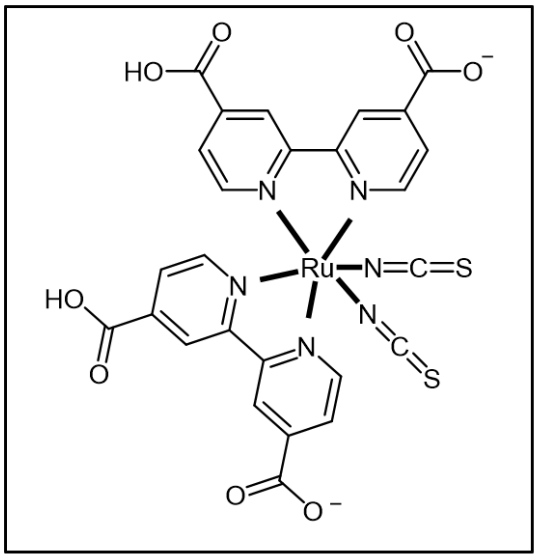

Figure 1-7 Molecular structure of N719 Di tetra butyl ammoinum Cis-bis (isothiocyanato) bis(4- carboxylic acid-4-carboxlate-2,2-bipyridine)-ruthenium(II). [80] .

The Ru complexes that used as sensitive organic dyes in DSSCs are N3, N719, N749 and Z907, where N3 is characterized by two groups of bi pyridine and two groups of thio cyanato ligands. Because of the NCS groups , they absorb up to 800 nm and provide high j_{sc}. In contrast, when V_{oc} is not high , N719 are different with two carboxyl groups where tetra butyl ammonium is associated with it instead of the H^+ **[81]** .

1.3 The literature survey

The electrochemical method has been adapted by Cirak, et al to prepare the TiO_2 NTs with a diameter of 26-115 nm and a length of 1.3 to 6.4μm**[43]** . Nyein et al, prepared TiO_2 NTs by anodization titanium foil in the electrolyte ethylene glycol containing fluoride and compared the addition of water and sodium hydroxide as an oxidants which was applied in a DSSCs where the efficiency of the cell was 2.4%**[44]** . Jinghua Hu and co-workers, attended the titanium dioxide nanowire film by hydrothermal process and used as photo-anode in dye-sensitive solar cells to improve the efficiency of these cells due to the rapid interfacial electron transmission**[45]** . Saera Jin et al, prepared Titanium dioxide nanowire by hydrothermal process using titanium foil in an alkaline. This corroded foil was used as a photoanode in the dye-sensitized solar cell and exhibited efficiency of 1.11%**[46]** . Ákos Kukovecza and co-workers studied the properties and applications of TiO_2 NTs & TiO_2 NWs from a surface science point and that the surface chemistry of one-dimensional titanates makes them excellent candidates' applications for heterogeneous catalytic, photocatalytic and energy storage**[47]**. Fatemeh Mohammadpour et al attended titanium dioxide nanotubes and were applied to dye-sensitive solar cells where cell efficiency improved to 0.8%**[48]**. Guohua Liu with the colleagues attended TiO_2 nanotube by an anodic oxidation of titanium alloy and have observed that the thickness of the layer increases with an increase in the application of voltages while the diameter is not affected where the inner diameter of the tube is 30-190 nm and the length of 5-40 mm**[49]**. Lianjie Qin et al synthesized the titanium dioxide nanotube by the electrochemical anodization of the high-purity titanium alloy in the electrolyte containing NH_4F and studied the effect of the anodic voltage and

time on the tube formation, where the diameter was within the range of 30-90 nm and the anodic time has effected on the length of tubes**[50]**. Pierre Pichat and co-workers have prepared titanium dioxide nanotube and improved photocatalytic efficiency observed to remove pollutants in water and air**[51]**. Indar Kustiningsih et al attended the titanium nanotubes & nanowires using commercial TiO_2 nanoparticles as a prefix via a sonication-hydrothermal integration method**[52]**. As well as, Yu-Zhen Zeng, Yu-Chang Liu et al attended the TiO_2 NTs using an anatase TiO_2 Powder and studied the effect of the pH values on the crystalline structure, photocatalytic activity, porosity, surface area**[53]**.

A. Rangitha and his colleagues attended the Titanium nanotubes and studied the effect of the reaction time on the nature of the composition of the tubes, whereas the length of the nanotubes 11.23nm and diameter 260nm**[54]**. A. F. Kanta Hitachi et al fabricated the TiO_2 NTs by anodization method for titanium foil in ethylene glycol electrolyte containing fluoride under constant voltage**[55]**. Lanfage Que et all have prepared TiO_2 3D NWs structure by hydrothermal method of Ti foil in an aqueous alkali and used as photoanode in dye-sensitive solar cells where the efficiency was 8.05%**[56]**.

As R. Camposecom et al in their study showed that the TiO_2 NTs prepared from TiO_2 Np in the hydrothermal method at a different concentrations of sodium hydroxide at 140 °C and later hydrochloric acid was added until reached pH 1**[57]**.

Ioan Roman et al were synthesized the titania nanotubes by anodization method in various substrates including titanium alloy in the electrolyte of ethylene glycol and glycerol and the influence of the anodization time on the length and diameter for the nanotubes**[58]**. Michal Nischk et al attended TiO_2

NTs which were vertically arranged by anodic oxidation of Ti foil in three electrolytes water, ethylene glycol and glycerol and studied the effect of voltage anodization, electrolyte structure, ultrasonic treatment and calcination time on the morphology of the thin films**[59]**. Vardan Galstyan and co-workers have prepared the TiO_2 NTs and demonstrated the effect of anodization parameters on the size and shape of the morphology of nanotubes**[60]**. Thu Thi Vu Hang Thi Au Lien Thi Tran et al synthesized Titania nanotubes by hydrothermal method from commercial titanium dioxide and studied the effect of both temperature and time of reaction and the effect of sodium hydroxide concentration on the morphology**[61]**.

W. Sharmoukh and co-workers were able to reach efficiency in dye sensitive solar cells of 3.94% by using TiO_2 NTs in conjunction with the ruthenium complex sensitizer**[62]**. Ju Hyung Kim et al attended the anatase phase of TiO_2 NTs through getting a thin layer of Titanium Dioxide on the surface of MWCNTs and then performed the process of calcination to obtain the pure phase of TiO_2 and remove MWCNTs at the same time**[63]**. kuan-chun Huang et al have prepared rutile/titania-nanotube in the manner of microwave irradiation and used it in photocatalysis which showed high efficiency under visible light spectrum**[64]**. A. Lambertia et al prepared highly ordered TiO_2 NTs by anodic oxidation of Ti foil and was applied in the dye-sensitive solar cells**[65]**. JIAO XingJian et all introduced anatase TiO_2 NWs by thermal oxidation method of Ti foil in an aqueous alkali,then transferred it to the FTO glass and used as photoanodes in dye-sensitized solar cells. Interestingly, it was found that it had less electron transfer resistance and longer electron diffusion length**[66]**. Nada F. Atta et al have fabricated highly order titanium dioxide nanotubes on Ti foil by employing electrochemical methods in HF-H_3PO_4 electrolyte with diameter of 110 nm

and applied in dye-sensitive solar cells by using dyes in the dark and under lighting where the efficiency of the cell arrived to 0.17%**[67]**. Himendra Jha et al introduced Titanium dioxide nanotubes through anodizing technique and studied changes in surface morphology and physical parameters such as pH and temperature.

However, it was used in the dye sensitive solar cells and showed an open circuit voltage effort higher than the commercial nanoparticles**[68]**. Jiquan Huang et all studied the effect of sodium hydroxide concentration in the formation of various Titania nanostructures. Nanowire consisted of a few concentrations, while high concentrations were produced in the nanoparticle formation and were applied in photocatalysis and adsorption. Strikingly, both were adsorbed to remove heavy metal ions while photocatalytic to remove pigments from the wastewater**[69]**. Akshay Kumar et all were able to prepare titanium dioxide nanowire with a rutile phase, on various basic materials such as glass slide ،FTO ،ITO etc, by controlled growth factors such as temperature and concentration of precursors were application as a photoanode in the dye sensitive solar cells and showed efficiency about 2.9%**[70]**.

Jun and co-workers have prepared TiO_2 NTs by electrochemical anodization method sensitized with dye N-719 and the surface TiO_2 NTs treatmented with $TiCl_4$ in conjunction with oxygen plasma exposition led to the improved power conversion efficiency of 7.37%**[71]**. Erdem Şennik and colleagues introduced the titanium dioxide nanotubes and applied it to hydrogen sensor, it was prepared the anodization process of the Ti foil in an aqueous solution containing the HF at 20°C. The length of the titanate tube was 1 μm and the diameter was 90 nm**[72].** Nawin Viriya et al attended Titania Nanotube and Nanowire in the hydrothermal process with sonication

pretreatment and revealed that the length of the tube increases with the application of sonication pretreatment**[73]**. Swati Bhardwaj et all prepared the TiO_2 NTs arranged in high order by the anodization of the Ti foil in (EG) electrolyte containing NH_4F and studied the effect of anodizing voltages on the formation tubes where it was found that increasing the anodization voltages causes reduction in the wall thickness , however, the porous diameter average was between 34nm to 58nm**[74]**. Yahya Alivov et all fabricated the TiO_2 NTs by an anodic oxidation of Ti foil in electrolyte containing ammonium fluoride and within the range of anodizing voltage from 10 to 240v**[75]**. Hun Park and co-workers have prepared highly order of TiO_2 NTs by electrochemical method, applied in dye-sensitive solar cells. The efficiency of the cell was 6.89%, which was found to be less efficient compared to TiO_2 nanoparticles based on DSSCs**[76]**. Tae-Sik Kang et all tried, to produce a high order of titania nanotubes using a nanoporous alumina templating approach with an external diameter of 295 nm and a length of 6 - 15 μm, it was used as a working electrode in dye-sensitive solar cells and showed a power efficiency of 3.5%**[77]**.

As Srimala Sreekantan et all were studied the effect of pH and anodization time in the formation of Titania nanotube, which was prepared by the anodization processes in the electrolyte contains Na_2SO_4 and NH_4F as the length within the range of 0.7 to 2.5 μm**[78]**. The others studied**[79]** synthesis of the anatase titanium dioxide nanowire by hydrothermal method and applied it in DSSCs that shows conversion efficiency of 2.42%.Hyung-Kee Seoa et all prepared titanium dioxide nanotube from titanium commercial dioxide oxide nanoparticles using the thermal method by treatment sodium hydroxide at a different range of temperature for 48 hours**[80]**. Daoai Wang et all attended TiO_2 nanotube in the hydrothermal process of titanium powder, with an

external diameter of 9-10 nm, an internal diameter of 3-4 nm and a length of several hundred nanometers**[81]**.

Karthik et all were attended a titanium dioxide nanotube with a length of up to 220 μm and applied in dye-sensitized dye cells and in hydrogen production by water photo electrolysis and achieved power efficiency of 6.9%**[82]**. Gopal and co-workers have prepared highly ordered TiO_2 NTs by anodic oxidation of Ti in fluoride-based electrolyte with different shapes, pore size, tubular length and wall thickness through changes in variables such as electrolyte concentration, pH, temperature bath, then applied in dye-sensitize solar cells after treatment with $TiCl_4$ and showed efficiency 2 .9%**[83]**. Kai Zhu, Nathan R . Neale et all fabricated the TiO_2 Nanotube by the anodic method of Ti alloy, where the tubes were arranged uniformly and with the length of several micrometers and with a perfect wall thickness. The pore diameter is about 30 nanometers and has been applied in dye sensitive solar cells, whereas, TNs showed higher efficiency than the Nps**[84]**.

Yoshikazu et all Also, partially synthesized the TiO_2 nanowire structure in the hydrothermal method, which showed that the efficiency of the dye-sensitised solar cells were of 6.01%**[85]**. Ryuhei has prepared the Anatase TiO_2 NWs by the hydrothermal method with a diameter range of 10 to 50 nm with some of nanowire packages of ~ 100 nm**[86]**. Yoshikazu Suzukiet all have prepared partial nanowire TiO_2 in the hydrothermal method and revealed that the conversion efficiency was of 6.01%**[85]**. Ryuhei Yoshida et all were able to prepare Anatase TiO_2 nanowire with sodium hydroxide concentration of 10 M and then treated with diluted hydrochloric acid and calcined at 600°C**[86]**. Y.X. Zhang et all successfully prepared the TiO_2 NWs in a simple hydrothermal way with a diameter range of 30 to 45nm**[87]**.

1.4 Aims of research

Presently with the increasing request for energy, especially electrical energy. It is very important to study solar energy sources which are one of the renewable energies that several advantages such as low cost, simple assembly, and environmentally friendly. Thus, the goal of the present research fabricates the dye-sensitized solar cell. The following items describe all steps of the work.

A- preparation of titanium dioxide nanotubes using the anodization electrochemical method. To achieve that, design a suitable homemade electrochemical cell which includes three electrodes to study three types of different electrolyte compositions (ethylene glygol-based electrolyte containing 1.5 ml H_2O and 0.5 g NH_4F, Water-based electrolyte containing o.1M Na_2SO_4 and 0.2 g NH_4F and lactic acid-based electrolyte containing 5 ml DMSO and 0.15 g NH_4F).

B- Study the influence of ultrasound waves on the growth of Titanium dioxide nanotubes by using one transducer under one intensity mode for all experiments.

C- Preparation the Titanium dioxide nanowires by using the hydrothermal method via homemade cell with the thermal sensor. Also, synthesis of it directly on the FTO glass.

D- Using the electrophoretic deposition method (EPD) synthesis the counter electrode of the dye-sensitized solar cell from the graphene nanoplates (GNP) at standard time.

E- Assembling dye-sensitized solar cell and use the N3 dye as sensitizer with a suitable electrolyte to determine the conversion efficiency by estimating the main parameters as short circuit photocurrent, open circuit photovoltage, maximum power and fill factor.

Chapter Two

Experimental part

2-1 Chemical materials

The substances used in the current research were recorded in Table (2-1) where these materials characterized by high purity and used without the need for additional purification.

Table (2-1): Materials used in the study

No.	*Material*	*Purity (%)*	*Supplier*
1	FTO glass	---	GOLO
2	Acetyl acetone	99.5%	CDH
3	Hydrochloric acid	37% w/w	THOMAS BAKER
4	Sodium hydroxide	99.0	B.D.H
5	Ethanol	99.9% v/v	HAYMAN
6	2- propanol	---	Riedel-deHaën
7	Ruthenium complex dye N3	99.9	ALDRICH
8	Hydrogen peroxide (30%)	99.0	Scharlau
9	Phosphoric acid (85%)	97.9	Analyticals Carlo Erba
10	Acetone	98	Sigma Alderich
11	Titanium Foil	99.7%	Sigma Alderich
12	Titanium(IV)butoxide	99	ALDRICH
13	Titanium (IV) oxide	99.5%	ALDRICH
14	Sodium sulfate anhydrous	99%	BDH chemicals

15	Lactic acid	92%	HIMEDIA
16	Dimethyl sulfoxide	----	BIOSOLVE
17	Ethylene glycol	99.9%	Barcelona Espane

2-2 Preparation methods of nanomaterials

2 -2-1 Preparation $TiO_{2(1,2,3)}$ Nanowire

Titanium dioxide nanowire was prepared using commercial titanium dioxide P25 (3 grams). It was mixed at room temperature with 150 ml sodium hydroxide (10 M) aqueous solution with continuous stirring for 15 minutes and then placed in a a Teflon-lined autoclave then heated for 12 hour at 160 °C and after cooled at room temperature then the resulting precipitate is washed with diluted hydrochloric acid (0.1M) and deionized water several times and then dried by drying oven at 80 ° C for 2 hours followed calcination by furnace at 700 °C for 1 hour . Thus, repeat the all steps of $TiO_{2(1)}$ NWs but change in heated time for 24 h and 36 h as shown in figure 2-2(a,b,c).

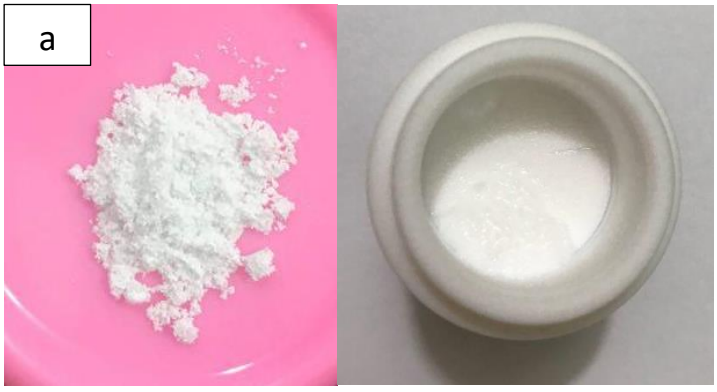

Figure 2-2 (a) preparation of $TiO_{2(1)}$ NWs

Figure 2-2 (b ,c) preparation of $TiO_{2(2,3)}$ NWs

2 -2-2 Preparation $TiO_{2(4)}$ Nanowire

Firstly, the glass (FTO) was ultrasonically cleaned in both acetone, iso propyl alcohol and deionized water sequentially for 15 minutes. Titanium dioxide nanowire is prepared by adding 1 ml of titanium (IV) butoxide to a mixture of deionized water and hydrochloric acid by 12:12 v/v to obtain a clear transparent solution. The solution is then transferred to the autoclave. Where the glass fluoride doped tin oxide is Place at an angle in the autoclave and heated to a temperature 180^0C for 3 hours as shown in figure 2-4.

Figure 2-3 preparation of $TiO_{2(4)}$ NWs

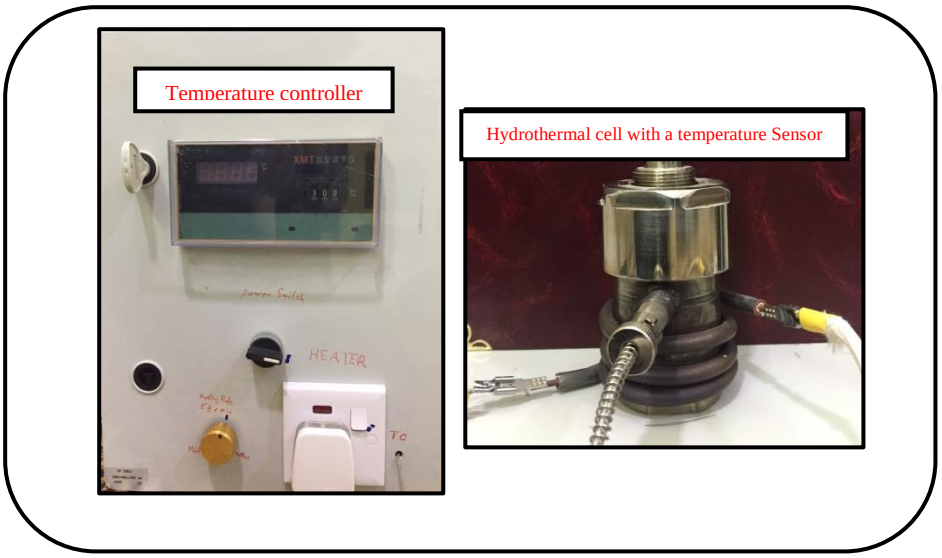

Figure 2-4: Hydrothermal cell with a temperature Sensor.

2 -2-3 Preparation $TiO_{2(1)}$ nanotube

The electrochemical anodization method used to prepare high order TiO_2 nanotubes on the Ti substrate which supplied from the Sigma –Aldrich with high purity 99.7% with 0.25 mm. ethylene glygol-based electrolyte containing 1.5 ml H_2O and 0.5 g NH_4F preparation as electrolyte solution and applied voltage at 20V in the presence and absence of the ultrasound for 30 min at 10 ^{0} C using three – electrode system which add a reference electrode as a Calomel electrode to control of the current values during the anodization process and recorded it with time. Before any test, it is necessary treated the Ti foil in sonication bath in both acetone, ethanol and then rinsed with deionized water and drying in nitrogen steam. The samples annealed and calcinated at 550 ^{0}C for 30 min as shown in figure 2-6.

Figure 2-5 preparation of *$TiO_{2(1)}$* NTs

2 -2-4 Preparation $TiO_{2(2)}$ nanotube

The electrochemical anodization method used to prepare high order TiO_2 nanotubes on the Ti substrate which supplied from the Sigma –Aldrich with high purity 99.7% with 0.25 mm. Water-based electrolyte containing o.1M Na_2SO_4 and 0.2 g NH_4F preparation as electrolyte solution and applied voltage at 20V in the presence and absence of the ultrasound for 30 min at 10 ^{0} C using three – electrode system which add a reference electrode as a Calomel electrode to control of the current values during the anodization process and recorded it with time. Before any test, it is necessary treated the Ti foil in sonication bath in both acetone, ethanol and then rinsed with deionized water and drying in nitrogen steam. The samples annealed and calcinated at 550 ^{0}C for 30 min as shown in figure 2-7 .

Figure 2-6 preparation of $TiO_{2(2)}$ NTs

2 -2-5 Preparation $TiO_{2(3)}$ nanotube

The electrochemical anodization method used to prepare high order TiO_2 nanotubes on the Ti substrate which supplied from the Sigma –Aldrich with high purity 99.7% with 0.25 mm. lactic acid-based electrolyte containing 5 ml DMSO and 0.15 g NH_4F preparation as electrolyte solution and applied voltage at 20V in the presence and absence of the ultrasound for 30 min at 10 ^{0}C using three – electrode system which add a reference electrode as a Calomel electrode to control of the current values during the anodization process and recorded it with time. Before any test, it is necessary treated the Ti foil in sonication bath in both acetone, ethanol and then rinsed with deionized water and drying in nitrogen steam. The samples annealed and calcinated at 550 ^{0}C for 30 min as shown in figure 2-8 .

Figure 2-7 preparation of $TiO_{2(3)}$ NTs

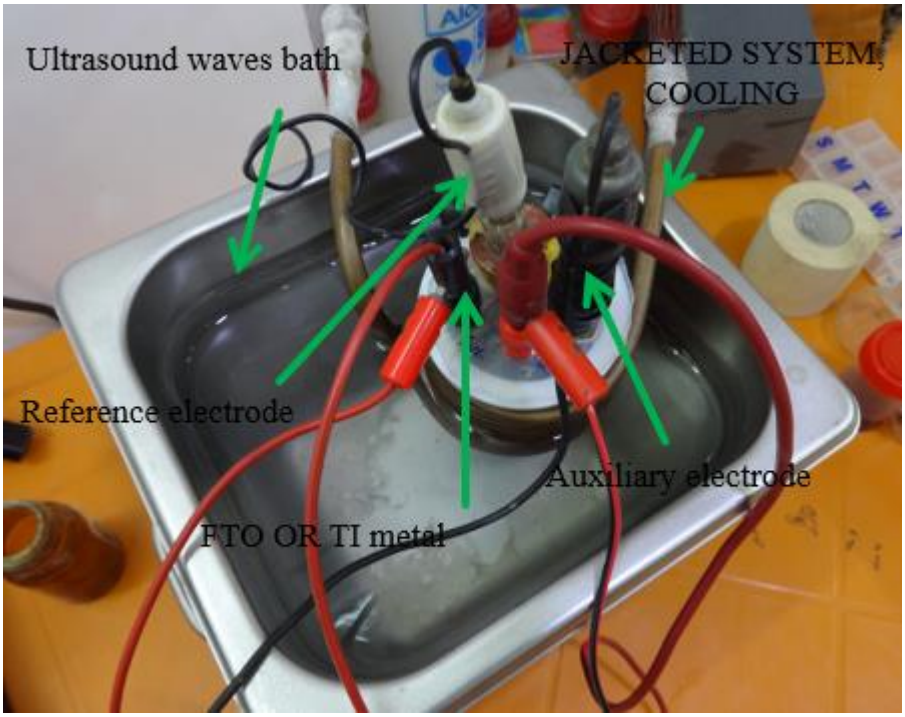

Figure 2-8 preparation System of TiO_2 NTs

2 -2-6 Preparation of counter electrode (CE) of DSSC

Weight a 0.01 gram of graphene nanoplates (GNP) suspension in 50 ml of deionized water and sonication for 15 min. After that, the FTO glass cleaned in a solvent (acetone and ethanol 2:4) and aqueous solutions in the sonication bath for 10 min. and dry by the nitrogen gas and then radiation by the U.V light source to enhance the adhesive the graphene nanoplatelets on the substrate through the electrophoretic method with applied 10 volts for the 90s. After this time, cleaned the CE by immersing it in deionized water to remove the residual of uncoated graphene nanoplatelets molecules, and checked the conductivity " resistance " of all surface to inspect to cover whole the surface by the GNP through selected a suitable point on it to measure.

Figure 2-9 Image preparation of counter electrode

2 -2-7 Preparation of electrolyte

The electrolyte prepared from "0.5 M N-methyl-N-butyl-imidazolium iodide (BMII) + 0.1 M LiI + 0.05 M I2 + 0.5 M 4-tert-butylpyridine" (TBP) in acetonitrile.

2 -2-8 Preparation of dye

It was prepared at concentration 0.0001 M in 50 mL of ethanol, thus photoelectrodes were immersed in dye for 24 hours .

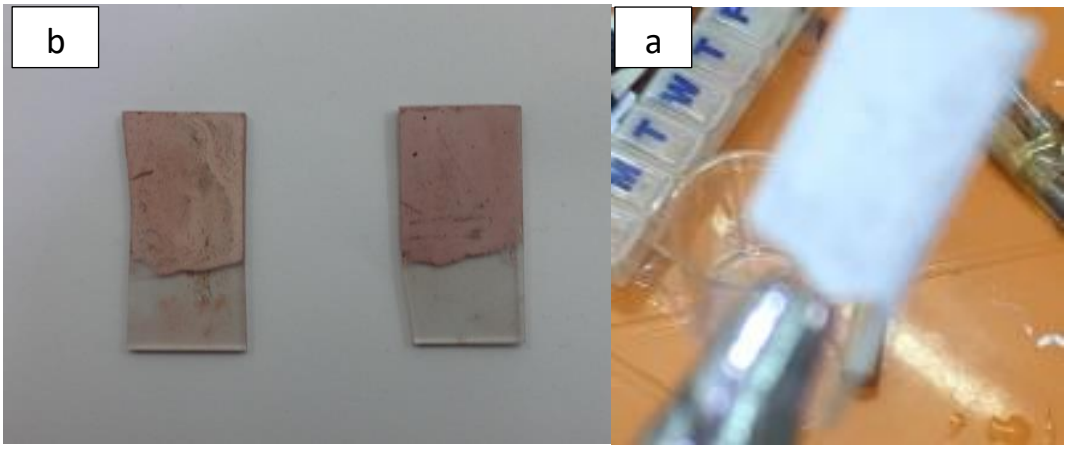

Figure 2-10 images of TiO_2 NWs before immersion in dye N3 (a) after immersion in dye N3 (b)

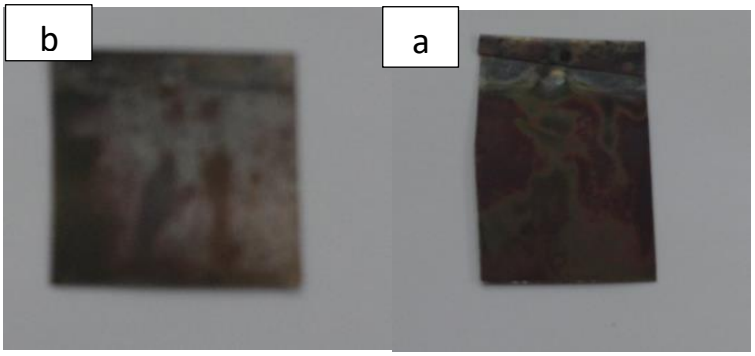

Figure 2-11 images of $TiO_{2(1)}$ NTs before immersion in dye N3 (a) in the presence of ultrasound (b) in the absence of ultrasound.

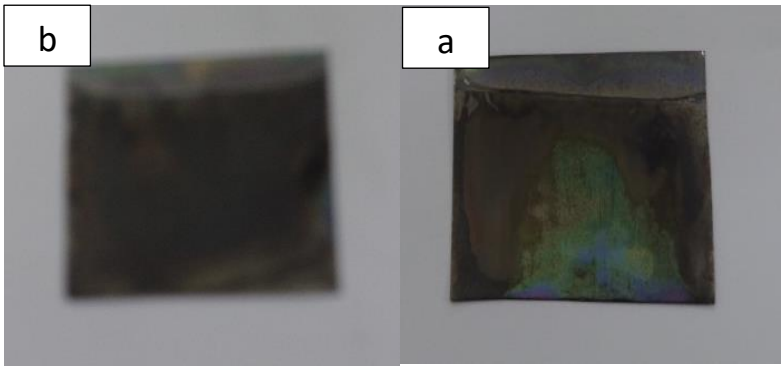

Figure 2-12 images of $TiO_{2(2)}$ NTs before immersion in dye N3 (a) in the presence of ultrasound (b) in the absence of ultrasound

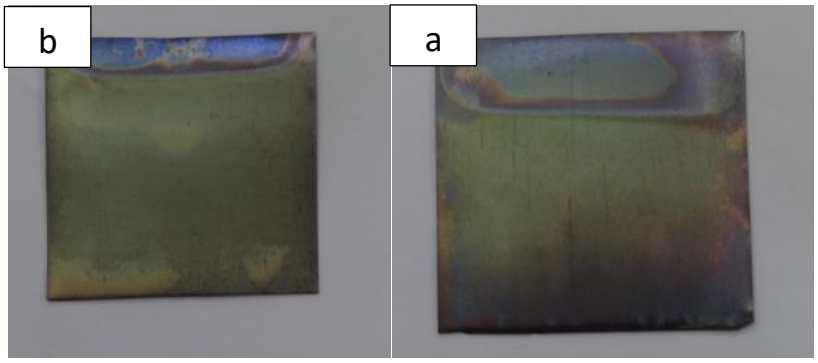

Figure 2-13 images of $TiO_{2(3)}$ NTs before immersion in dye N3 (a) in the presence of ultrasound (b) in the absence of ultrasound

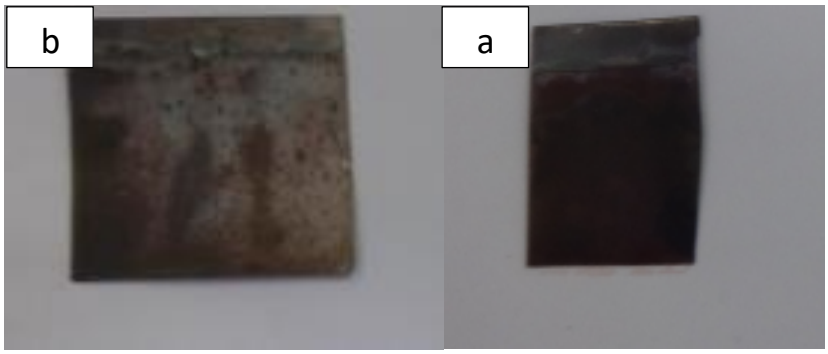

Figure 2-14 images of $TiO_{2(1)}$ NTs after immersion in dye N3 (a) in the presence of ultrasound (b) in the absence of ultrasound

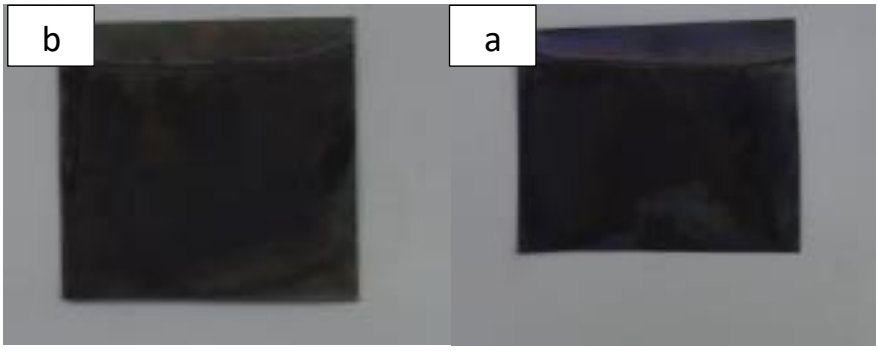

Figure 2-15 images of $TiO_{2(2)}$ NTs after immersion in dye N3 (a) in the presence of ultrasound (b) in the absence of ultrasound

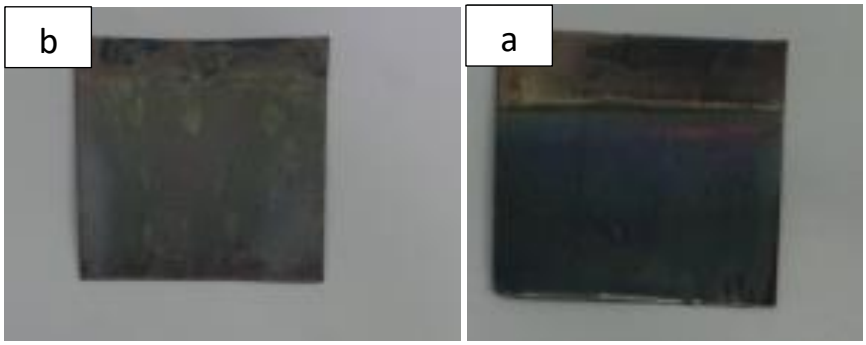

Figure 2-16 images of $TiO_{2(3)}$ NTs after immersion in dye N3 (a) in the presence of ultrasound (b) in the absence of ultrasound

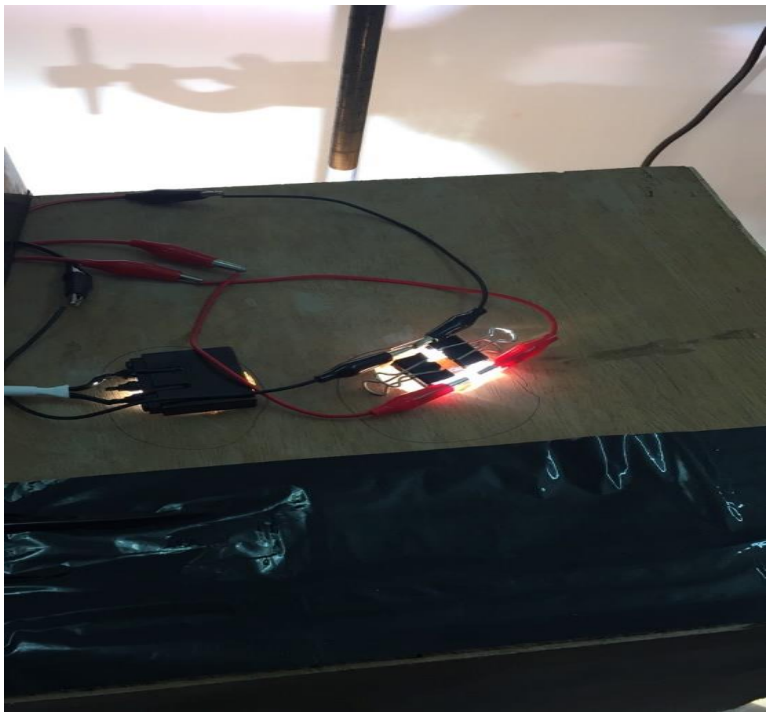

Figure 2-17 Images preparation of DSSCs

2-3 Identification of the prepared Nanomaterials

1- Phase and crystalline size

X-ray diffraction technique was used to study the crystalline properties of prepared materials using a single-wavelength light (o.15056) from source CuKα with the use of nickel as a filter. where the range taken from the angles of deviation (2θ) in this measurement is within the range (10-80) degree, X-ray diffraction spectra were recorded in the service laboratory. in Baghdad university, college of Education. Ibn Al-Haytham. using X-Ray diffraction(6000XRD) specie phaser, company Shimadzu , Japan.

2- Field - Emission scanning electron microscopy (FESEM)

This technique was utilized to study the morphology properties of the nanomaterials prepared in terms of shape, size and the nature of the assemblies.This measurement was done by accelerating the voltages 15.0 kv

with a magnification force ranging from 1.00 – 170 kx for models and other models from 5 to 200 as well EDX – mapping was also used to estimate the number of elements in prepared samples in Tehran university and sharif technology service complex.

3- Raman spectroscopy

Raman spectroscopy was used to study the crystalline phases of prepared nanomaterials and the knowledge of transitions electronic.Raman spectra of solid materials were recorded using laser beams and a range of wavelengths (100-1000) cm^{-1}, Raman Spectra was registered at the college of Science - Tehran University using Raman Microscopy type Takram N1-541, Japan.

4- Atomic force microscopy (AFM)

It was used to utilized outer surface composition(Topography) , surface roughness and square root rate of surface roughness using the tapping mode .in college of science -Baghdad university.

5- Transmission electron microscopy (TEM))

It was studied the external composition, the crystalline phase and the average size of the nanomaterials in Sharif technology service complex-Tehran-Iran using (TEM) type AB912, company Leo Germany.

6- Analysis of the surface area and the porosity nature of surface (BET,BJH)

The surface properties of titanium dioxide nanowire were studied on the one hand of surface area and the distribution of pore diameter and pore size using isotherm BET (adsorption – desorption) and BJH method for the distribution of pore diameters and the use of liquid nitrogen at a temperature of 77 K, in

Sharif technology service complex-Tehran-Iran using B.E.T surface area analyzer type NOVA 2200 ,company Quantachrome instruments , It is a common technique used to diagnose surface area and pore size by using isotherm adsorption - desorption and the distribution of pore size BJH (Barrett-Toyner-Halenda)

The figure below demonstrates the different class of adsorption isotherms

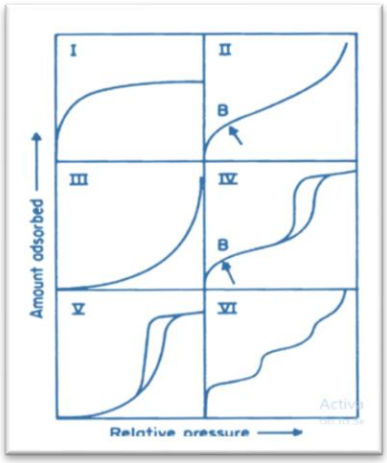

Figure 2-18 classes of adsorption isotherm

Isotherm adsorption is divided into six categories

-The first class of isotherm adsorption

As this type of isotherm is characterized by monolayer adsorption, adsorption appears to increase rapidly with relative pressure and finally reaches a plateau at the pressure high enough as this type of isotherm obtain for the microporous solids have relatively small outer surfaces.

-The second class of isotherm adsorption

This type of isotherm shows multi-layer adsorption so the plateau disappears and thus adsorption continues to increase even when the relative pressure is finished at the unit. This type of species appears at the macroporous adsorbents.

-The third class of isotherm adsorption-

The type of isotherm characteristic that curve uptake is convex at a full range of relative pressure.

-The fourth class of isotherm adsorption-

the class of isotherm is characterized by a hysteresis loop that contributes to the filling or discharging of the mesopores through capillary condensation. The lower section of the hysteresis loop represents The gradual addition of the adsorbent gas and the upper branch represents the gradual withdrawal of the adsorbent gas, it can be considered as a combination of type I and II for adsorption. Adsorption increases with the pressure within the low-pressure zone and are then subjected to monolayer and multilayer adsorption

-The fifth class of isotherm adsorption

This type of isotherm is characterized that S- curve adsorbents and shows a hysteresis loop.

-The sixth class of isotherm adsorption

it is similar the second type of isotherm, which appears multi-layer adsorption, on a regular non-porous surface. It occurs in steps. the step high represent the capacity of the monolayer for each adsorbed layer. It is stable for two or three adsorbents layers. The acuity steps depend on the system and the

temperature .Isotherm of adsorption can be analyzed and classification of models into three various types of porosity.

1- Microporous that less than 2 nm .

2-Mesoporous which was between 2 – 50 nm .

3-Macroporous that more than 50 nm .

7- DRS Spectroscopy

This technique was used to calculate the energy gap and to study the potential electronic transitions where the spectral reflection of ultraviolet radiation was recorded at the college of Physics - Sharif - Tahran-Iran type MIRA3 company Quantachrome Instruments , USA

8- PV power analyzer

Used to measure the current and voltage values of dye sensitive solar cells with Si calibrated cells to calibrate the intensity of light falling on the cell at the same moment power supply type Net zamachlubgerat In addition to other measuring devices including a Bdigital multimeter 3465 and light source a xenon lamp intensity 84 mW/cm^2 .

Chapter Three

Results and Discussion

3-1 Characterization of the prepared nanomaterials

3-1-1 Characterization of Titanium dioxide nanotubes

3-1-1-1 Phase and crystalline size

The TiO_2 nanomaterials structure were tested in their solid-state using X-ray diffraction (XRD), to determine some of their structural properties such as crystalline phase, crystalline size, and purity. where the XRD spectra to the TiO_2 nanomaterials appear that all the position of apparent diffraction peaks has high matching with peaks of the Joint Committee on Powder Diffraction Standards (JCPDS)**,** there are diffraction peaks to be reviewed when the size of the crystals is very small. the review at the diffraction peaks of titanium dioxide nanomaterials indicates the formation of these nanomaterials, according to literature, the crystal size decreases when the increase in the review of these peaks **[125]**. The amplitude of the X-ray diffraction peaks is due to four main things: micro–strains, such as lattice deformation, crystalline fracture due to crystallization defects, domain size of the crystal and field size distribution **[126, 127].** when the prepared crystals are neither tight nor distorted, the review, in this case, instructs the crystal size **[128]**. The Debye-Scherrer equation was used to calculate the crystalline size for titanium dioxide nanomaterials as follows **[126]**:

$$D = \frac{k\lambda}{\beta \cos\theta} \qquad \ldots\ldots\ldots (1-3)$$

D is represents the average crystalline size, k is representing the shape factor, ordinarily about 0.9, λ is the X-ray wavelength, which is CuKα = 0.15056nm, β represents the full width of half the maximum height FWHM, θ is the angle of deviation, and the angle is used at the highest peak to calculate the crystalline size of the particles. In applying this equation, the average

crystalline size of TiO_2 nanomaterials was found to be between 8.48 nm and 38.02 nm.

Then calculate the d-spacing using the Bragg's law **[129]**

$$d = \frac{n\lambda}{2\sin\theta} \qquad \ldots\ldots\ldots(2-3)$$

Where d is the spacing between crystalline levels, n is an integer (1,2,3…et) The (XRD) technique was used to identify the crystalline phase and from the characteristic peaks shown by the X-ray diffraction spectra 101 and 110 for the anatase and rutile phase, respectively. The phase depends entirely on the preparation of method and the nature of the precursor as well as the temperature at which the calcination process takes .

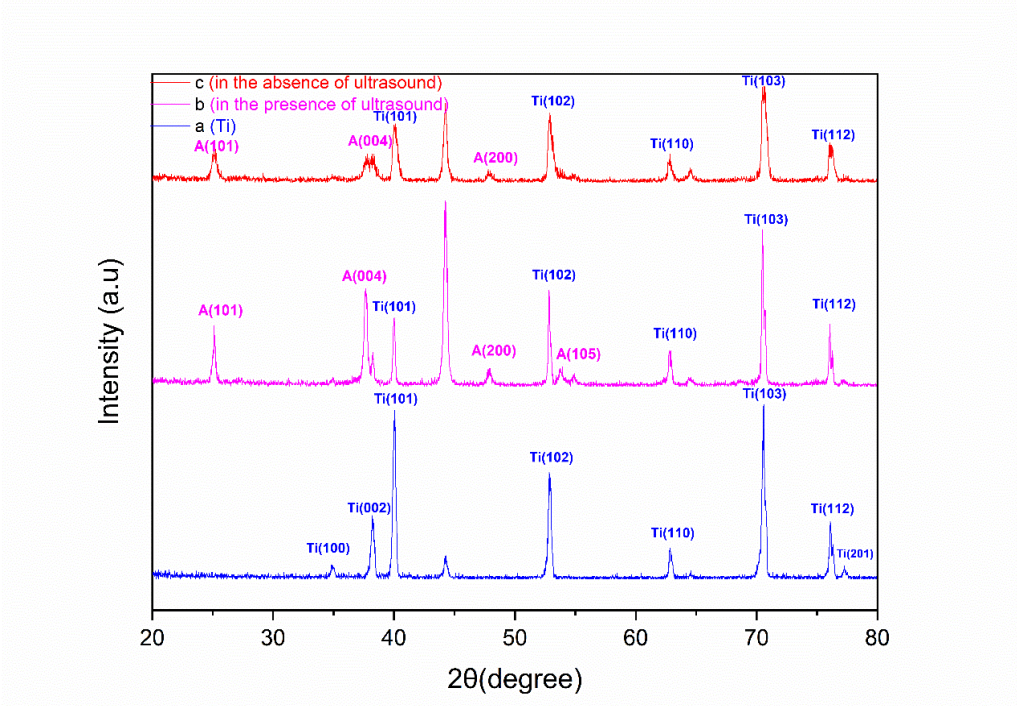

Figure (3-1): show XRD for standard diffraction pattern (a) and annealed TNT/Ti arrays in the presence of ultrasound (b) and annealed TNT/Ti arrays in the absence of ultrasound (c) in an electrolyte solution (ethylene glycol) containing both NH_4F and H_2O

Table (3-1): Data X - ray diffraction variables for TiO_2 prepared in an electrolyte solution (ethylene glycol) containing both NH_4F and H_2O

in the presence of ultrasound					
2Θ(deg)	FWHM	Crystal Size(nm)	Intensity	d- spacing(Å)	Miller index
25.1541	0.27330	15.20	43	3.53751	(101)
37.6646	0.30200	14.19	101	2.38631	(004)
47.8692	0.36000	12.32	13	1.89872	(200)
53.7966	0.30000	15.16	15	1.70267	(105)
54.9062	0.20000	22.85	8	1.67085	(211)
in the absence of ultrasound					
2Θ(deg)	FWHM	Crystal Size(nm)	Intensity	d- spacing(Å)	Miller index
25.1857	0.49000	8.48	28	3.53314	(101)
37.6956	0.44000	9.74	19	2.38442	(004)
47.8692	0.48000	9.24	8	1.89872	(200)

Figure 3-1 (b, c) in an electrolyte solution (ethylene glycol) containing both NH_4F and H_2O in the presence and absence of ultrasound shows TiO_2 NTs after annealing at 550°C for 30 min in an atmosphere of oxygen that the anatase crystal structure. XRD measurements refers to have TiO_2 NTs the anatase phase, whereas the crystalline form could be observed after annealing and represented three strong diffraction peaks where the diffraction is indexed (JCPDS 21-1572), both TiO_2 NTs in the presence of ultrasound and in the absence of ultrasound possess the diffraction peaks at (25.15°, 37.69°, 47.86°) and (25.18°, 37.69°, 47.86°) can be specified to the (101), (004), (200) anatase crystal faces, Consecutively. It is worth mentioning that the increase

in the intensity of the peak of TiO_2 NTs indicates the increase in the length of nanotube.

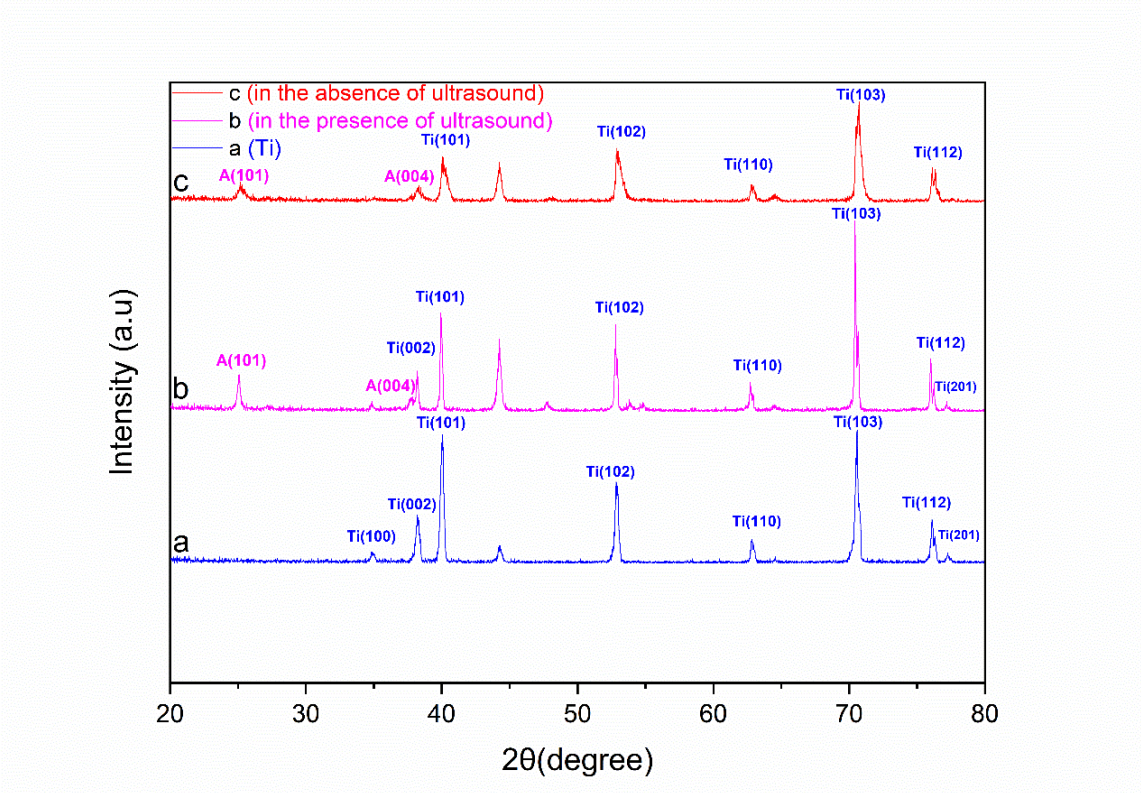

Figure (3-2): shows XRD for standard diffraction pattern (a) and annealed TNT/Ti arrays in the presence of ultrasound (b) and annealed TNT/Ti arrays in the absence of ultrasound in water-based electrolyte containing both Na_2SO_4 and NH_4F

Table (3-2): Data X - ray diffraction variables for TiO_2 prepared in water-based electrolyte containing both Na_2SO_4 and NH_4F

in the presence of ultrasound					
2Θ(deg)	FWHM	Crystal Size(nm)	Intensity	d- spacing(Å)	Miller index
25.0915	0.22530	18.44	44	3.54619	(101)
37.7356	0.21340	20.08	13	2.38199	(004)

in the absence of ultrasound					
2Θ(deg)	FWHM	Crystal Size(nm)	Intensity	d- spacing(Å)	Miller index
25.2606	0.46000	9.03	17	3.52283	(101)
37.7555	0.20000	21.43	4	2.38078	(004)

Figure 3-2 (b, c) in water-based electrolyte containing both Na_2SO_4 and NH_4F in the presence and absence of ultrasound shows TiO_2 NTs after annealing at 550˚C for 30 min in an atmosphere of oxygen that the anatase crystal structure. XRD measurements refers to have TiO_2 NTs the anatase phase, whereas the crystalline form could be observed after annealing and represented three strong diffraction peaks where the diffraction is indexed (JCPDS 21-1272), both TiO_2 NTs in the presence of ultrasound and in the absence of ultrasound possess the diffraction peaks at (25.09°, 37.73°) and (25.26°, 37.75°) can be specified to the (101), (004) anatase crystal faces, Consecutively. It is worth mentioning that the increase in the intensity of the peak of TiO_2 NTs indicates the increase in the length of nanotube **[82].**

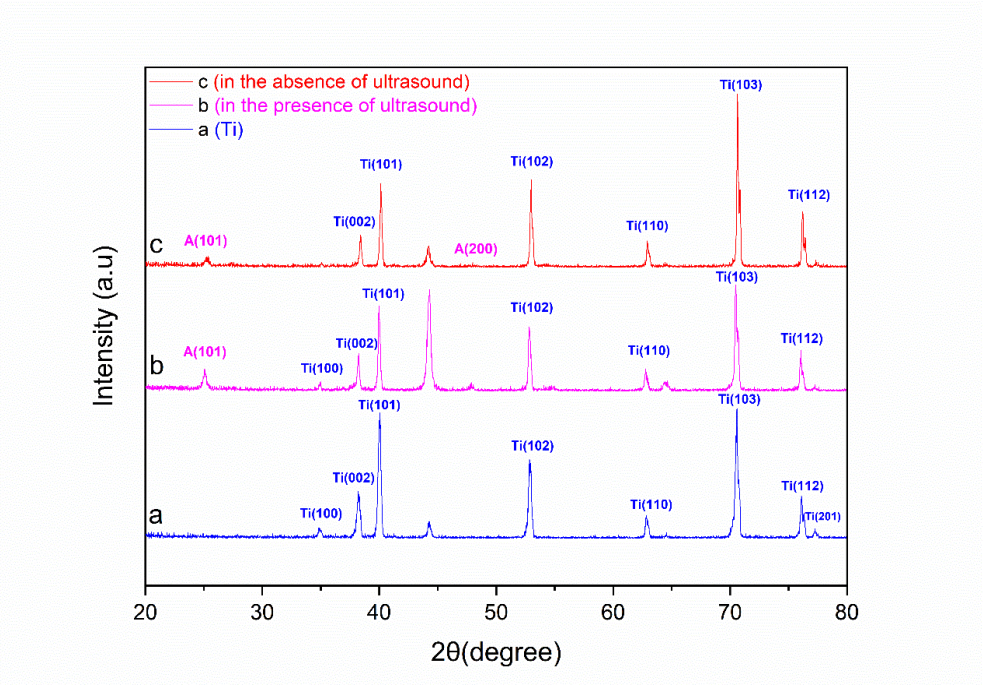

Figure (3-3): shows XRD for standard diffraction pattern (a) and annealed TNT/Ti arrays in the presence of ultrasound (b) and annealed TNT/Ti arrays in the absence of ultrasound in lactic acid-based electrolyte containing o.15 wt NH_4F and 5 vol H_2O

Table (3-3): Data X - ray diffraction variables for TiO_2 prepared in lactic acid-based electrolyte containing o.15 wt NH_4F and 5 vol H_2O

in the presence of ultrasound					
2Θ(deg)	FWHM	Crystal Size(nm)	Intensity	d- spacing(Å)	Miller index
25.1058	0.29000	14.33	24	3.54420	(101)
37.8455	0.14000	29.05	6	2.37532	(004)
47.8608	0.11670	38.02	9	1.89904	(200)
in the absence of ultrasound					
2Θ(deg)	FWHM	Crystal Size(nm)	Intensity	d- spacing(Å)	Miller index
25.3015	0.12200	34.07	11	3.51723	(101)

Figure (3-3,b) in lactic acid-based electrolyte containing o.15 wt NH_4F and 5 vol H_2O showed X-ray diffraction TiO_2 NTs after annealing at 550˚C for 30 min that the anatase crystal structure, which is evidenced from the diffraction peaks (101) at 2θ = 25.10˚ (101) , 37.73°(004) , 47.84°(200) consisting only of the anatase peak while **figure (3-3,c)** in the absence of ultrasound show that the crystalline form could be noticed after annealing and represented the strong diffraction peaks where the diffraction is indexed (JCPDS 21-1272), the diffraction peak at 25.30°can be specified to the (101) anatase crystal face.

3-1-2 Characterization of Titanium dioxide nanowires

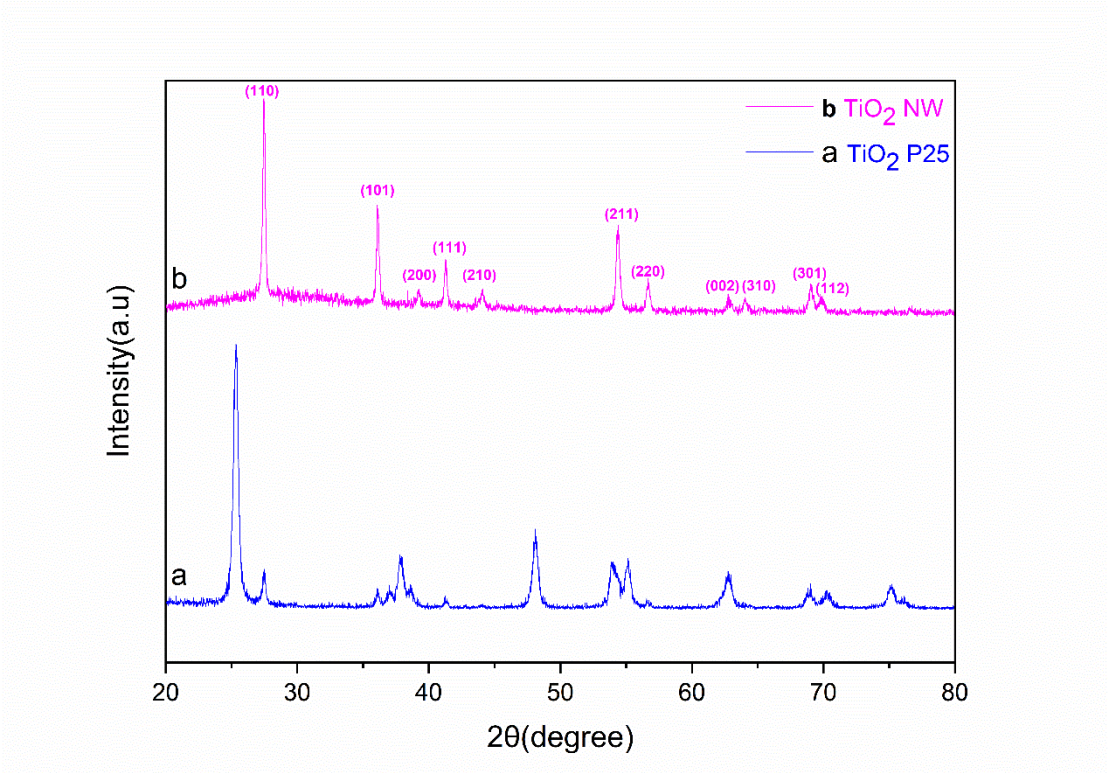

Fig. (3-4) The XRD patterns of TiO_2P25 and (a) as-synthesized TiO_2 NW arrays (b) in 3 hour .

from the figure (3-4), the XRD data show an excellent agreement with the standard rutile structure of TiO_2 (PDF card-TiO_2-00-021-1276), The absence

of any peaks for other impurities is proof of the high purity of the product **[130].**

Table (3-4): data X- ray diffraction variables for TiO_2 powder prepared in 3 hour

2Θ(deg)	FWHM	Crystal Size(nm)	Intensity	d- spacing(Å)	Miller index
27.5022	0.21970	19.00	252	3.24058	(110)
36.1348	0.22730	18.77	119	2.48375	(101)
39.2349	0.19100	22.54	22	2.29435	(200)
41.2924	0.22390	19.36	59	2.18465	(111)
44.0763	0.21000	20.83	24	2.05291	(210)
54.3627	0.26730	17.05	116	1.68626	(211)
56.6575	0.24800	18.58	39	1.62329	(220)
62.7767	0.21330	22.27	17	1.47897	(002)
64.0396	0.19330	24.75	20	1.45281	(310)
69.0381	0.27330	18.01	34	1.35932	(301)
69.8113	0.26000	19.02	14	1.34614	(112)

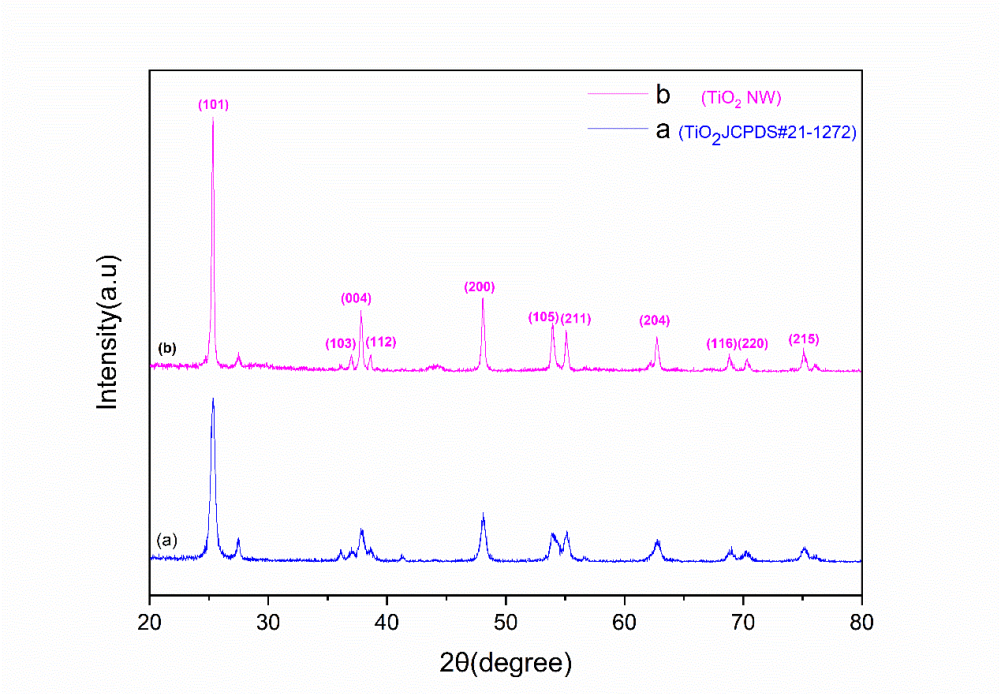

Fig. (3-5) The XRD patterns of TiO_2P25 and (a) as-synthesized TiO_2 NW arrays (b) in 12 hour

Figure 3-5 illustration XRD patterns of the TNWs prepared at hydrothermal temperatures at 180° C for 12 hours. where XRD data a model diffraction peaks corresponding to the reflection of the standard pure anatase TiO_2 material (JCPDS Card No.21-1272) a main peak centered at 25.39° can be ascribed to the (101) facet of anatase TiO_2. The absence of any peaks for other impurities is proof of the high purity of the product **[131]**.

Table (3-5): Data x - ray diffraction variables for TiO_2 powder prepared in 12 hour

2Θ(deg)	FWHM	Crystal Size(nm)	Intensity	d-spacing(Å)	Miller index
25.3980	0.21840	19.03	338	3.50408	101
37.0536	0.19500	21.93	26	2.42425	103

37.8964	0.19100	22.45	96	2.37225	004
38.6688	0.22000	19.54	22	2.32662	112
48.1194	0.20930	21.22	140	1.88943	200
53.9830	0.18950	24.02	89	1.69723	105
55.1433	0.20020	22.85	79	1.66423	211
62.7718	0.20490	23.19	64	1.47907	204
68.8182	0.23330	21.07	26	1.36313	116
70.3692	0.18400	26.97	33	1.33683	220
75.1118	0.21600	23.68	42	1.26375	215

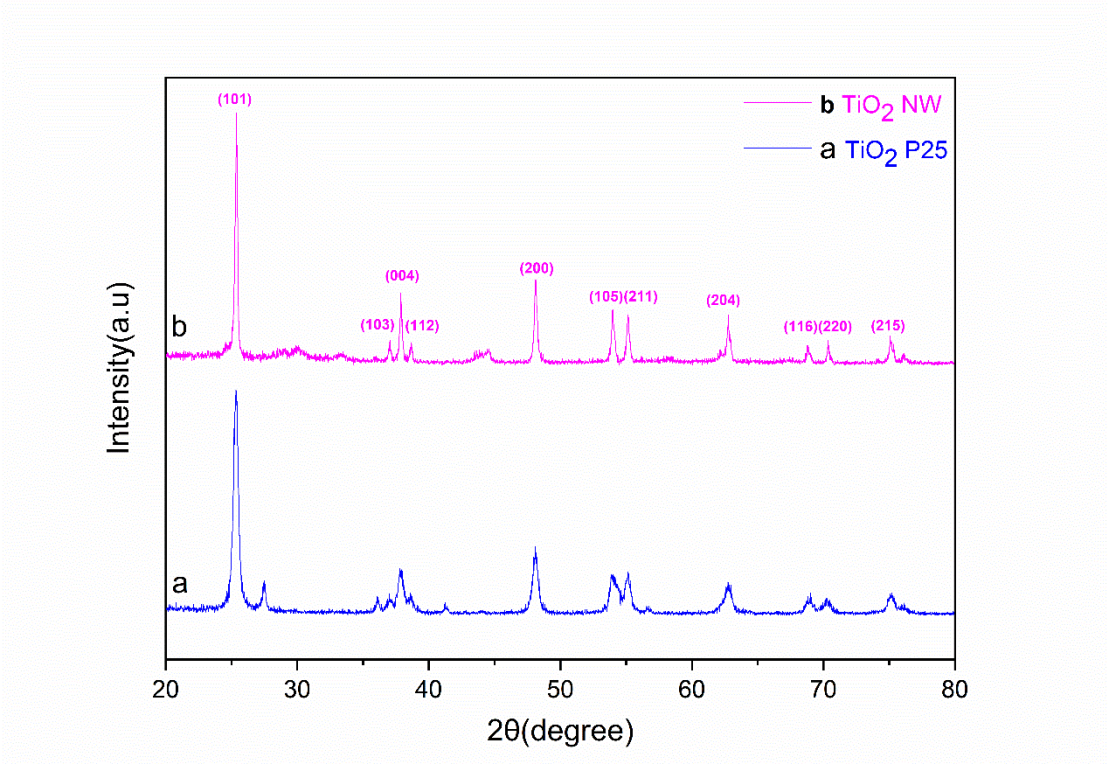

Fig. (3-6) The XRD patterns of TiO_2P25 and (a) as-synthesized TiO_2 NW arrays (b) in 24 hour

Figure (3-6) Shows XRD patterns the anatase phase of TiO_2 that peaks are corresponding to the planes (101) (004) (200) (204) (116) (220) of anatase titanium dioxide structure (JCPDS Card No.21-1272). The absence of any peaks for other impurities is proof of the high purity of the product.

Table (3-6): data x - ray diffraction variables for TiO_2 powder prepared in 24 hour

2Ɵ(deg)	FWHM	Crystal Size(nm)	Intensity	d- spacing(Å)	Miller index
25.3559	0.21870	19.01	506	3.50981	(101)
36.9862	0.22000	19.44	**29**	2.42851	(103)
37.8388	0.23000	18.64	122	2.37573	(004)
38.6065	0.22330	19.24	29	2.33023	(112)
48.0712	0.18690	23.76	182	1.89122	(200)
53.9351	0.23450	19.40	104	1.69862	(105)
55.1012	0.19910	22.97	89	1.66540	(211)
62.7159	0.22500	21.11	80	1.48026	(204)
68.8206	0.22200	22.14	36	1.36308	(116)
70.3028	0.22330	22.21	30	1.33793	(220)
75.0984	0.21300	24.02	51	1.26394	(215)

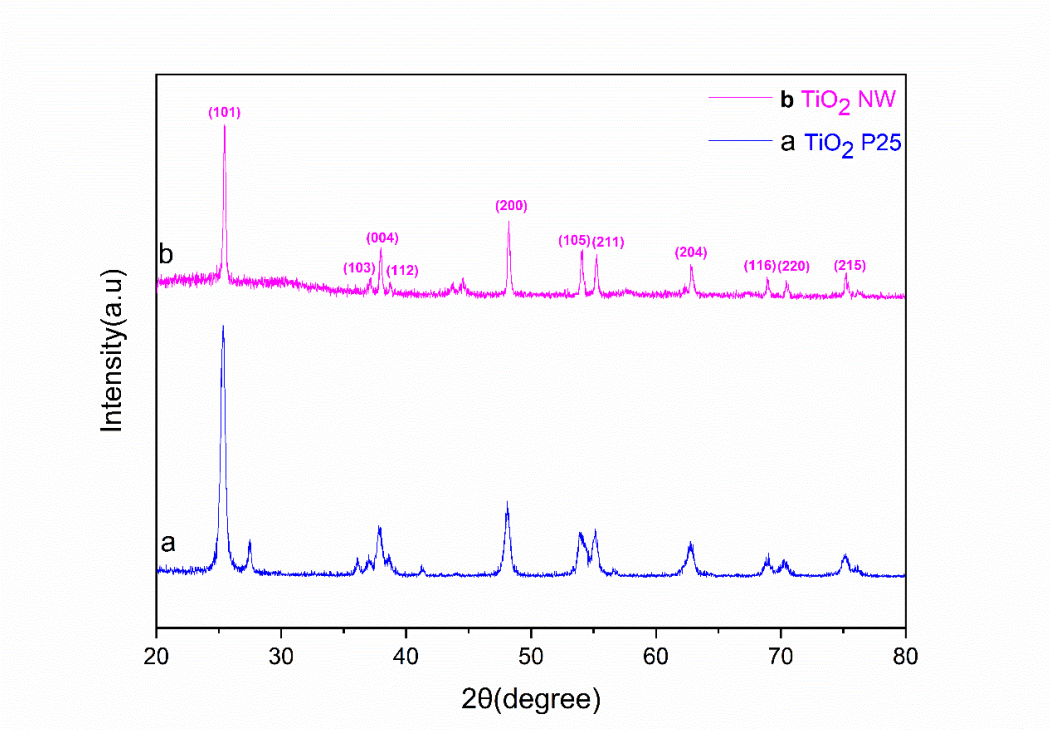

Figure (3-7): The XRD patterns of TiO_2P25 and (a) as-synthesized TiO_2 NW arrays (b) in 36 hour

Figure (3-7) b Shows X-ray diffraction (XRD) only the anatase structure of TiO_2 where diffraction peaks corresponding to the reflections of the standard pure anatase TiO_2 material (JCPDS card No.21-1272, a major peak concentrated at 25.28° can be imputed to the (101) fact of anatase TiO_2**[131]** (. While (3-7) (a) explain the X-ray diffraction patterns of the TiO_2 P25 Degussa and TiO_2 NWs, as the model is recorded at high temperature at 700 °C in order to detect changes in phase structure and crystal size

Table (3-7): data x - ray diffraction variables for TiO_2 powder prepared in 36 hour

2Θ(deg)	FWHM	Crystal Size(nm)	Intensity	d- spacing(Å)	Miller index
25.4923	0.22260	18.68	206	3.49134	(101)
37.9807	0.19930	21.52	61	2.36718	(004)
38.7264	0.16330	26.33	15	2.32329	(112)
48.2142	0.19970	22.25	110	1.88594	(200)
55.2236	0.20030	22.85	59	1.66200	(211)
62.3036	0.16000	29.62	8	1.48906	(213)
62.8474	0.18530	25.65	49	1.47747	(204)
68.9441	0.20500	24.00	28	1.36094	(116)
70.4511	0.18000	27.58	24	1.33548	(220)
75.2098	0.18000	28.44	38	1.26235	(215)

3-1-1-2 Raman spectroscopy

Raman spectroscopy was used to characterize of the nanomaterials as prepared and identified crystalline phase and crystalline structure. The compositions of titanium oxide showed that the anatase phase is the dominant phase, which has a tetragonal structure according to a literature. It is known that the active vibrational forms of the anatase phase are six forms as follows (A1g, 2B1g, 3Eg) while the vibrational shape (A2u, Eu) is active in both Raman spectra and infrared region.

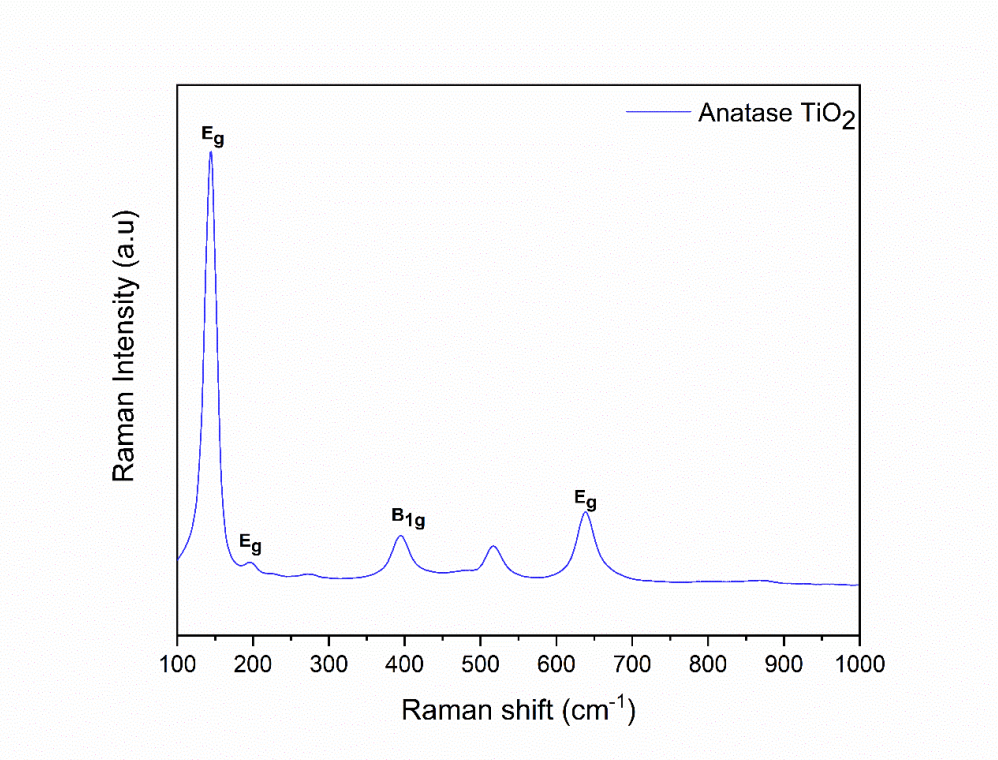

Figure (3-8) Raman spectrum of TiO_2 nanowire arrays prepared in 12 hour

Figure 3-8 Explain Raman scattering spectra for titanium dioxide Nanowire where Raman peaks are located at (145 (Eg) ،396 (B1g) ،638 (Eg) cm^{-1}) and correspond to the typical peaks of anatase titanium dioxide **[132]**.

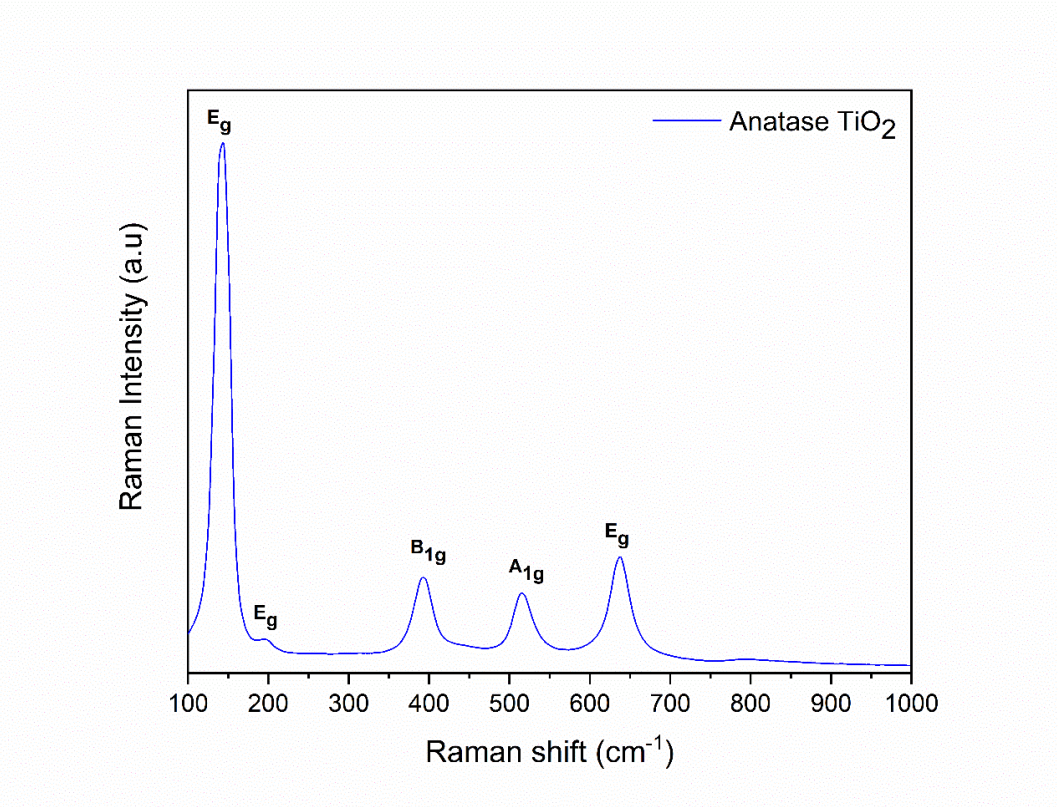

Figure (3-9) Raman spectrum of TiO_2 nanowire arrays prepared in 24 hour

Figure (3-9) illustrates the Raman spectra of the titanium dioxide nanowires where Raman peaks are located at 145، 390، 514، 638 cm^{-1} and correspond to the typical peaks of anatase titanium dioxide.

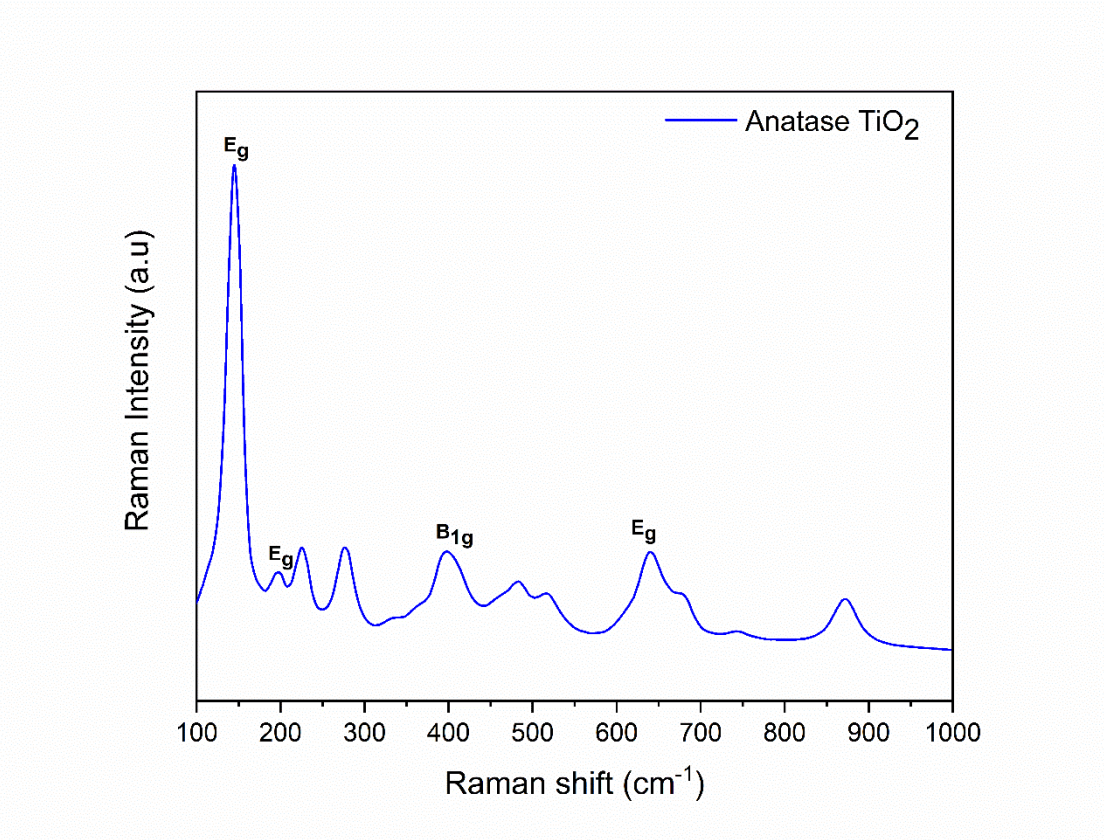

Figure (3-10) Raman spectrum of TiO_2 nanowire arrays prepared in 36 hour

Figure (3-10) shows the Raman spectra of titanium dioxide nanowires, there is apparent peaks at the region (145, 396, 638) that attributed to the appearance of pure anatase phase. This demonstrates that the method used in the preparation of titanium dioxide nanowires is a qualitative method for preparation of the pure anatase phase **[132]**. The peak that is shown at 144 cm^{-1} considered that characteristic peak of the anatase phase and the peak that shown at 638 cm^{-1} (Eg) is indicated to set the vibration of the stretch Ti-O while the peak at 396 cm^{-1} (Eg) that indicate position bend vibration O-Ti-O.

Standard TiO_2 (anatase)	Eg	Eg	B1g	A1g	Eg
	143	196	396	514	637
TiO_2-Nanowire (anatase) prepared in 12 hour	145	-	396	-	638
TiO_2-Nanowire (anatase) prepared in 24 hour	145	-	390	514	638
TiO_2-Nanowire (anatase) prepared in 36 hour	145	-	396	-	638

Table (3-8): Peaks locations of the anatase phase for both standard and prepared TiO_2

3-1-1-3 UV-Diffuse Reflectance Spectroscopy (UV.DRS)

The band gap of the titanium dioxide nanowire was estimated using the technique (UV. DRS) and the absorption spectra of the nanomaterials showed that the maximum wavelength is in the range 416 nm. This is due to the transfer of the charge from the valence band of the orbital 2p for the oxide to the valence band of the orbital 3d for the titanium**[133]**. This indicates that the Titanium nanomaterials prepared is appears in the UV region. The energy band gap of titanium dioxide nanomaterials can be measured by using wavelength and according to the following equation :

$$E_g = \frac{1240(eV.nm)}{\lambda} \qquad \ldots\ldots\ldots(3-3)$$

Where E_g is energy band gap, λ is wavelength at extension the edge of the absorbent band, Whose values through the spectrum are equal to (416,415 and 397 nm) respectively at different times as in Figures (3-11 ,3-12and 3-13) , It

was found through the equation (3-3) that the energy band gap of the TiO_2 NWs are equal to (2.98 , 2.98 and 3.12eV) respectively .

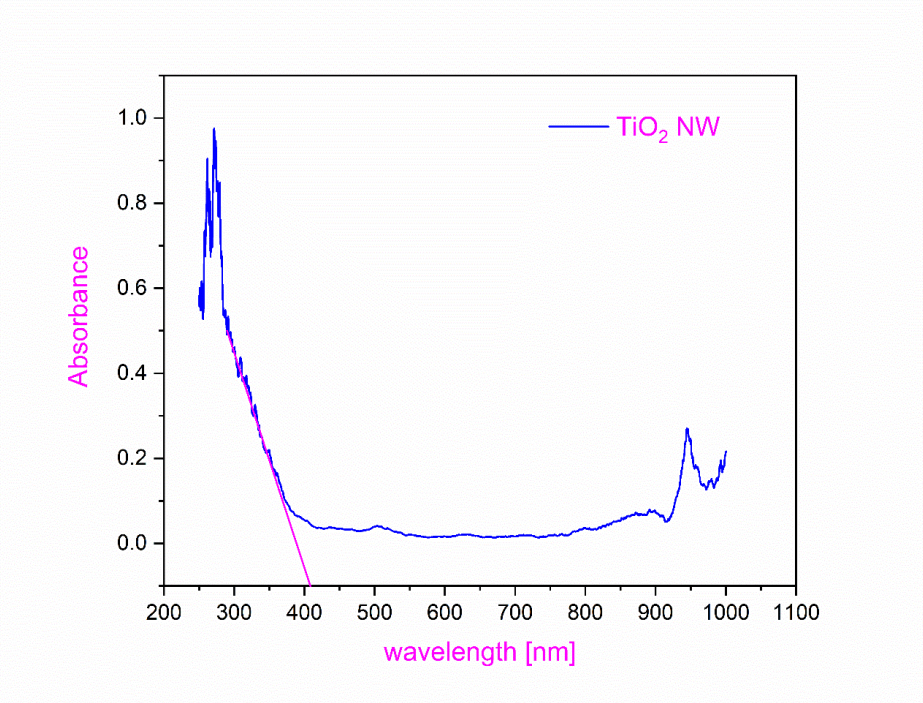

Figure (3-11) DRS spectra of $TiO_{2(1)}$ nanowire

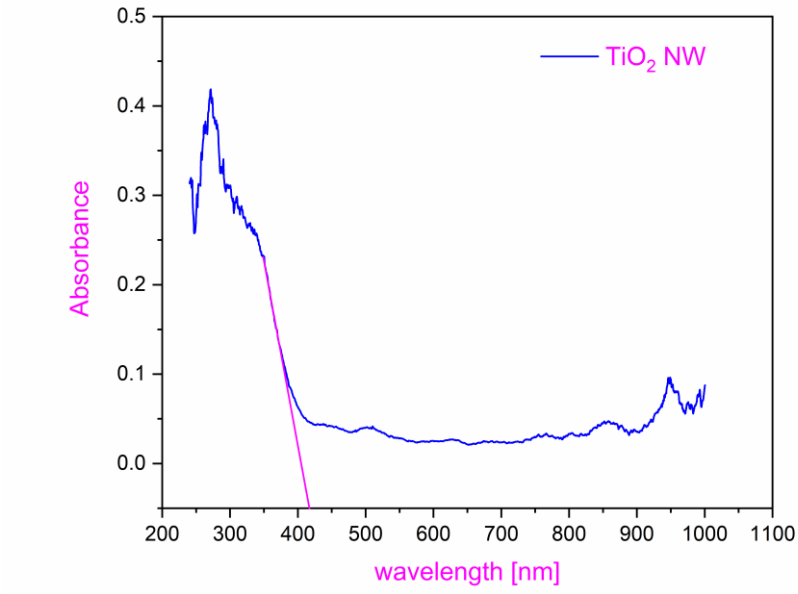

Figure (3-12) DRS spectra of $TiO_{2(2)}$ nanowire

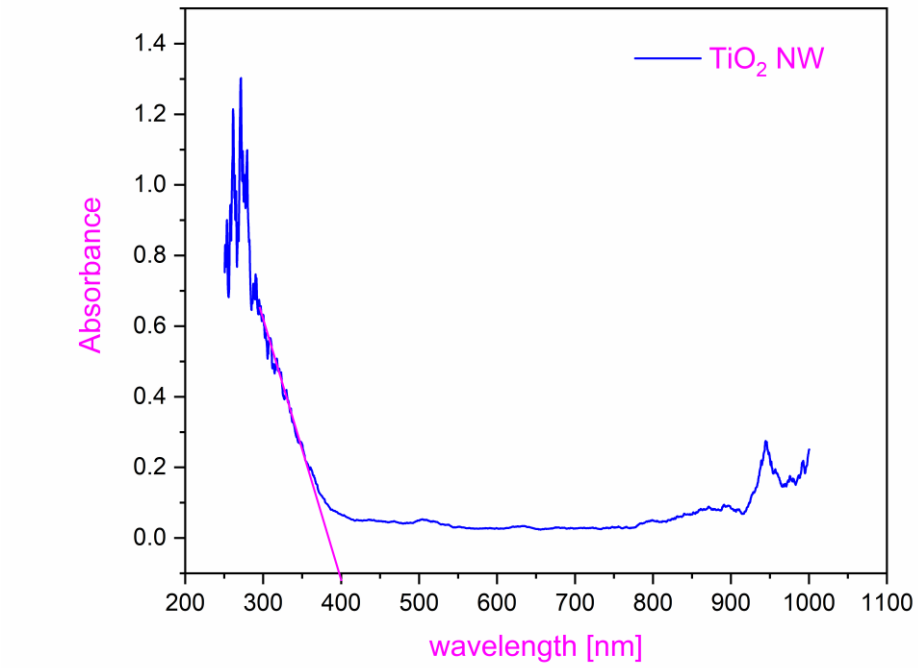

Figure (3-13) DRS spectra of $TiO_{2(3)}$ nanowire

The energy band gap can also be calculated through the Tauc plot method ، according to the following equation **[134]**:

$$\alpha h\upsilon = A\,(h\upsilon - E_g)^{1/2} \qquad \ldots\ldots\ldots (3-4)$$

Where α is absorption factor ،h is constant Planck, υ is frequency of light, A is constant of proportion, Eg is energy band gap. The Tauc plots are shown in figures (3-14,3-15and 3-16) and the calculated energy gaps are listed in table (3-9)

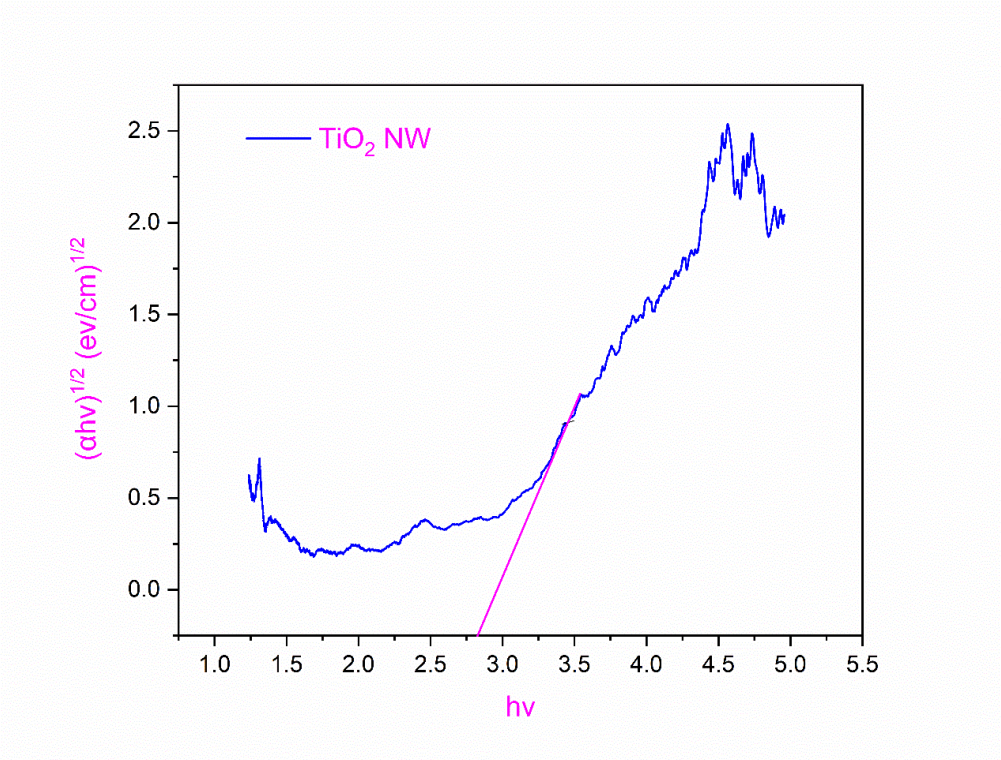

Figure (3-14) Tauc plot for $TiO_{2(1)}$ nanowire

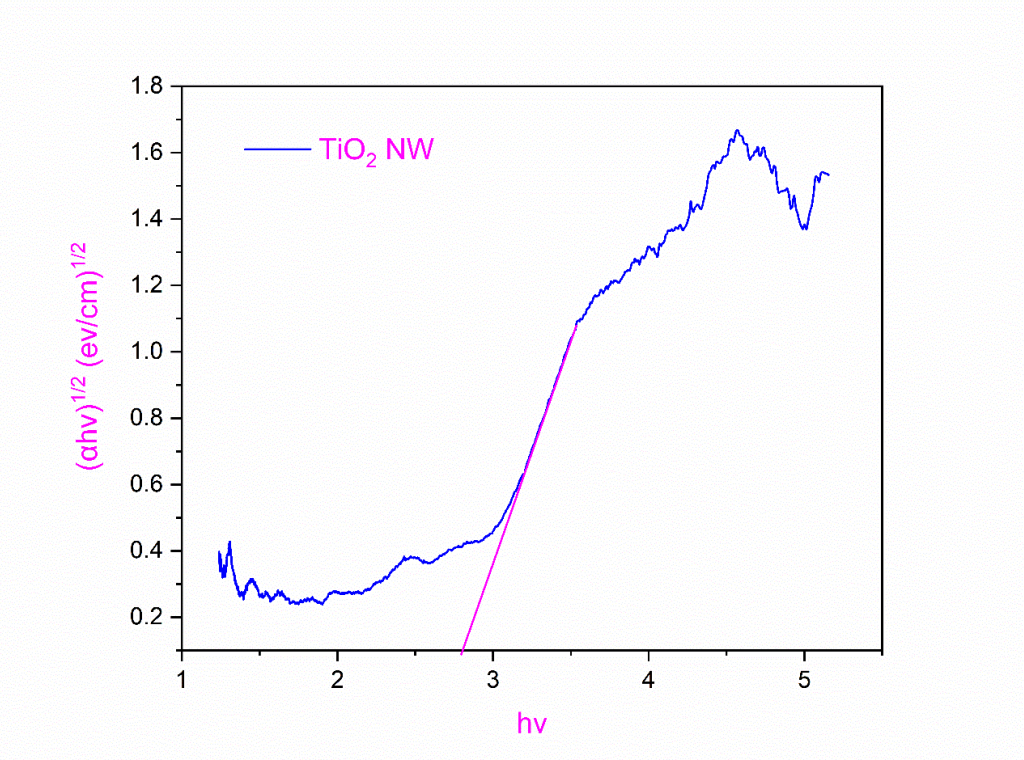

Figure (3-15) Tauc plot for $TiO_{2(2)}$ nanowire

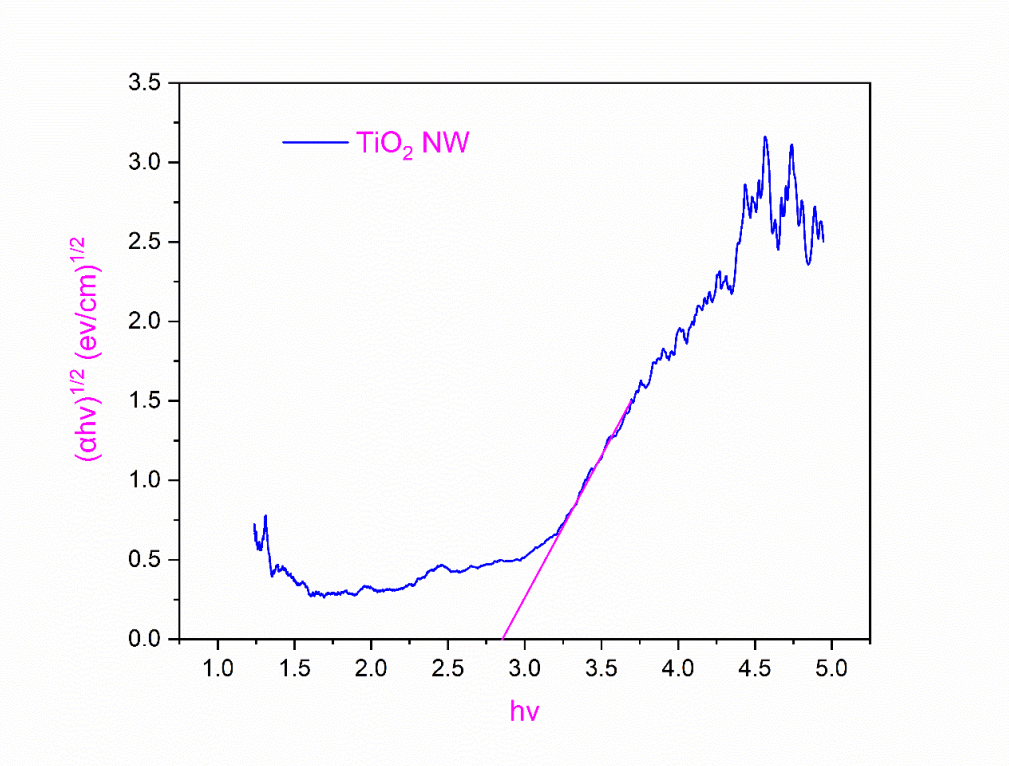

Figure (3-16) Tauc plot for $TiO_{2(3)}$ nanowire

Table (3-9): Calculated energy gap (eV)

Sample	Time	Energy gap (eV)
1	12 h	2.82
2	24 h	2.79
3	36 h	2.85

3-1-1-4 Scanning electron microscopy (SEM)and Energy-dispersive X-ray spectroscopy (EDX)-mapping

The characteristics of the surface for titanium dioxide nanotubes have been studied regarding size, shape and assembly using the scanning electron microscope technique. The characteristics are highly dependent on nature and shape surface. The elements compositions and dispersion, were estimated by EDX-mapping.

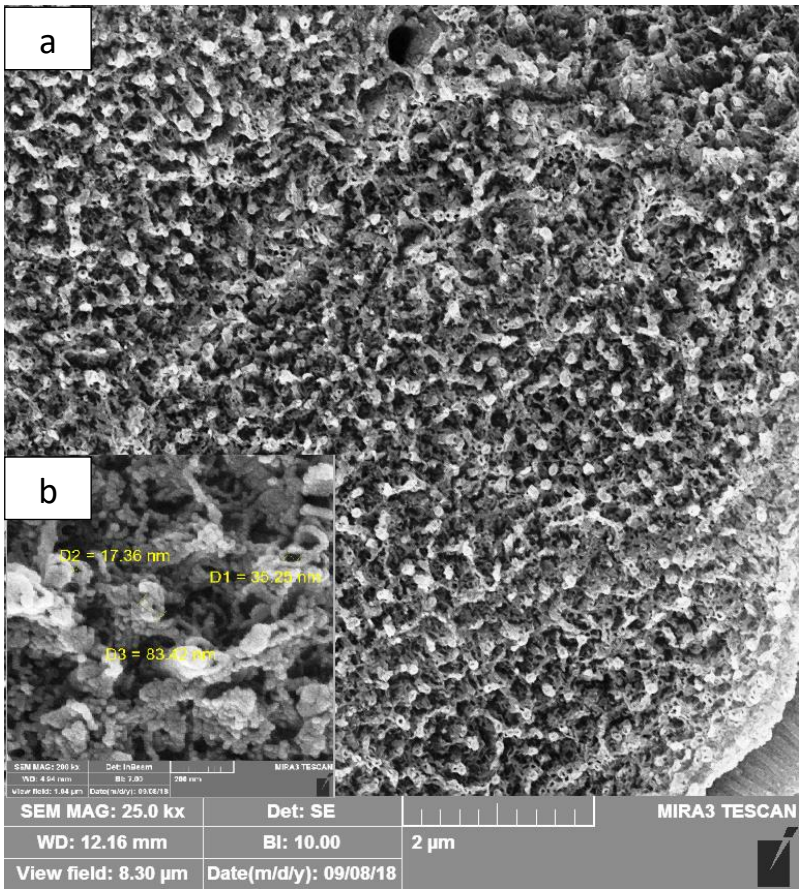

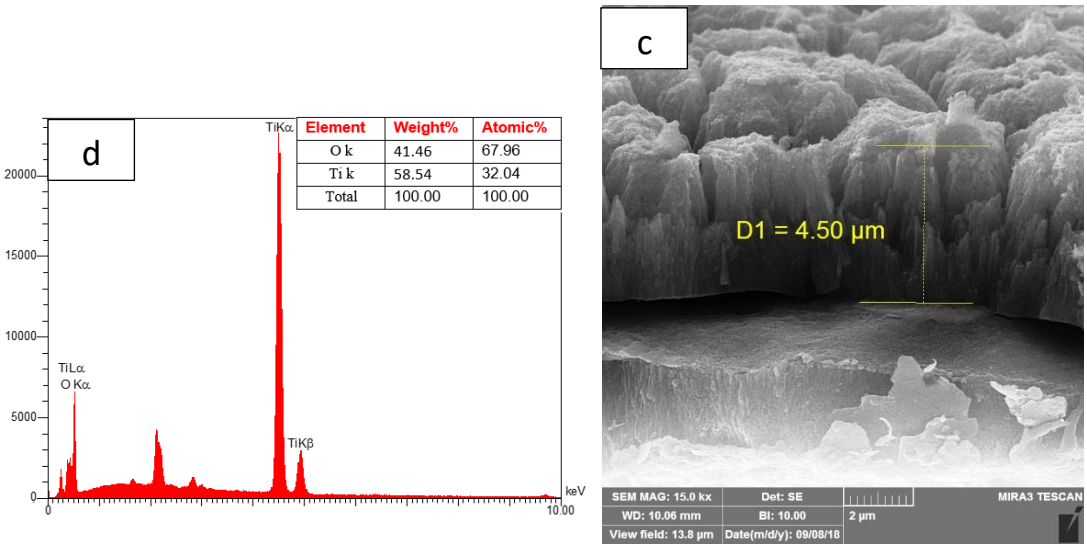

Fig. (3-17) SEM images of the TiO_2 NTs arrays (a) top view (scale bar) = 2µm, (b) pore diameter and (c) cross-sectional view and (d) EDX-spectrum in an electrolyte solution (ethylene glycol) containing both NH_4F and H_2O

The figure (3-17 a,b,c) showed that Titanium dioxide Nanotubes grew directly on titanium foil after anodizing process in an electrolyte solution (ethylene glycol) containing both NH_4F and H_2O in the absence of ultrasound. it is found to be irregular, as well as the presence of fragile debris on the surface because the TiO_2 NTs accompished with other participates from electrolyte solution. It is difficult to obtain a smooth surface **[135]**. Thus, the cross-sectional show that TiO_2 NTs with a length of 4.50µm and a tube diameter of 17.36 nm. (3-17 d) shows a quantitative analysis of the EDX spectra. It is illustrated the presence of oxygen and titanium elements which can be taken as evidence of existence TiO_2 NTs.

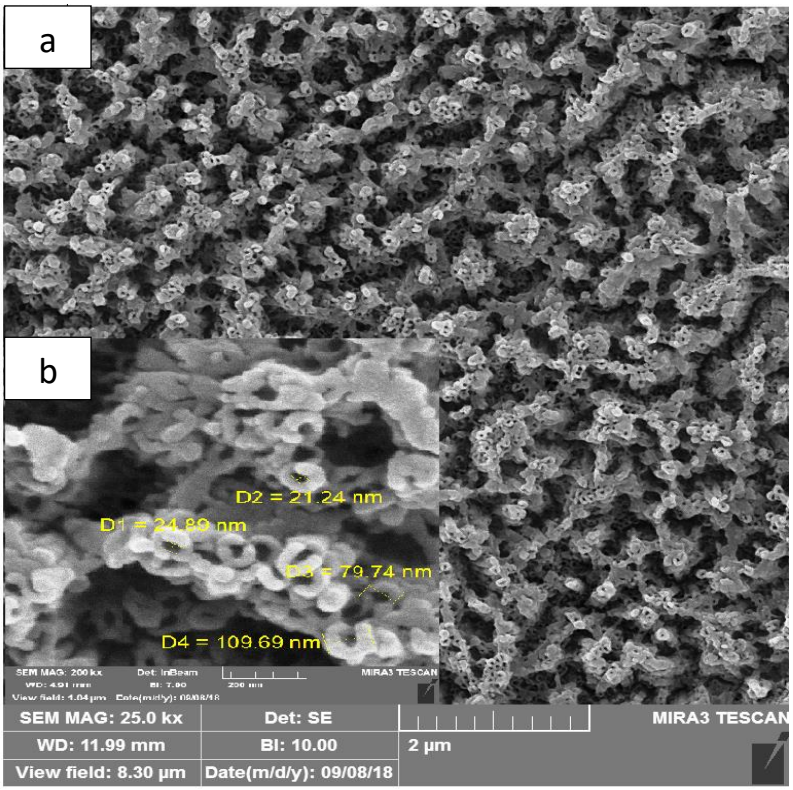

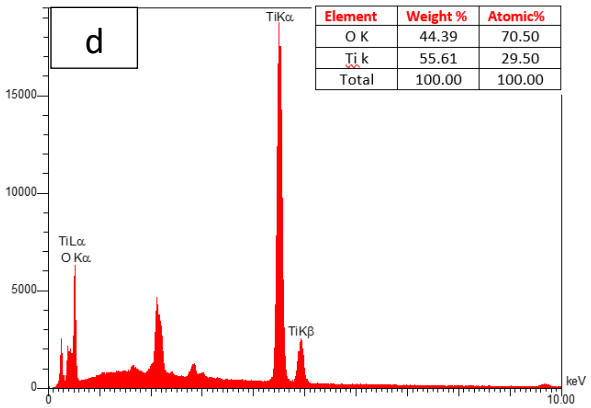

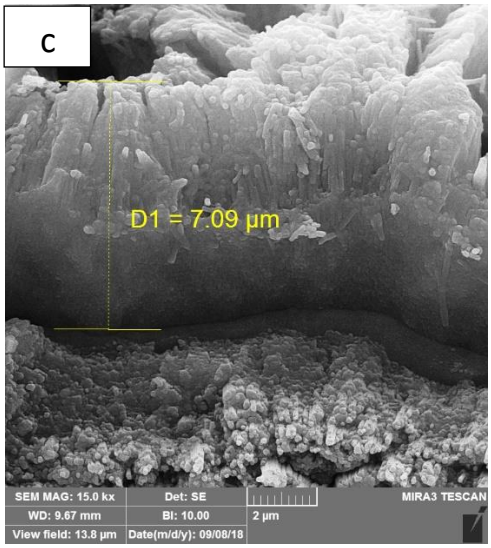

Fig. (3-18) SEM images of the TiO_2 NTs arrays (a) top view (scale bar) = 2µm , (b) pore diameter and (c) cross-sectional view and (d) EDX-spectrum in an electrolyte solution (ethylene glycol) containing both NH_4F and H_2O

The figure (3-18 a ,b,c) showed that Titanium dioxide Nanotubes grew directly on titanium foil after anodizing process in an electrolyte solution (ethylene glycol) containing both NH_4F and H_2O in the presence of ultrasound . it is found to be irregular, as well as the presence of fragile debris on the surface because the TiO_2 NTs accompished with other participates from electrolyte solution. It is difficult to obtain a smooth surface**[135]**. Thus, the cross-sectional show that TiO_2 NTs with a length of 7.09 μm and a tube diameter of 21.24 nm. (3-18 d) shows a quantitative analysis of the EDX spectra. It is illustrated the presence of oxygen and titanium elements which can be taken as evidence of existence TiO_2 NTs.

Fig.(3-19a ,b,c) show SEM images of titanium dioxide nanotubes obtained by electrochemical anodization Ti foil in water-based electrolyte in the presence of ultrasound at 10 c at 20 V for 30 min and then annealed and calcinated at 550 C for 30 min , with a highly ordered, vertically oriented and smooth wall. The inner diameter and a membrane thickness of the TiO_2 NTs are nearly (30.82, 45.97) nm and 0.76 μm or 762.29 nm, respectively. It is observing the presence of some precipitates on the surface of the TiO_2 NTs because nanotubes are accompished with other participates from electrolyte solution. Quantitative analysis of the EDX spectra in figure (3-18) d exhibit the presence of oxygen and titanium elements which can be taken as evidence of existence TiO_2 NTs

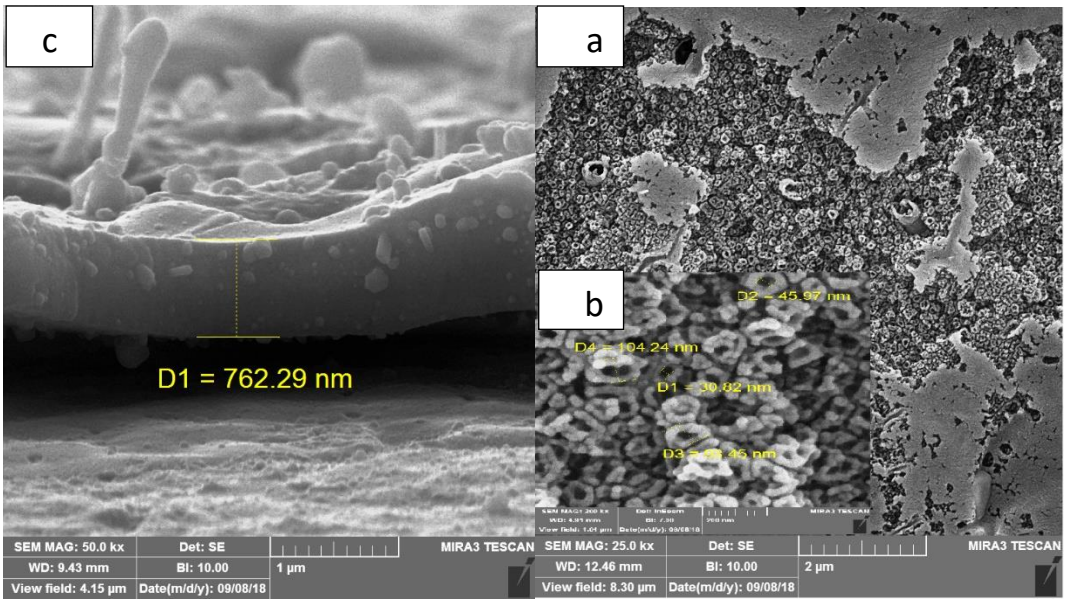

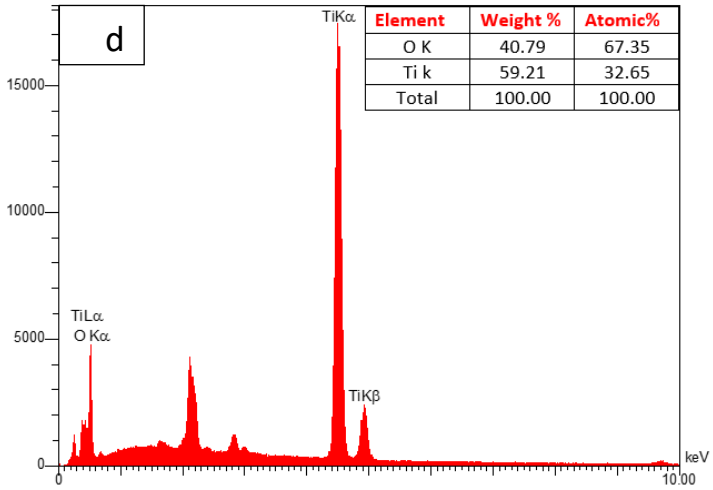

Element	Weight %	Atomic%
O K	40.79	67.35
Ti k	59.21	32.65
Total	100.00	100.00

Fig. (3-19) SEM images of the TiO_2 nanotube arrays (a) top view (scale bar) = 2µm, (b) pore diameter and (c) cross-sectional view and (d) EDX – spectrum in water-based electrolyte containing o.1M Na_2SO_4 and 0.2 wt NH_4F

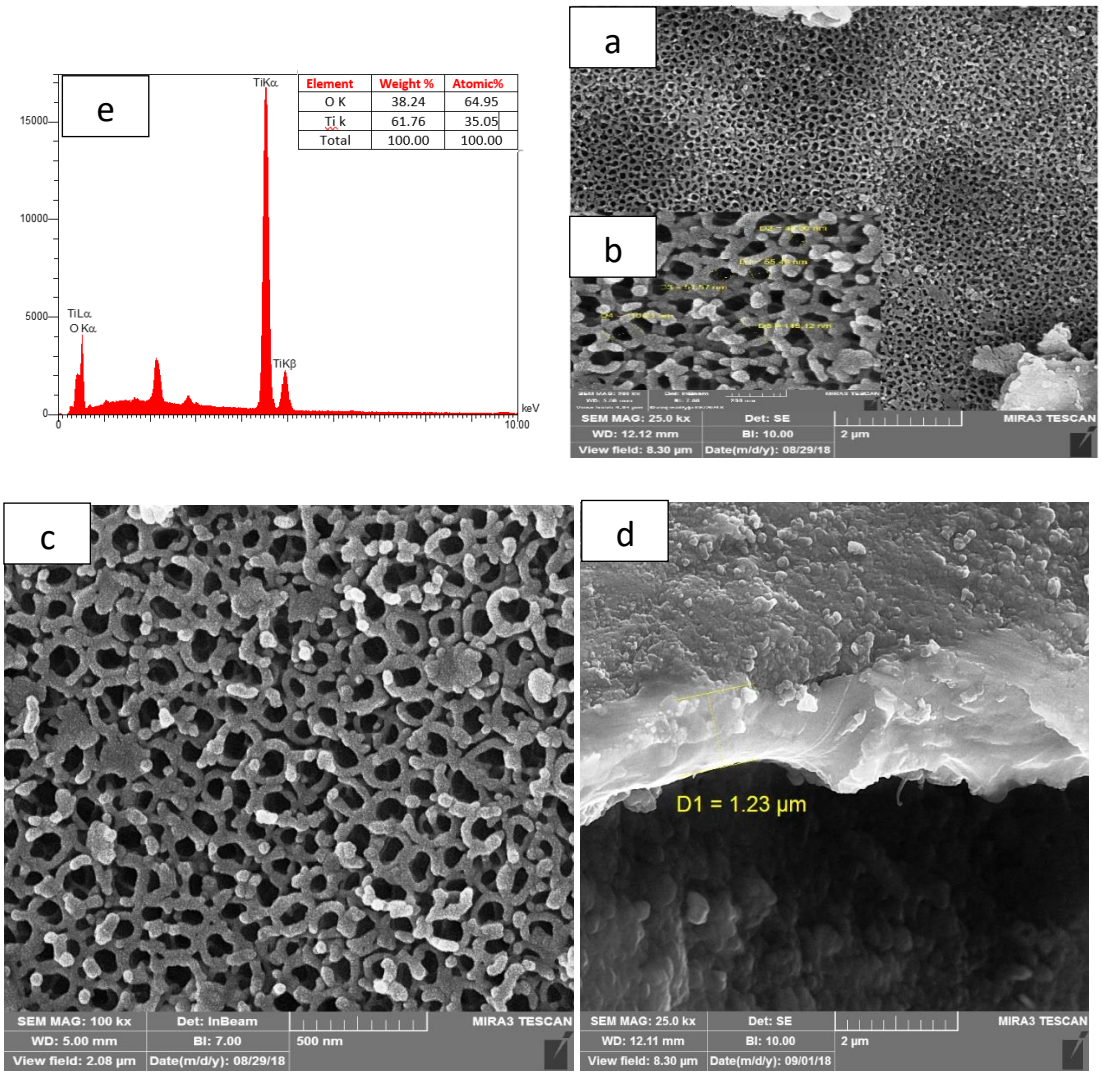

Fig. (3-20) SEM images of the cylinder-shaped TiO_2 NTs arrays (a) , (c) top view (scale bar) = 2µm , (b) pore diameter and (d) cross-sectional view and (e) EDX- spectrum in water-based electrolyte containing o.1M Na_2SO_4 and 0.2 wt NH_4F

Figure (3-20) (a),(c) shows that TiO_2 NTs obtained by electrochemical anodization of Ti foil in water-based electrolyte containing 0.1M Na_2SO_4 and 0.2 wt NH_4F in the absence of ultrasound at 10 c at 20 V for 30 min and then annealed and calcinated at 550 C for 30 min a cylinder TiO_2 NTs are vertically placed side-by-side and the thickness of the membrane is 1.23 µm while the (3-20 b) indicate the tube diameter that is (47.00, 55.43 and 57.57

nm) (3-20 e) shows a quantitative analysis of the EDX spectra. It is illustrated the presence of oxygen and titanium elements which can be taken as evidence of existence TiO_2 NTs.

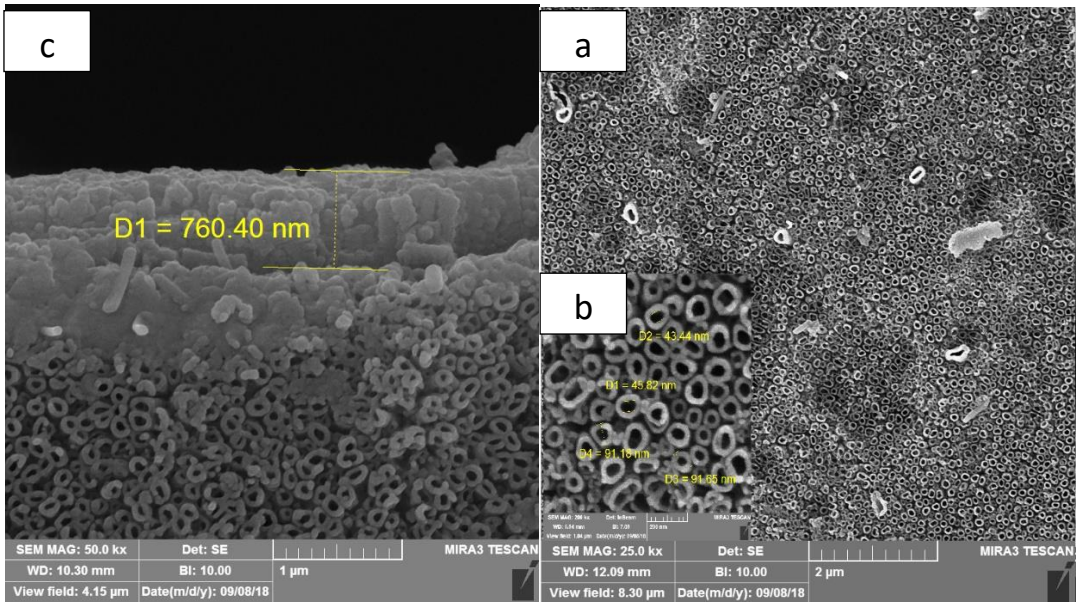

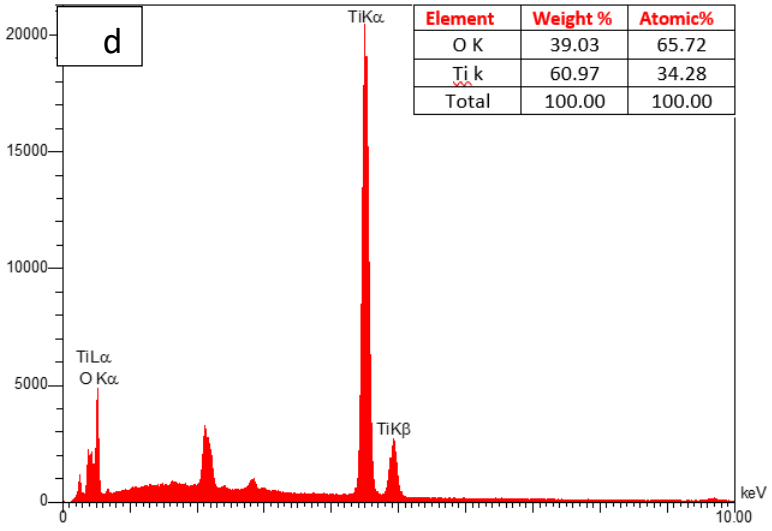

Fig. (3-21) SEM images of the TiO_2 nanotube arrays (a) top view (scale bar) = 2µm , (b) pore diameter and (c) cross-sectional view and (d) EDX – spectrum in lactic acid-based electrolyte containing o.15 wt NH_4F

Figure (3-21 a,b,c) shows the SEM images of the TiO_2 NTs obtained by electrochemical anodization of Ti foil in lactic acid-based electrolyte containing o.15 wt NH_4F and 5 vol H_2O in the presence of ultrasound at 10 c at 20 V for 30 min and then annealed and calcinated at 550 C for 30 min ,where the shape a show magnification 2 µm .It is shown the high order of the TiO_2 nanotube **[136]**and Fig.(3-21 b) showed the size of the pores and the diameter of the tube as well as the thickness of the wall where (45.82, 43.44)nm (91.18,91.65) nm and 760.40 nm respectively . figure (3-21 d) shows a quantitative analysis of the EDX spectra. It is illustrated the presence of oxygen and titanium elements which can be taken as evidence of existence TiO_2 NTs .

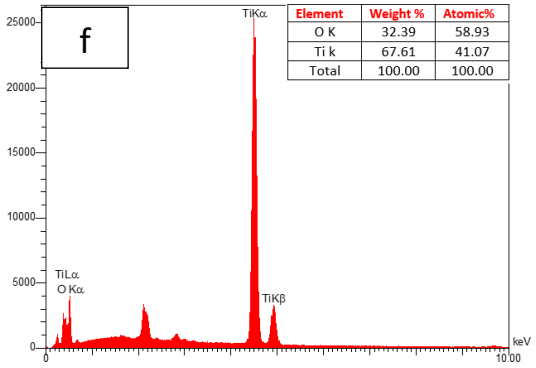

Element	Weight %	Atomic%
O K	32.39	58.93
Ti k	67.61	41.07
Total	100.00	100.00

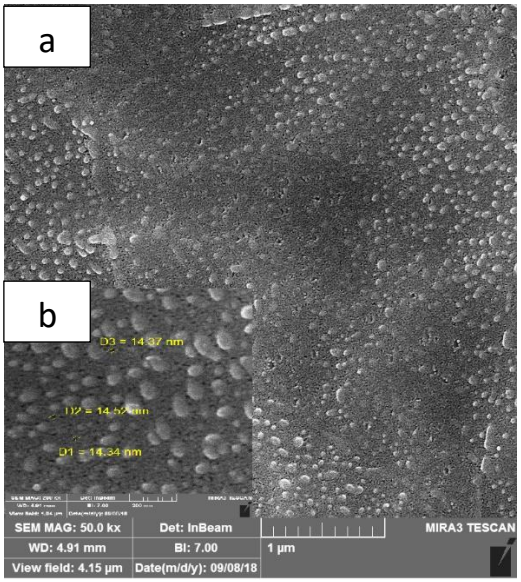

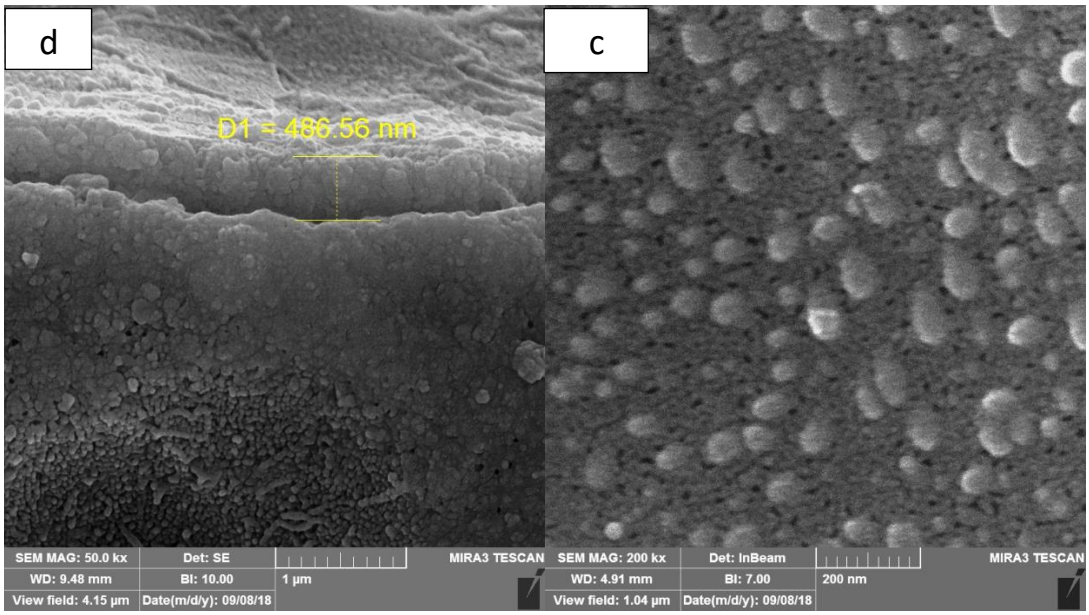

Fig. (3-22) Show SEM (a ,b ,c) top images and (d) cross- sectional , of NTs array and (f) EDX-spectrum in a DMSO electrolyte

Figure (3-22 a,b,c,d) shows NTs array grown at 20 V in a DMSO electrolyte in the absence of ultrasound the pores may appear clogged in such cases, although a complete clogging does not take place as this prevents the electrolyte species from reaching the bottom of the tubes thus terminating the anodization process. (3-22 f) shows a quantitative analysis of the EDX spectra. It is illustrated the presence of oxygen and titanium elements which can be taken as evidence of existence TiO_2 NTs

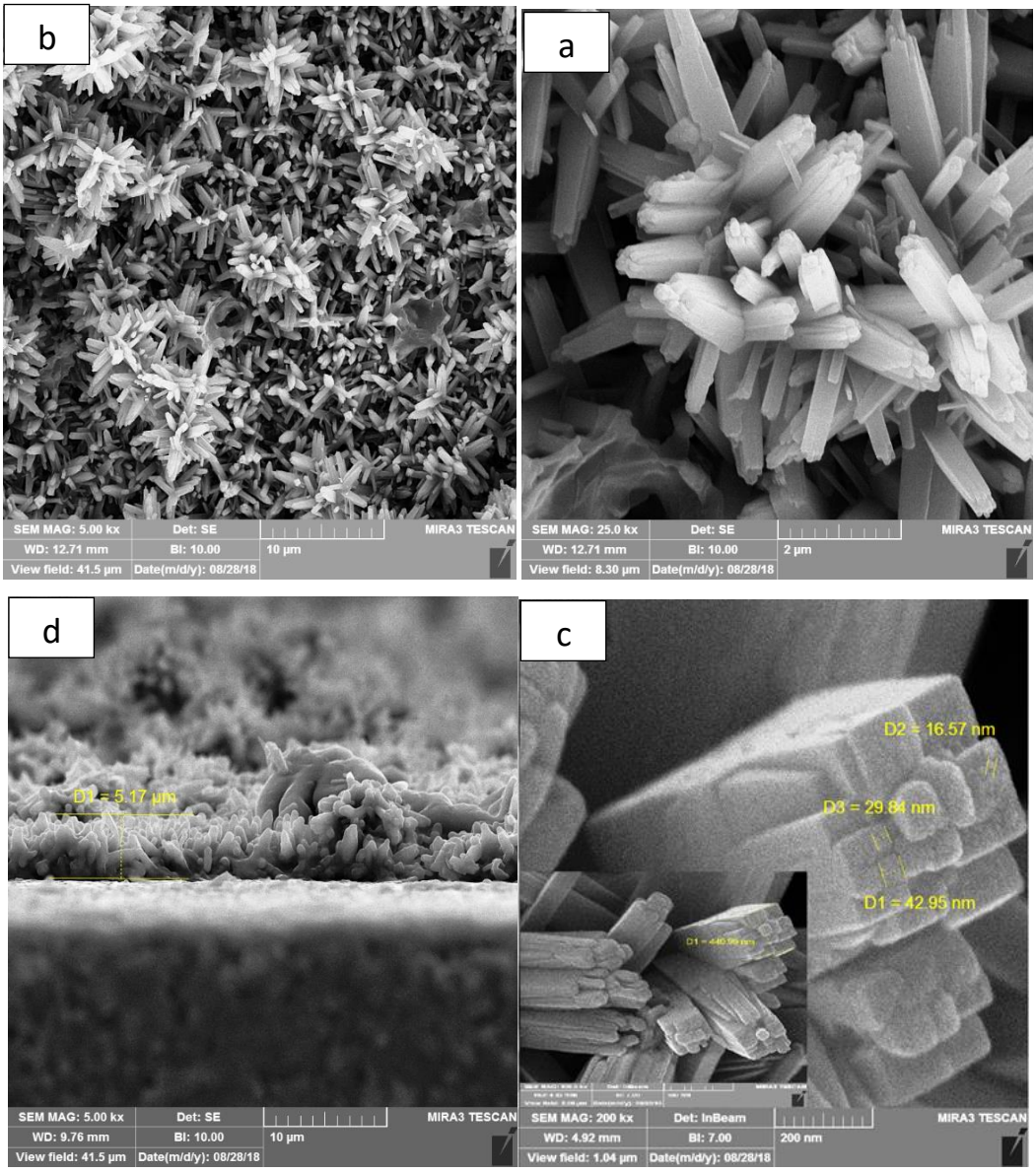
b
SEM MAG: 5.00 kx
Det: SE
MIRA3 TESCAN
WD: 12.71 mm
BI: 10.00
10 µm
View field: 41.5 µm
Date(m/d/y): 08/28/18
a
SEM MAG: 25.0 kx
Det: SE
MIRA3 TESCAN
WD: 12.71 mm
BI: 10.00
2 µm
View field: 8.30 µm
Date(m/d/y): 08/28/18
d
D1 = 5.17 µm
SEM MAG: 5.00 kx
Det: SE
MIRA3 TESCAN
WD: 9.76 mm
BI: 10.00
10 µm
View field: 41.5 µm
Date(m/d/y): 08/28/18
c
D2 = 16.57 nm
D3 = 29.84 nm
D1 = 42.95 nm
SEM MAG: 200 kx
Det: InBeam
MIRA3 TESCAN
WD: 4.92 mm
BI: 7.00
200 nm
View field: 1.04 µm
Date(m/d/y): 08/28/18

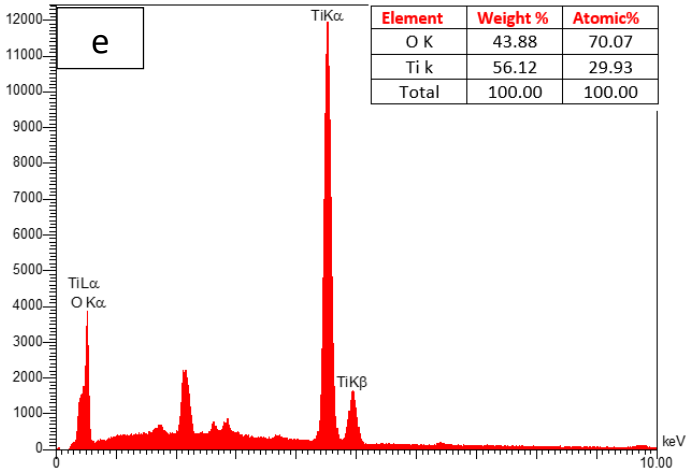

Element	Weight %	Atomic%
O K	43.88	70.07
Ti k	56.12	29.93
Total	100.00	100.00

Fig 3-23 Shows SEM images of TiO_2 nanowire (a ,b) Top morphology and (c , d) scale of diameter and (e) cross-section (f) EDX spectrum prepared in 3 hour

Figure (3-23 a,b,c,d) shows SEM images the top surface of the nanowire at different magnification forces .it has the high order and the nanowire arrays can be seen densely packed on the FTO glass substrate, as nanowire has tetragonal crystallographic levels and the side profile images show a nanowire arrangement vertically on the glass surface **[137]**, and the length of the nanowire is around 5.17µm. (3-23 e) shows a quantitative analysis of the EDX spectra. It is illustrated the presence of oxygen and titanium elements which can be taken as evidence of existence TiO_2 NWs.

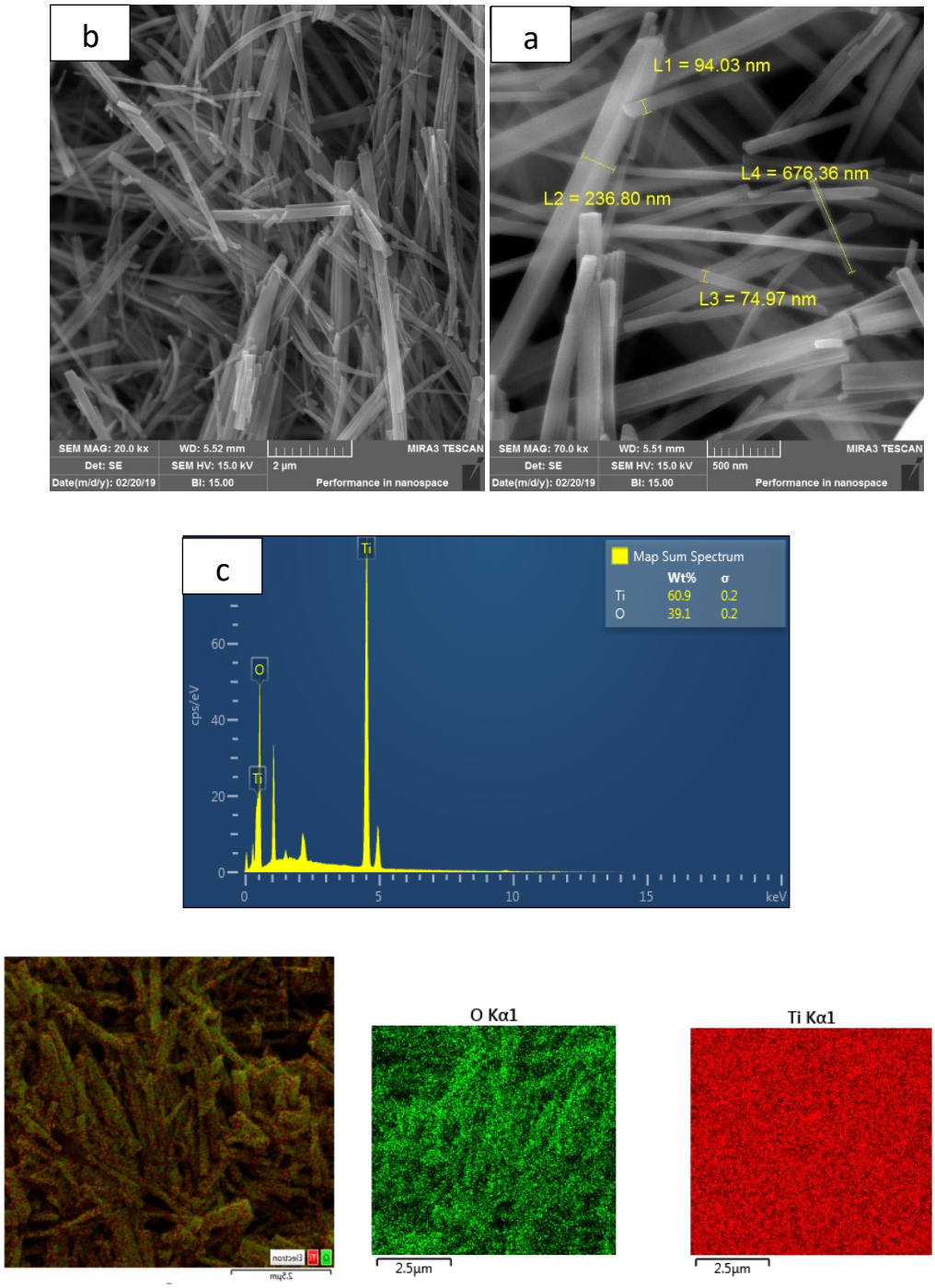

Fig 3-24 Shows SEM images of TiO_2 nanowire (a) Top morphology and (b) scale of diameter and (c) EDX spectrum prepared in 12 hour

Figure (3-24 a,b) represents the SEM images of TiO_2 nanowire with different magnification images the diameter ranging 74.97-94.03 nanometer and appearance of small amounts of particles caused by the high temperature

of the process calcination **[123]**. (3-24 c) shows a quantitative analysis of the EDX spectra. It is illustrated the presence of oxygen and titanium elements which can be taken as evidence of existence TiO_2 NWs.

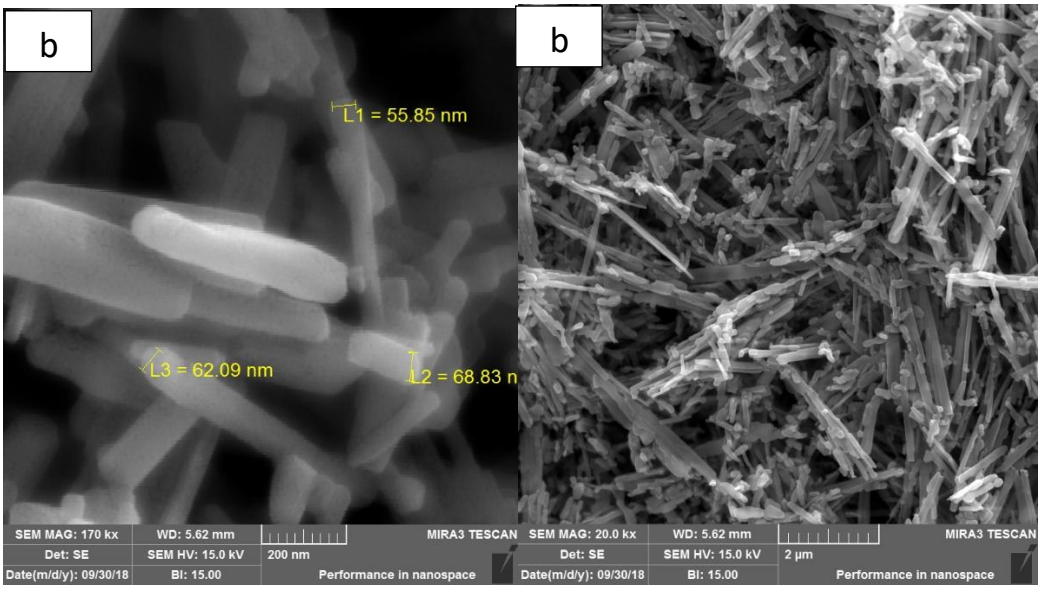

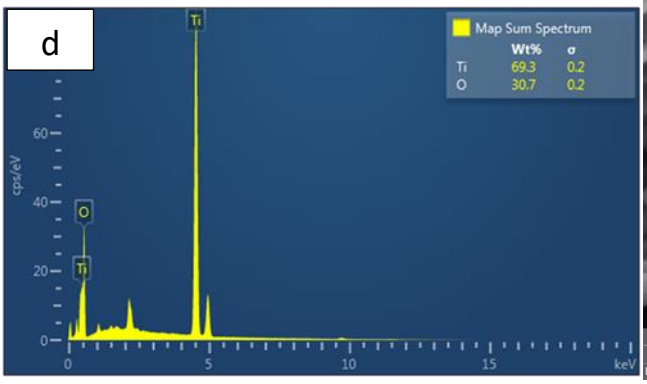

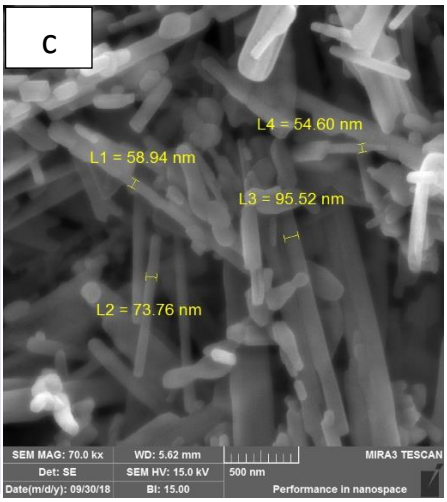

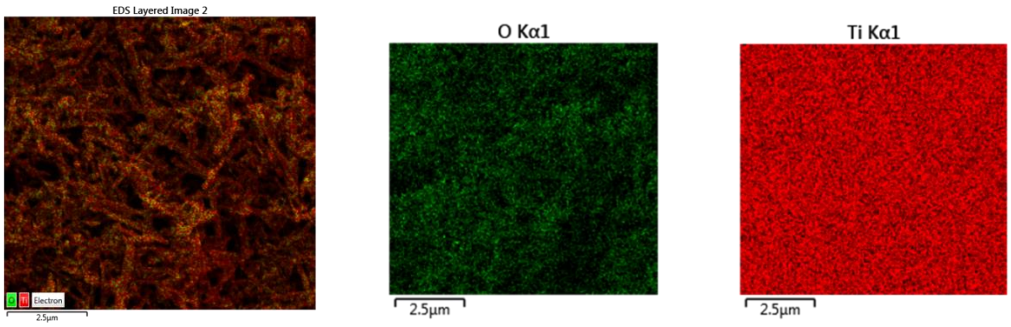

Fig 3-25 Shows SEM images of TiO_2 nanowire (a) Top morphology and (b,c) scale of diameter and (d) EDX spectrum prepared in 24 hour

Figure (3-25 a,b,c) shows SEM images with a wire-like structure, the diameter ranging 54-95 nanometer and appearance of small amounts of particles caused by the high temperature of the process calcination. (3-25 d) shows a quantitative analysis of the EDX spectra. It is illustrated the presence of oxygen and titanium elements which can be taken as evidence of existence TiO_2 NWs.

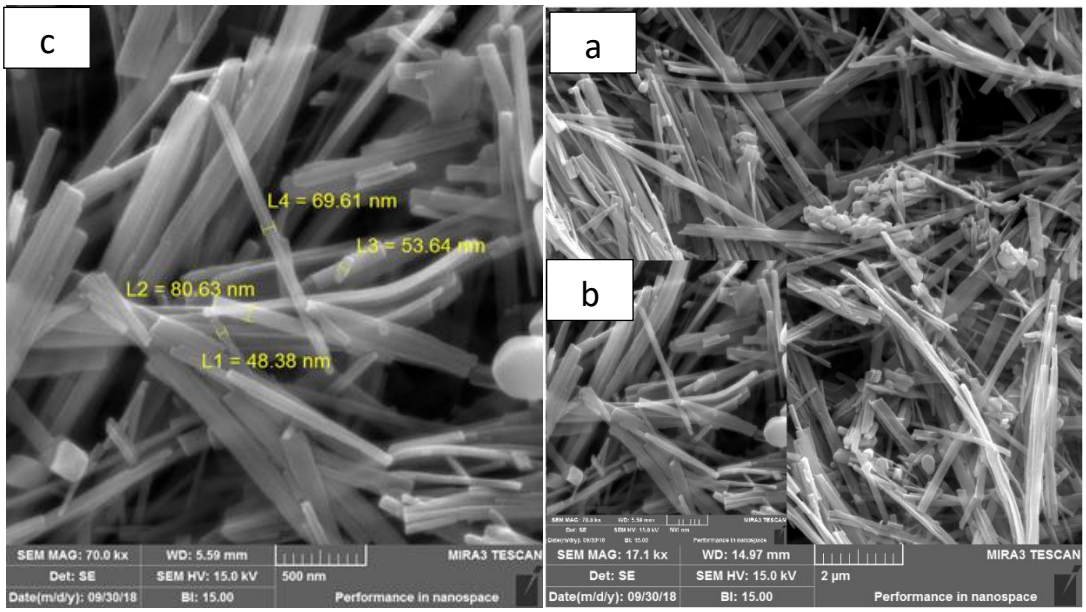

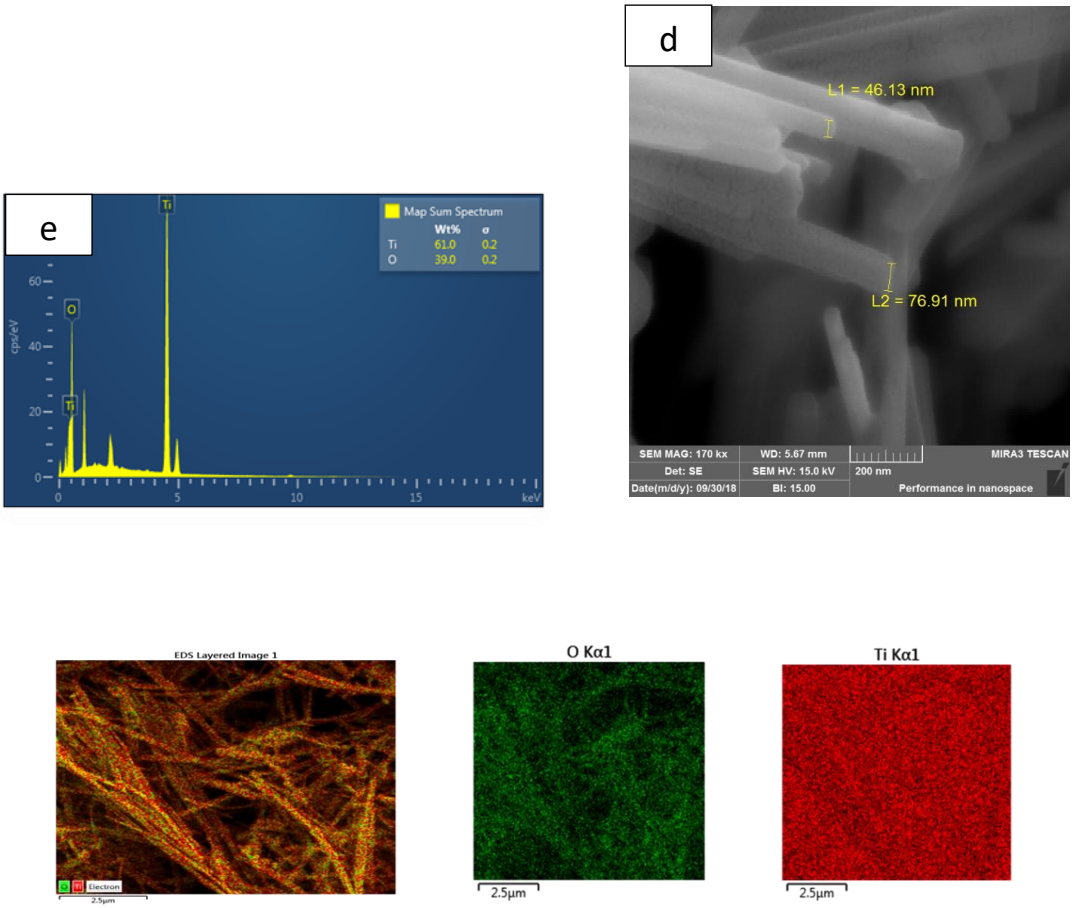

Fig 3-26 Shows micrographs of TiO_2 nanowire, consisting of well anatase nanowires and small amounts of particles (a) low magnification (b) high magnification (c,d) scale of diameter (e) EDX spectra and mapping prepared in 36 hour .

Figure (3-26 a,b,c)illustrates the typical SEM micrographs of the Nanowire. It is shown that the sample is composed of high-density Nanowire with small amounts of molecules, as well as characterized by a high abundance in quantity, some of the nanowire assembled to bundles in the solution or during the preparation SEM of the sample. The diameter and length of nanowires were about 48.38 – 80.63 nm and several µm. He reasons for the presence of small particles is due to the high temperature of the process calcination **[123]**. (3-26 e) shows a quantitative analysis of the EDX

spectra. It is illustrated the presence of oxygen and titanium elements which can be taken as evidence of existence TiO_2 NWs.

3-1-1-5 Surface Area Analysis BET (Brunauer-Emmett-Teller)

It is a common technique used to identify surface area and pore size by using isotherm adsorption - desorption and the distribution of pore size BJH (Barrett-Toyner-Halenda)

Figure 3-27 a The N_2 adsorption – desorption isotherms of the TiO_2 nanowire show III type and the hysteresis loop not present .The (BET) surface area of TiO_2 nanowire is 8.849 m^2/g , pore volume 2.0332 cm^3(STP) /g and the figure 3-27 b BJH pore diameter is 12.52 nm compared with TiO_2 P25 Degussa (surface area 56 m2/g , pore volume 0.250 cm^3(STP)/g and pore diameter 17.50 nm), pore size distribution with peak at 12.52 refers the presence of a mesoporous structure (2- 50 nm).

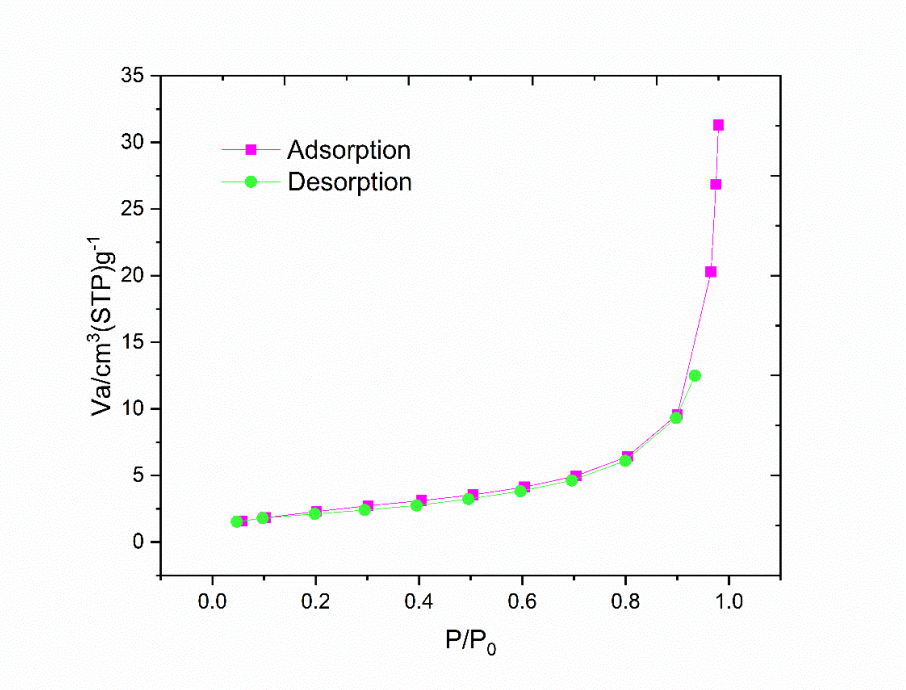

Fig. 3-27 a Isotherm adsorption-desorption nitrogen of $TiO_{2(1)}$ nanowire according to the BET method.

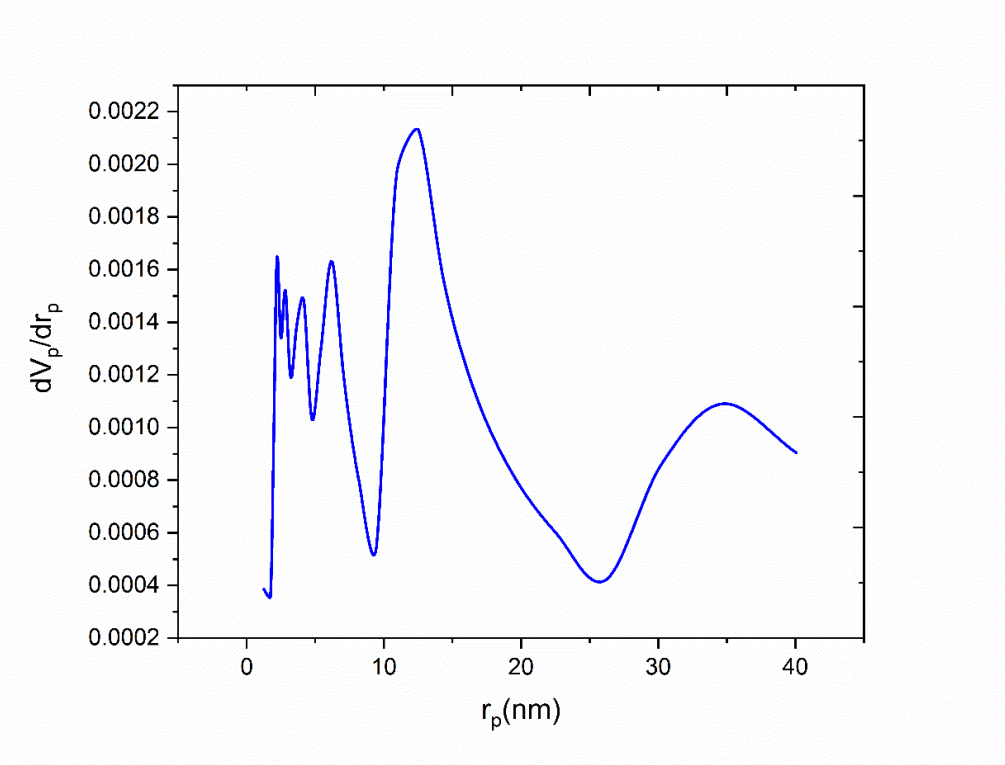

Fig.3-27 b Distribution of pore size of $TiO_{2(1)}$ nanowire according to the BJH method .

Figure 3-28 a The N_2 adsorption – desorption isotherms of the TiO_2 nanowire show III type and the hysteresis loop not present .The (BET) surface area of TiO_2 nanowire is 18.49 m^2/g , pore volume 1.70 cm^3(STP) /g and the figure 3-28 b BJH pore diameter is 9.02 nm compared with TiO_2 P25 Degussa (surface area 56 m^2/g , pore volume 0.250 cm^3(STP)/g and pore diameter 17.50 nm), pore size distribution with peak at 12.52 refers the presence of a mesoporous structure (2- 50 nm).

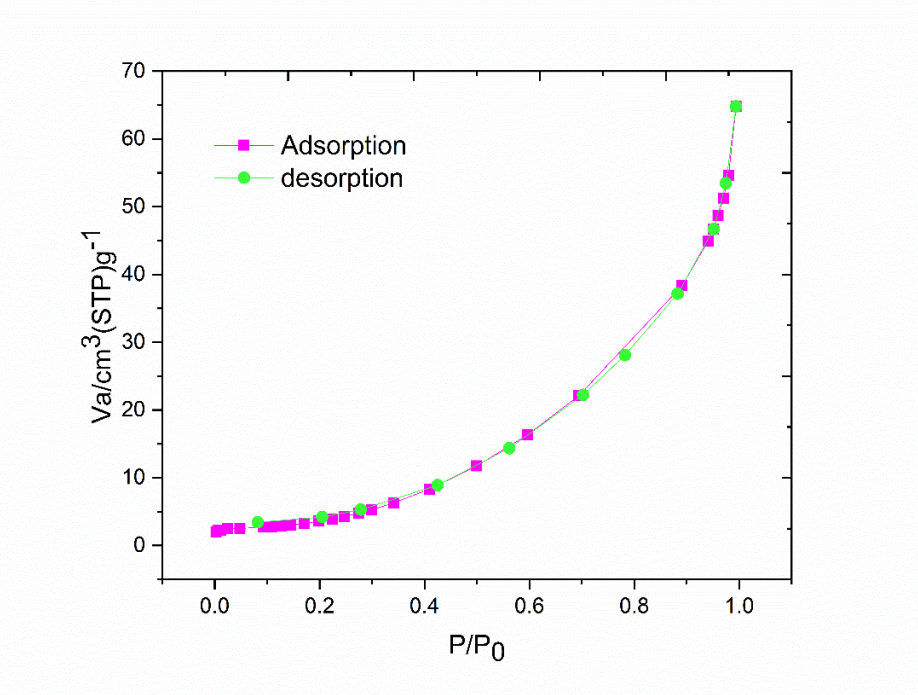

Fig. 3-28 a Isotherm adsorption-desorption nitrogen of $TiO_{2(2)}$ nanowire according to the BET method .

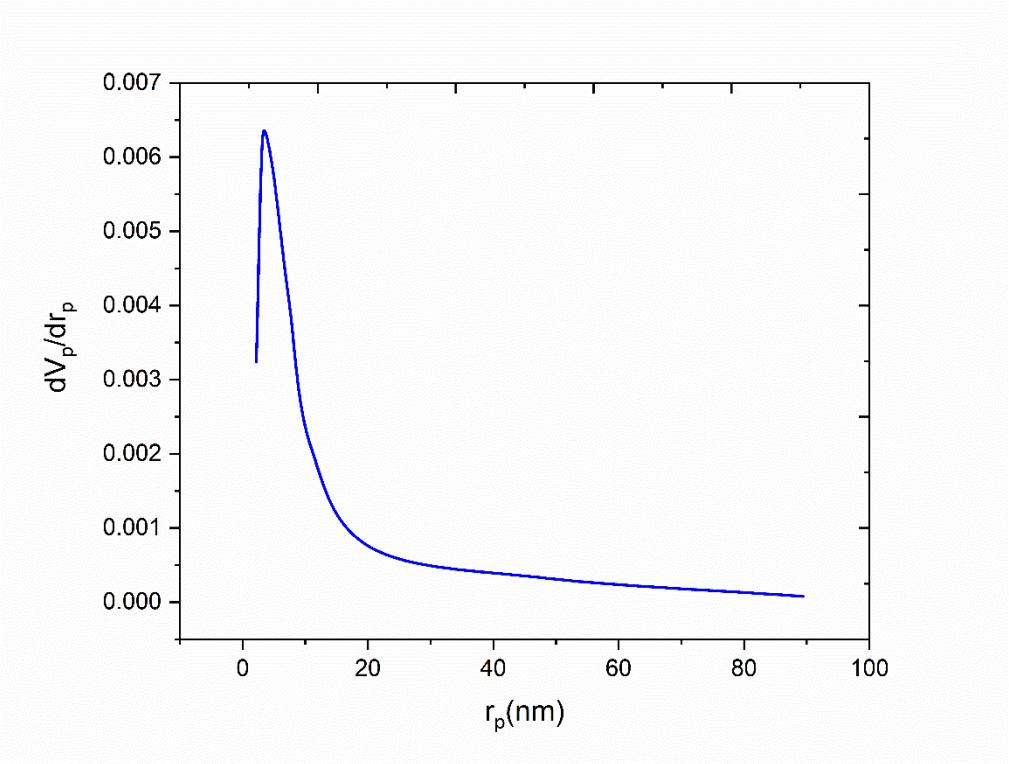

Fig.3-28 b Distribution of pore size of $TiO_{2(2)}$nanowire according to the BJH method .

Figure 3-29 a the N_2 adsorption – desorption isotherms of the TiO_2 nanowire shows III type and the hysteresis loop no present .The (BET) surface area of TiO_2 nanowire is 10.261 m^2/g , pore volume 2.3576 cm^3(STP) /g and the figure 3-29 b show BJH pore diameter is 12.52 nm compared with TiO_2 P25 Degussa (surface area 56 m^2/g , pore volume 0.250 cm^3(STP)/g and pore diameter 17.50 nm), pore size distribution with peak at 12.52 refers the presence of a mesoporous structure (2- 50 nm).

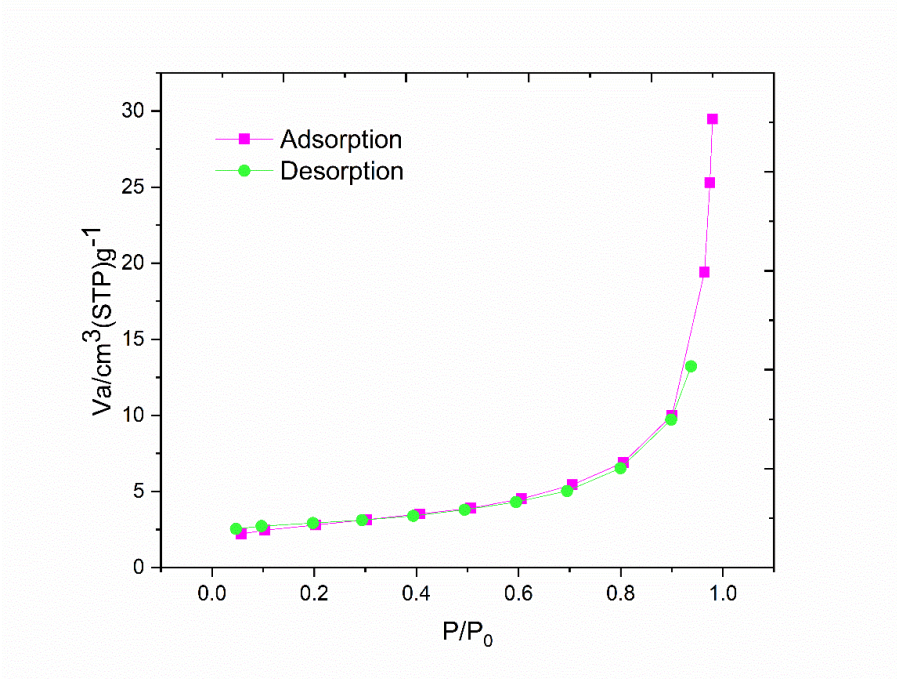

Fig. 3-29 a Isotherm adsorption-desorption nitrogen of $TiO_{2(3)}$ nanowire according to the BET method.

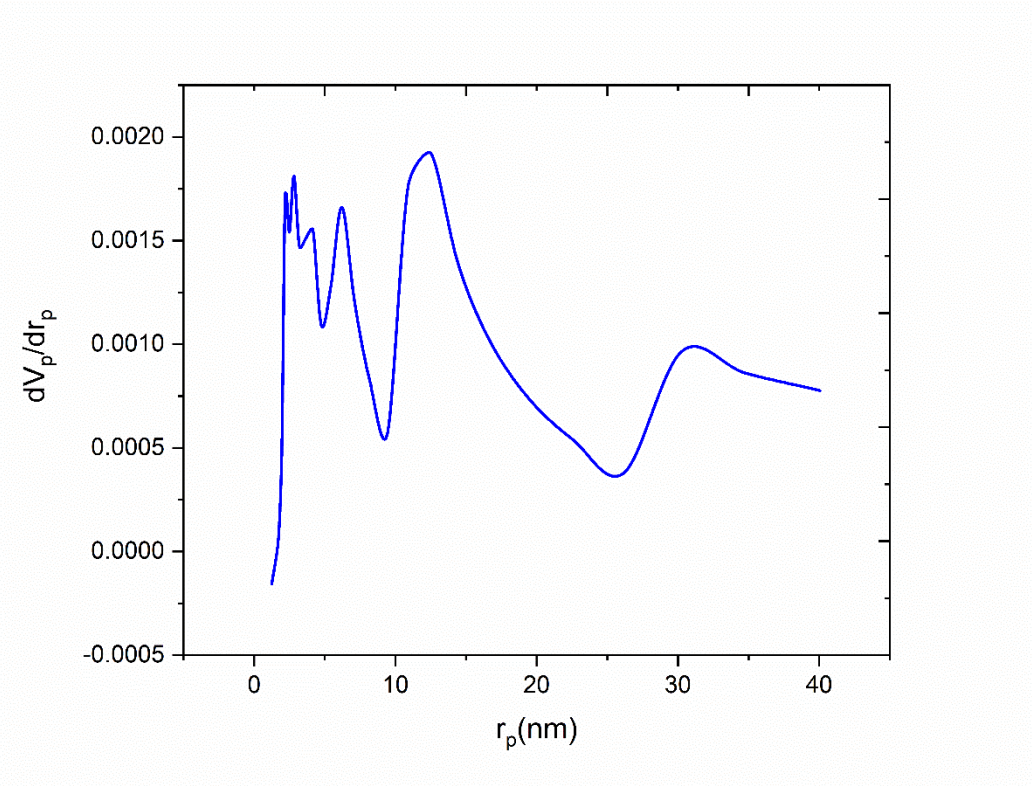

Fig. 3-29 b Distribution of pore size of $TiO_{2(3)}$nanowire according to the BJH method .

property	Sample (12h)	Sample (24)	Sample (36)
Surface area (m^2/g)	8.849	18.49	10.261
Pore volume (cm^3/g)	2.0332	1.70	2.3576
Pore diameter (nm)	12.52	9.02	12.52
Isotherm type	III	III	III
Type of pore	Meso-porous	Meso-porous	Meso-porous

3-1-1-6 Transmission electron microscopy (TEM)

Transmission electron microscope (TEM) is used to study the crystalline structure of the surface and the shape, size and distribution of crystals. The strength of the magnification showed that nanowire had a rough surface and tended to form packets of nanowire as shown in figure 3-30.

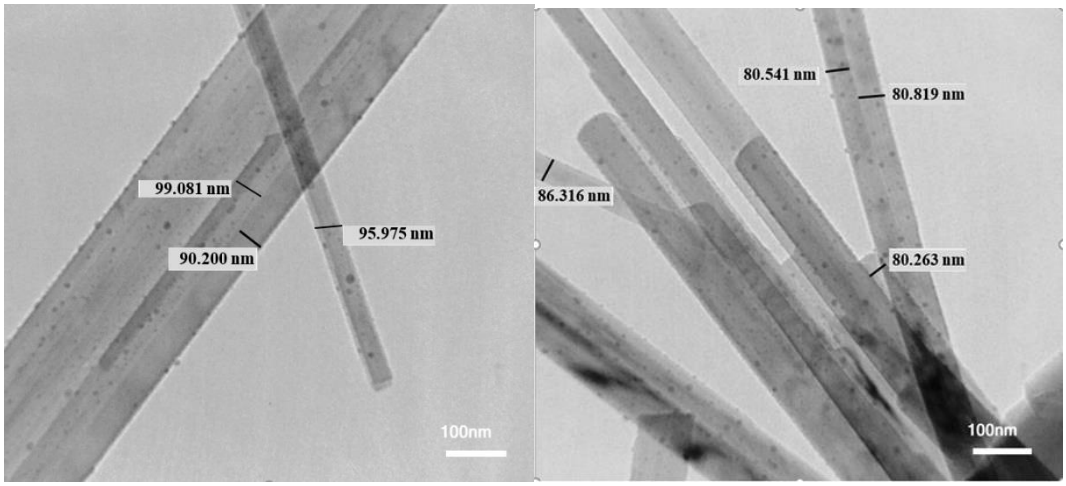

Fig. 3-30 TEM image of TiO_2 nanowire (obtained by the calcination at 700 ˚C for 1 hour) prepared in 12 hour.

Figure 3-31 TEM images appeared that the TiO_2 NWs have diameters in the range of 54.02 – 89.617 nm, and tend to form bundles. the NWs had length from hundreds of nanometers to several micrometers.

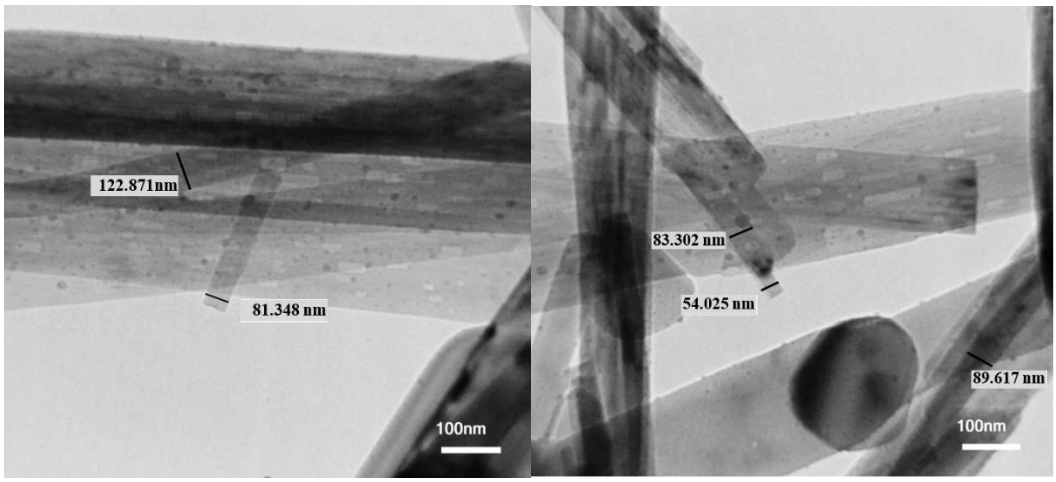

Fig. 3-31 TEM image of TiO2 nanowire (obtained by the calcination at 700˚C for 1 hour) prepared in 24 hour.

Where the nanowire was shown accurate picture by a transmission electron microscope. Nanowire also had smooth surface after calcination. It has few hundred nanometers and consists of anatase mono-crystalline or bundles of mono-crystalline as shown in figure 3-32.

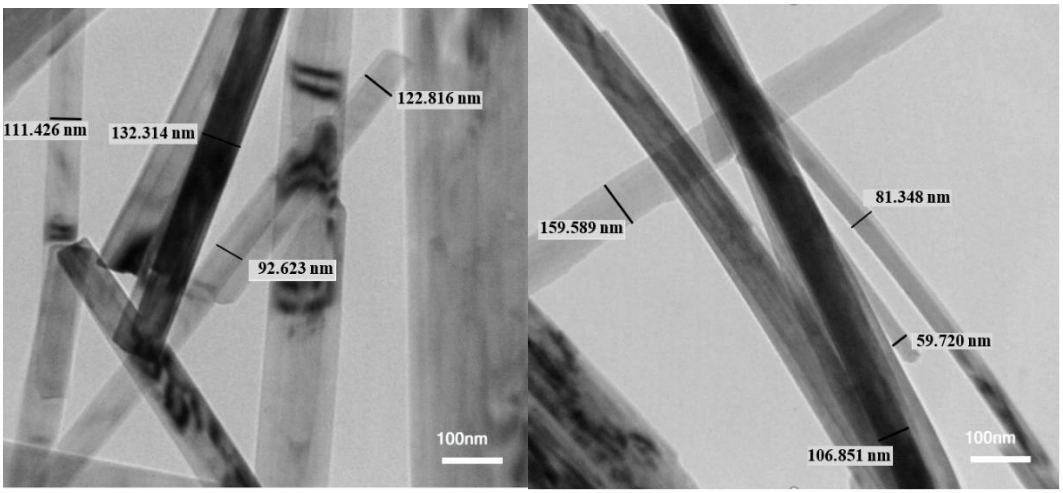

Fig.3-32 TEM micrographs of TiO_2 nanowire (obtained by the calcination at 700˚C for 1 hour) prepared in 36 hour.

3-1-1-7 *Atomic Force Microscopy (AFM)*

AFM is a commonly used technique, it is recognized the nature of the surface structure and the average thickness. AFM analysis gives the main factors in the description of surface topography, which include mean roughness (Ra) and the root mean square roughness (Rq), The third factor is the surface Skewness and is symbolized by the symbol (Rsk). It is used to measure the symmetry of the profile around an average line, where it has values equal to zero, ie, the distribution is identical to the heights and dips. The negative value indicates the dips more than the heights and the positive value indicate the higher than the dips and asymmetrical, fourth factor is surface Kurtosis (Rku) It has three values. If it is 3, it means the distribution of the data according to a Gaussian curve. It is called Mesokurtic. If it is less than 3, the surface is plane and is called Platykurtic but If it is larger than 3 the surface has more peaks than dips, it is called leptokurtic**[135]** A diagram of surfaces with positive and negative R_{sk} values, as well as with R_{Ku} values lower and higher than 3 is displayed in bellow Figure

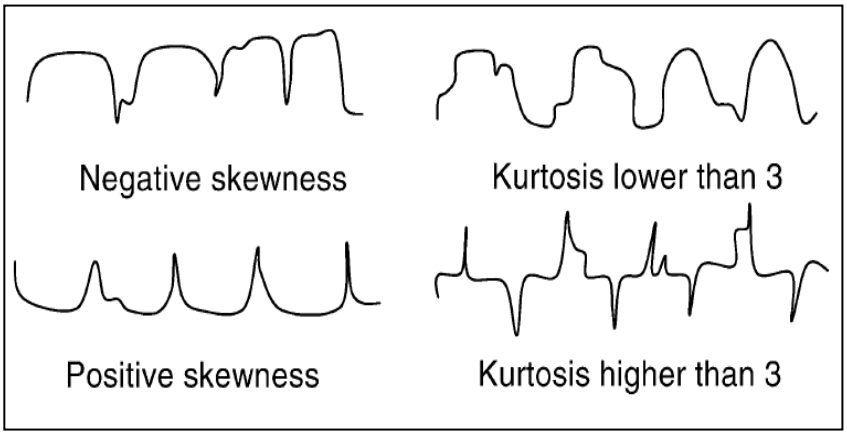

Figure 3-33: Differences in shape and surface nature at different values of surface Skewness (R_{sk}), Kurtosis (R_{ku})

Table3-11: The statistical roughness coefficients of prepared samples (A, C, E,) for TiO_2 $NTs_{(1,2,3)}$ in the absence of ultrasound ,(B,D,F) for TiO_2 $NTs_{(1,2,3)}$ in the presence of ultrasound and (G, H, I) for TiO_2 nanowires (12,24 and 36) h

Amplitude Factors	R_a (nm	R_q	R_{sk}	R_{ku}	Vertical distance	Thickness (nm)
A	4.83	5.61	-0.311	1.92	2.10	18.53
B	5.8	6.68	-0.00703	1.79	1.51	22.78
C	1.91	2.36	-0.00325	2.36	0.98	10.83
D	2.63	3.25	0.186	2.65	3.18	15.51
E	5.14	5.94	0.000588	1.8	0.52	20.57
F	4.52	5.21	0.00134	1.79	3.26	17.86
G	2.06	2.43	-0.0962	1.99	0.84	10.12
H	34.2	39.1	0.0436	1.75	104.08	128.22
I	15.9	18.3	7.95e-005	1.8	21.28	63.08

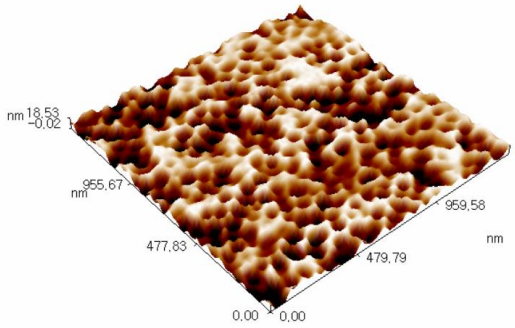

A (3D)

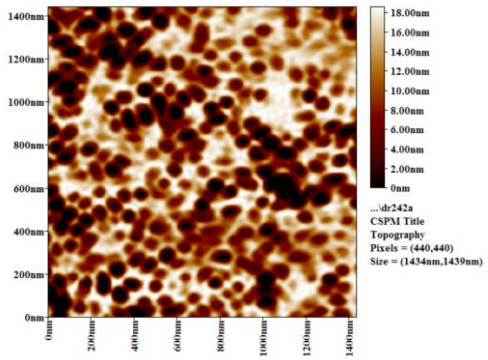

A (2D)

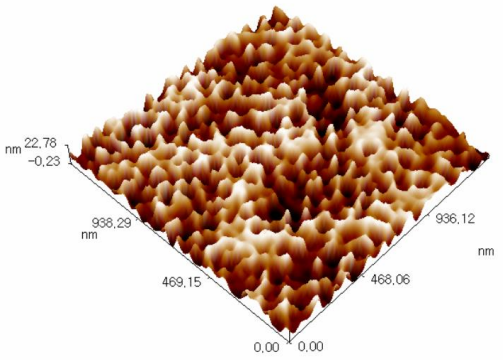

B (3D)

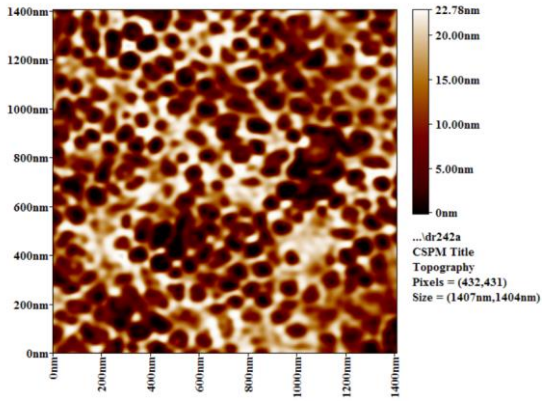

B (2D)

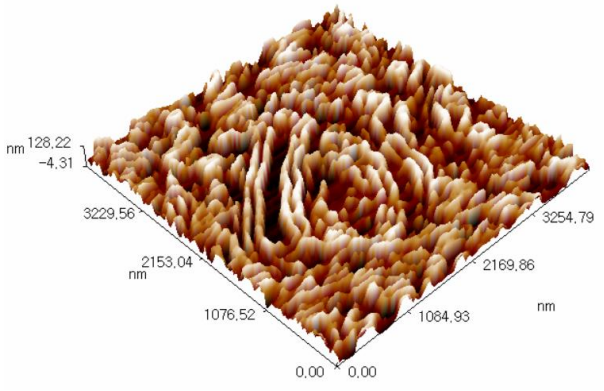

C (3D)

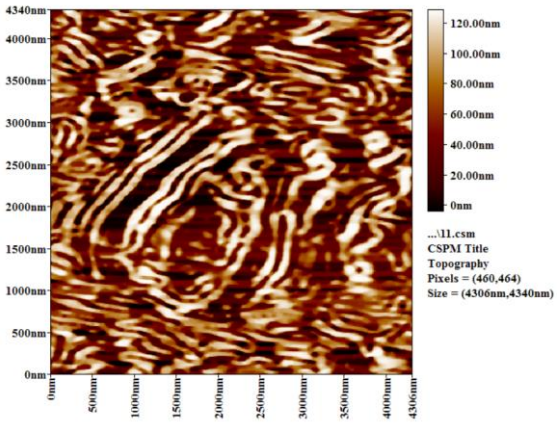

C (2D)

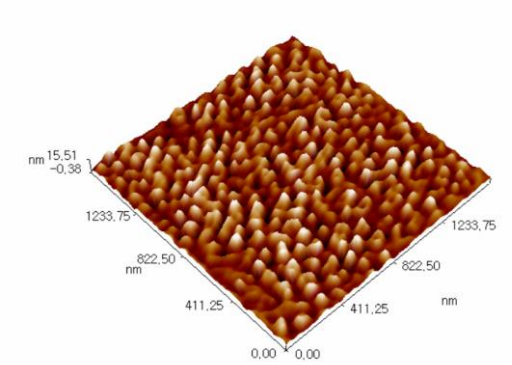

D(3D)

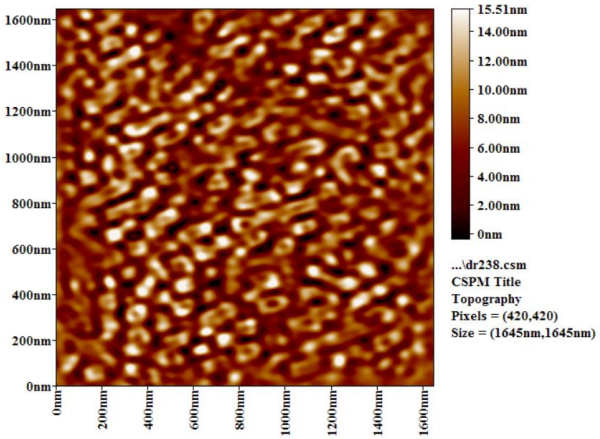

D (2D)

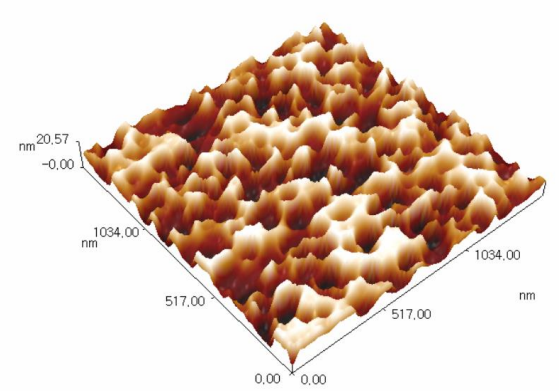

E (3D)

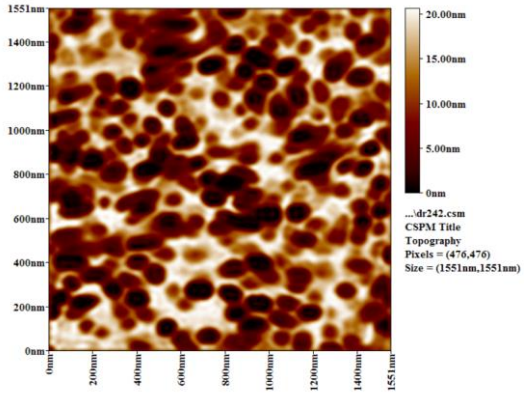

E (2D)

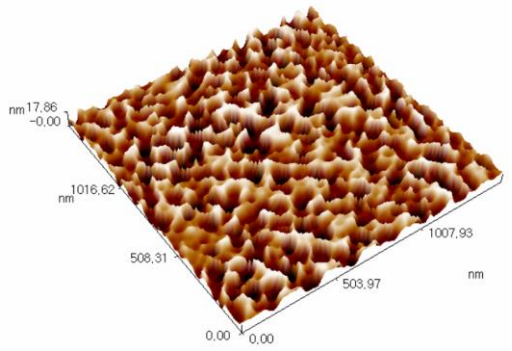

F (3D)

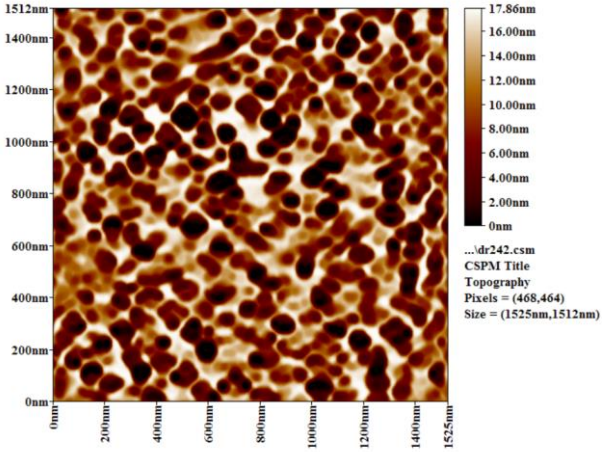

F (2D)

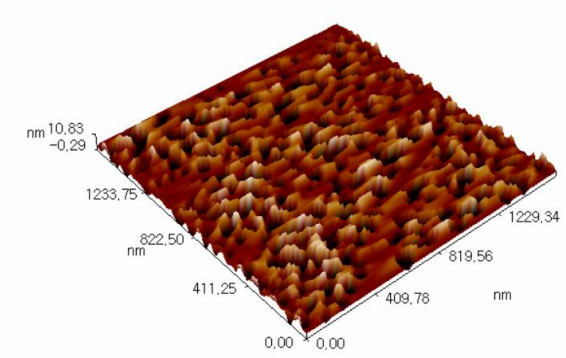

G (3D)

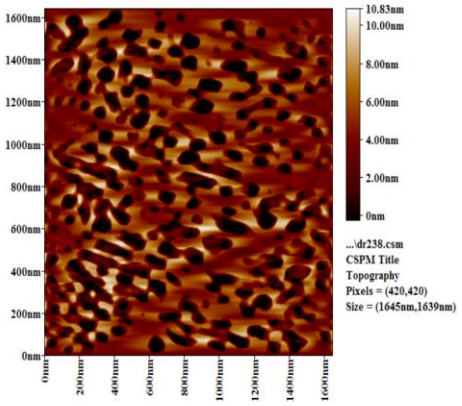

G (2D)

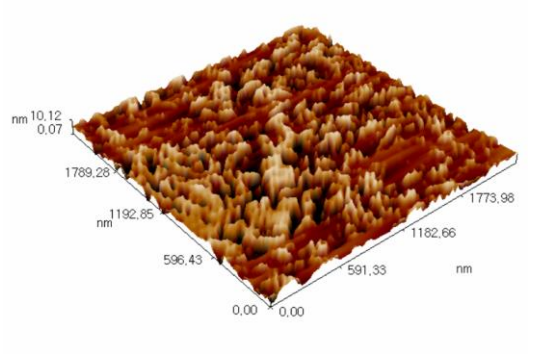

H (3D)

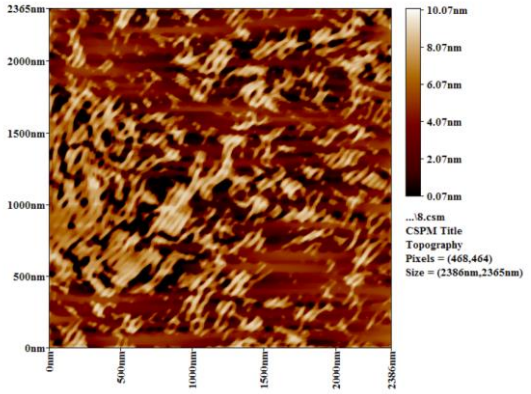

H (2D)

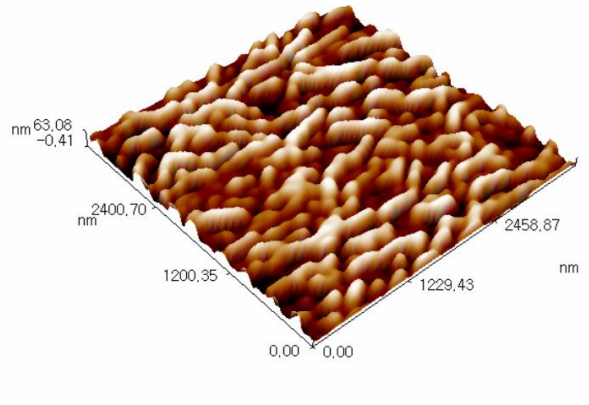

I (3D)

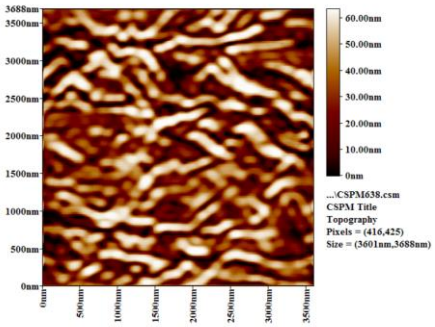

I (2D)

Figures 3-34 appear the two- and three-dimensions AFM images (A, C, E,) for TiO_2 $NTs_{(1,2,3)}$ in the absence of ultrasound , ,(B,D,F) for TiO_2 $NTs_{(1,2,3)}$ in the presence of ultrasound and (G, H, I) for TiO_2 nanowires (12,24 and 36) h

3-1-1-8 Influence of applied potential with change of current density

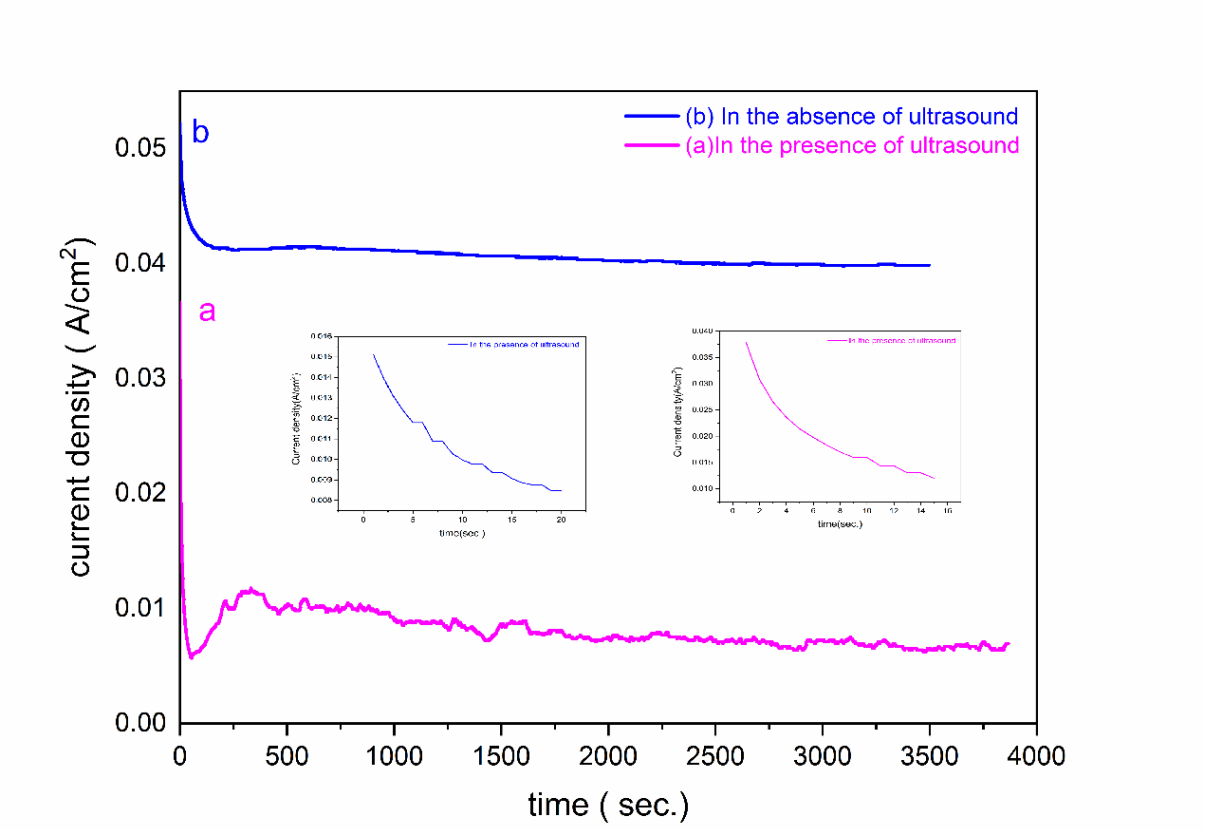

Figures 3-35 current density – time curve for anodized Ti at 20 v for 30min (a) in the presence of ultrasound (b) in the absence of ultrasound in an electrolyte solution (ethylene glycol) containing both NH_4F and H_2O.

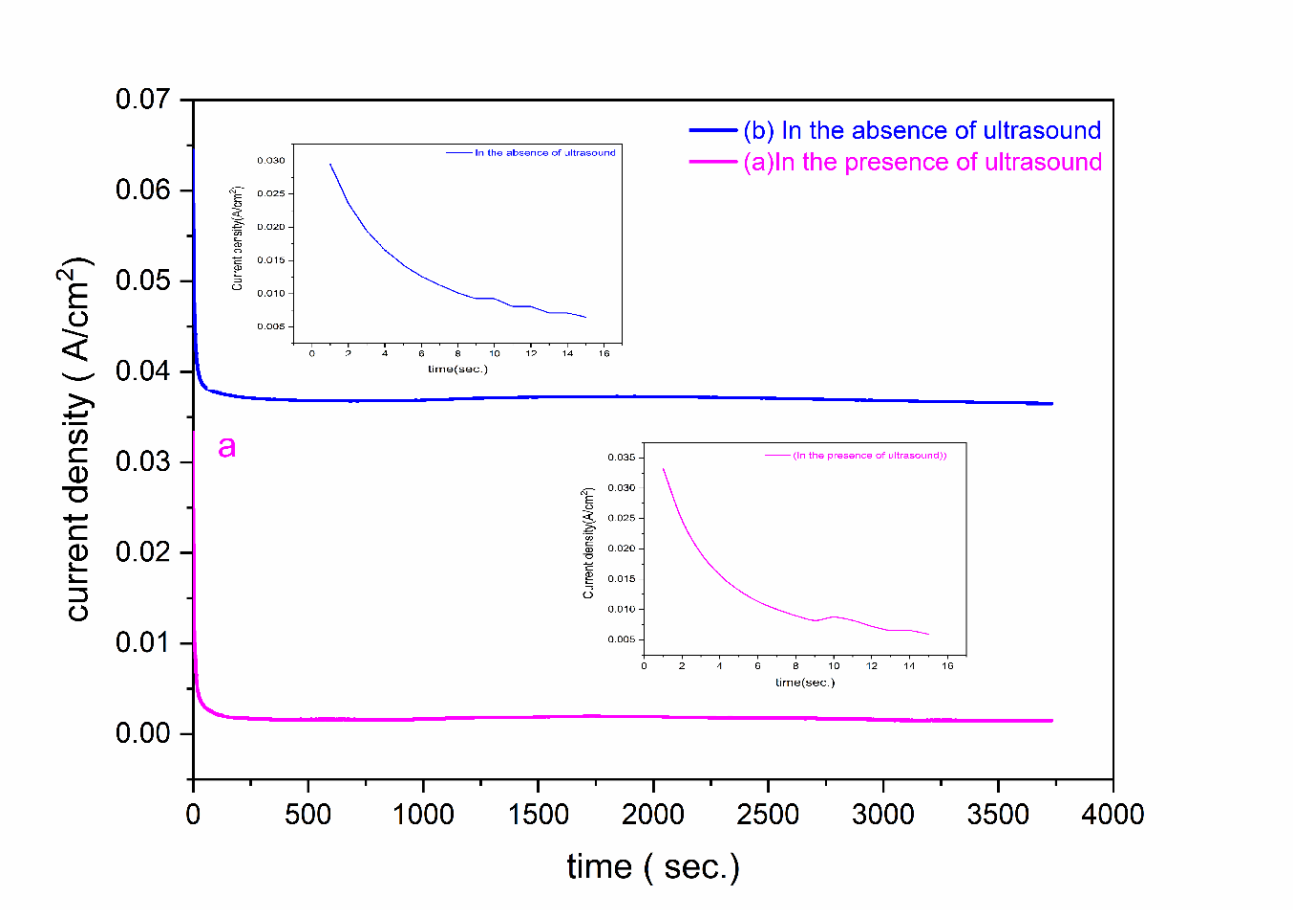

Figures 3-36 current density – time curve for anodized Ti at 20 v for 30min (a) in the presence of ultrasound (b) in the absence of ultrasound in water-based electrolyte containing both Na_2SO_4 and NH_4F

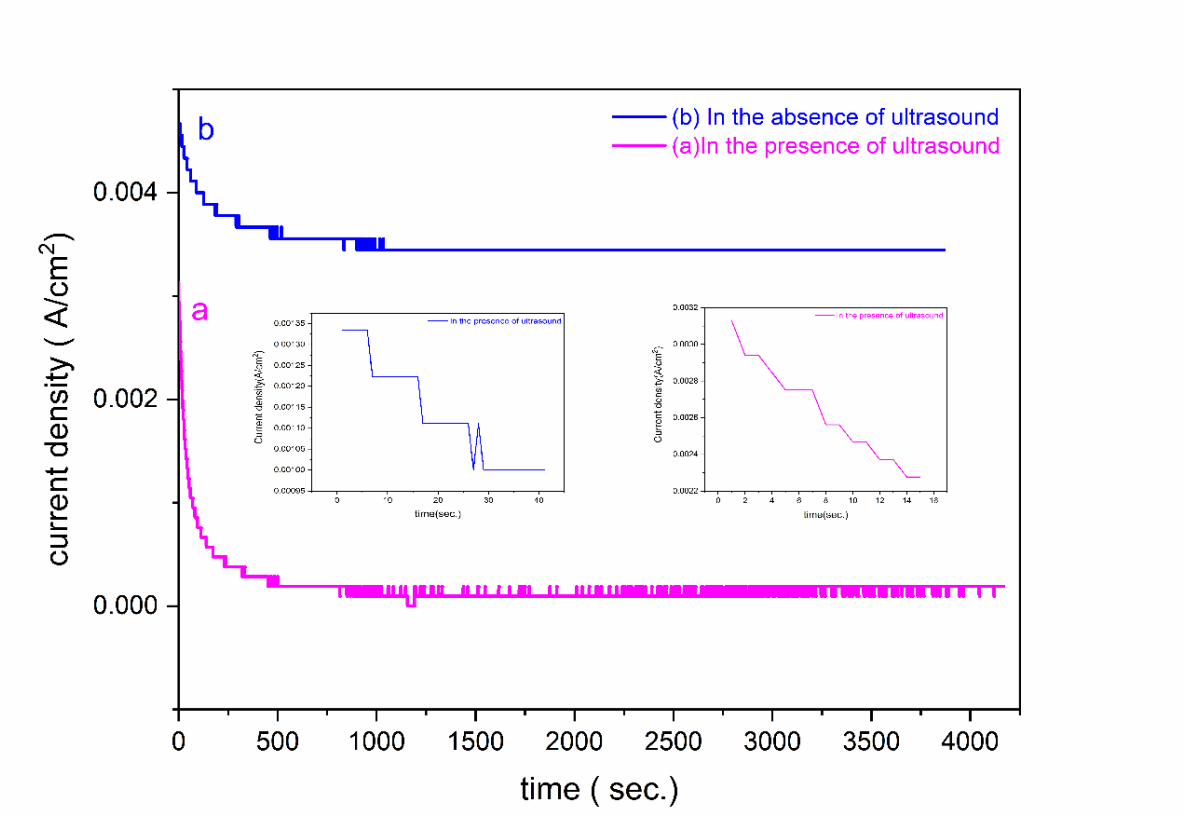

Figures 3-37 current density – time curve for anodized Ti at 20 v for 30min (a) in the presence of ultrasound (b) in the absence of ultrasound in lactic acid-based electrolyte containing o.15 wt NH_4F and 5 vol H_2O.

Figure 3-35 **(** in an electrolyte solution (ethylene glycol) containing both NH_4F and H_2O in the presence and absence of ultrasound) 3-36(in water-based electrolyte containing both Na_2SO_4 and NH_4F in the presence and absence of ultrasound) and 3-37 (in lactic acid-based electrolyte containing o.15 wt NH_4F and 5 vol H_2O) showed three different cases of the porous oxide layer where at the beginning of the anodizing process in the presence of ultrasound , a rapid decrease in current intensity to the lowest value due to the high resistance to the layer of oxide and the movement of ions such as (O^{-2},OH^{-},Ti^{+4} and F^{-1}) during the high resistance barrier layer necessary in order to maintain the process of oxidation, the presence of fluorine ions is caused the drilling of the oxide layer(the first case) and suddenly rises the current to the maximum value that leads to growth of porosity and will cause a decrease in resistance layer barrier (the second case) and when the

current reach the steady state that means formation the titanium dioxide nanotube (three case) classical interpretation due to the speed of oxide formation at the interface of the metal /oxide equivalent to the speed of decay at oxide / electrolyte interface **[138]**. It is observed that increases the fluoride concentration caused increase of the total charge density**[139]**

The formation mechanism of TiO_2 NTs

$$Ti \rightarrow Ti^{+4} + 4e^- \quad \ldots\ldots\ldots(1)$$

$$Ti^{+4} + 4OH^- \rightarrow Ti(OH)_4 \quad \ldots\ldots\ldots(2)$$

$$Ti^{+4} + 2O^{-2} \rightarrow TiO_2 \quad \ldots\ldots\ldots(2)b$$

$$Ti(OH)_4 \rightarrow TiO_2 + 2H_2O \quad \ldots\ldots\ldots(3)$$

$$TiO_2 + 6\,F^- + 4\,H^+ \rightarrow [TiF_6]^{-2} + H_2O \quad \ldots\ldots\ldots\ldots(4)$$

$$Ti(OH)_4 + 6\,F^- \rightarrow [TiF_6]^{-2} + 4OH^- \quad \ldots\ldots\ldots\ldots(5)$$

$$Ti^{+4} + 6\,F^- \rightarrow [TiF_6]^{-2} \quad \ldots\ldots\ldots\ldots(6)$$

3-2 Performance of DSSCs

The measurement of solar cell variables depended on the intensity of the current and voltage curve (J-V) , examples incident photon to current conversion efficiency (IPCE) These variables were used to verify the performance of the solar cell (DSSCs) in addition to short circuit photocurrent density(J_{sc}) , open circuit photo voltage (V_{oc}) and Fill factor (FF) ,all these variables can be determined by (J-V) While J_{sc} variable depends on the amount and chemical composition of the dye as well as the electrochemical properties of the thin films used as photoelectrodes for the DSSCs and electrolyte **[140]** .

The open circuit voltage represents the difference between the Fermi level of the semiconductor thin film (photoelectrode) and the oxidation and reduction potential in the medium used as electrolyte, where the variable is affected by the recombination and absorption velocity of the photo sensor **[47]**. while the filling factor is defined by the following equation

$$FF = (I_{max} \times V_{max})/(J_{sc} \times V_{oc}) \qquad \ldots\ldots\ldots (3-3)$$

I_{max} and V_{max} represent the voltage and the photocurrent density which can be obtained from the external maximum energy of the DSSCs whereas the fill factor has to do with the resistance of the device (DSSCs) either IPCE is used to describe the efficiency of converting light into an electric current at a particular wavelength.

The important factor in the performance of the DSSCs conversion efficiency of the total solar energy into electric energy that can be described by the following equation:

$$\eta = J_{sc} \times V_{oc} \times FF / P_{in} \qquad \ldots\ldots\ldots (4-3)$$

P_{in} : represents incident photo intensity **[141]**.

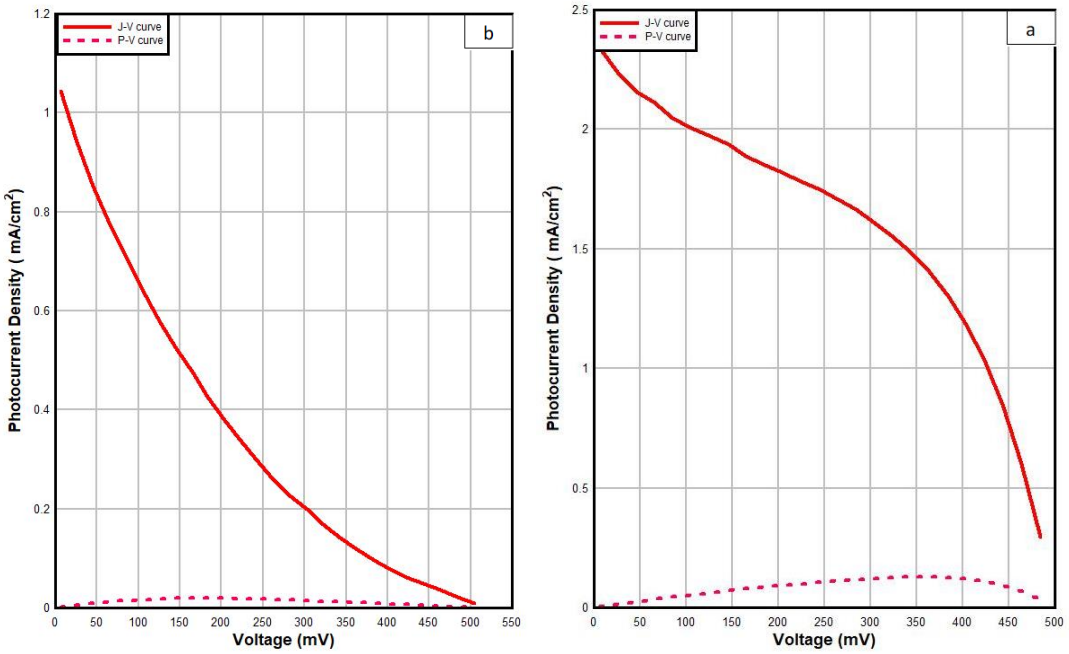

Figure 3-38: photocurrent-voltage curve of TiO_2 nanotube in an electrolyte solution (ethylene glycol) containing both NH_4F and H_2O the presence of ultrasound (a) and in the absence of ultrasound (b)

Figure 3-38 illustrates the electric parameters of the DSSC its good conversion efficiency in the presence of ultrasound if compared with the synthesis it in without ultrasound and use the graphene nanoplatelets as the counter electrode. The lower values of the short circuit current are related to the higher resistance of FTO glass substrate that coated by graphene nanoplatelets (counter electrode) as shown from the values of series resistance in Table 3-12 as well the nature of nanotubes to adsorb the dye molecules **[135, 142]**. the photocurrent-voltage parameters such as open circuit voltage (V_{oc}), short circuit current density (J_{sc}), Voltage at max power point (V_{mpp}), current at max power point (I_{mpp}), fill factor (FF) and cell conversion efficiency (η) as well series resistance (R_s)= and shunt resistance are estimated from the J-V curves a tabulated in Table 3-12 .

Table3-12.: photocurrent – voltage parameters of dye-sensitized NT solar cell.

DSSC's	V_{oc} / V	J_{sc} / mA/cm^2	V_{mpp} / V	I_{mp} / mA	FF	η	R_s / Ω	R_{sh} / Ω
TNT's in the presence of ultrasound effect	0.500	2.336	0.363	1.404	0.436	0.637	218.3220	3424.689
TNT's in the absence of ultrasound effect	0.518	1.040	0.164	0.119	0.144	0.097	5589.415	7690.799

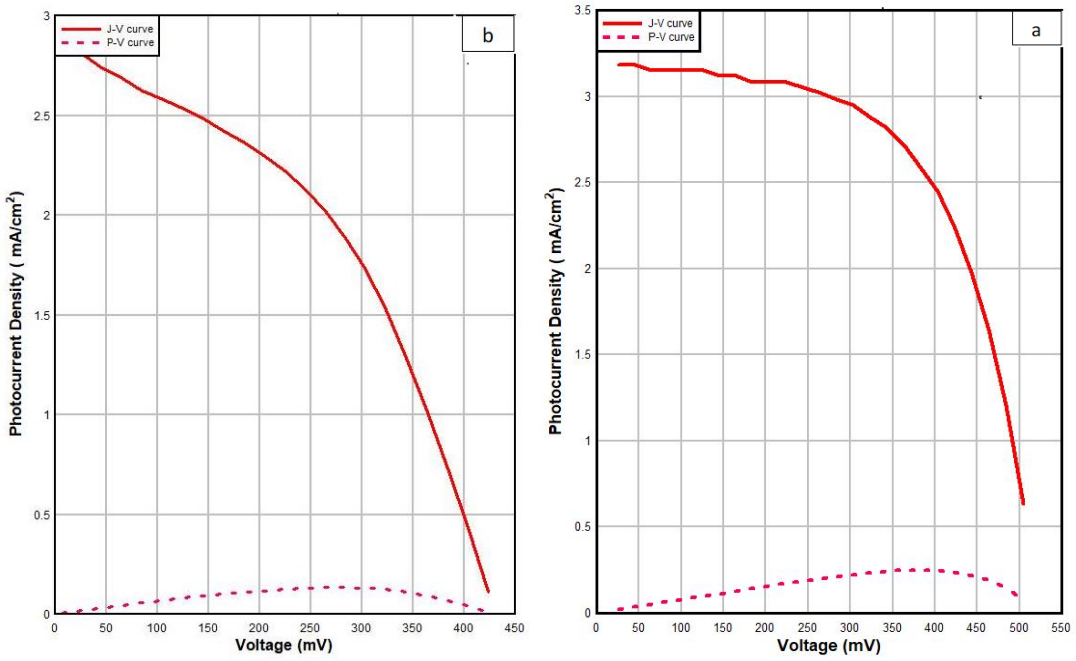

Figure 3-39 : photocurrent-voltage curve of TiO_2 nanotube in water-based electrolyte containing both Na_2SO_4 and NH_4F in the presence of ultrasound (a) and in the absence of ultrasound (b)

Figure 3-39 illustrates the electric parameters of the DSSC its good conversion efficiency in the presence of ultrasound if compared with the

synthesis it in without ultrasound and use the graphene nanoplatelets as the counter electrode.

the photocurrent-voltage parameters such as open circuit voltage (V_{oc}), short circuit current density (J_{sc}), Voltage at max power point (V_{mpp}), current at max power point (I_{mpp}), fill factor (FF) and cell conversion efficiency (η) as well series resistance (R_s)= and shunt resistance are estimated from the J-V curves a tabulated in Table3-13.

Table3-13.: photocurrent – voltage parameters of dye-sensitized NT solar cell.

DSSC's	V_{oc} / V	J_{sc} / mA/cm^2	V_{mpp} / V	I_{mp} / mA	FF	η	R_s / Ω	R_{sh} / Ω
TNT's in the presence of ultrasound effect	0.522	3.148	0.384	2.580	0.603	1.238	114.234	2544.229
TNT's in the absence of ultrasound effect	0.429	2.896	0.283	1.884	0.429	0.666	223.671	2763.372

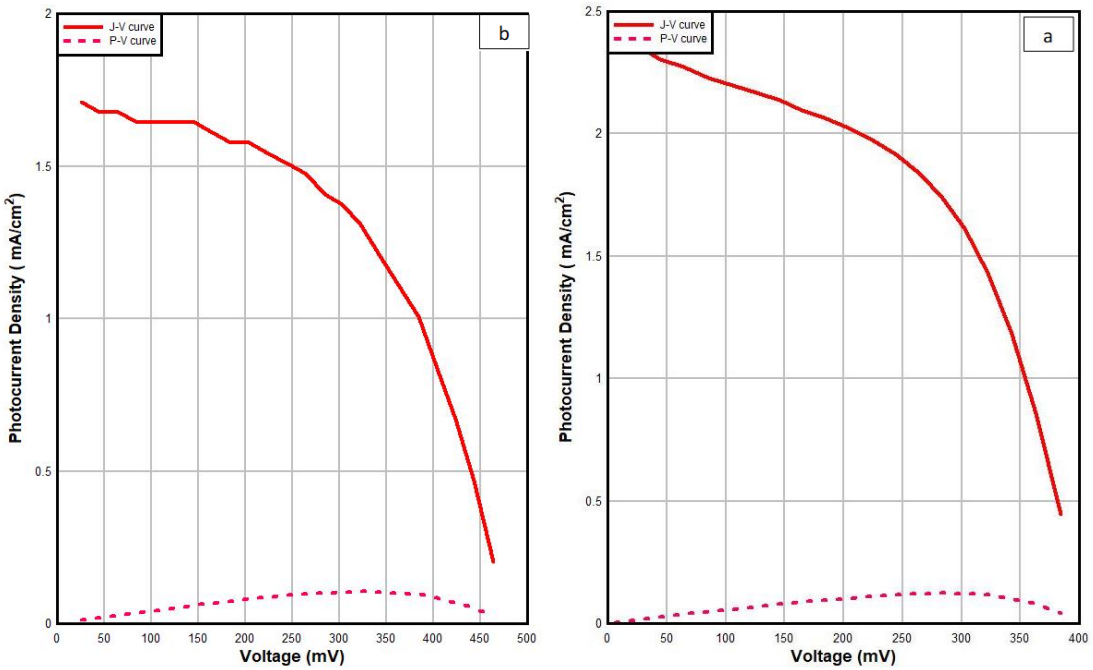

Figure 3-40: photocurrent-voltage curve of TiO_2 nanotube in lactic acid-based electrolyte containing o.15 wt NH_4F and 5 vol H_2O in the presence of ultrasound (a) and in the absence of ultrasound (b)

Figure 3-40 show the electric parameters of the DSSC its good conversion efficiency in the presence of ultrasound if compared with the synthesis it in without ultrasound and use the graphene nanoplatelets as the counter electrode.

the photocurrent-voltage parameters such as open circuit voltage (V_{oc}), short circuit current density (J_{sc}), Voltage at max power point (V_{mpp}), current at max power point (I_{mpp}), fill factor (FF) and cell conversion efficiency (η) as well series resistance (R_s)= and shunt resistance are estimated from the J-V curves a tabulated in Table 3-14.

Table3-14.: photocurrent – voltage parameters of dye-sensitized NT solar cell.

DSSC's	V_{oc} / V	J_{sc} / mA/cm^2	V_{mpp} / V	I_{mp} / mA	FF	η	R_s / Ω	R_{sh} / Ω
TNT's in the presence of ultrasound effect	0.402	2.416	0.283	1.740	0.507	0.615	163.075	3310.982
TNT's in the absence of ultrasound effect	0.477	1.688	0.322	1.308	0.523	0.526	272.620	4739.313

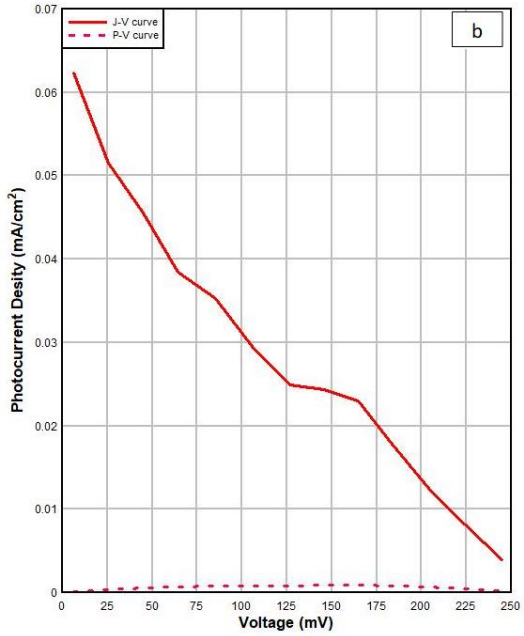

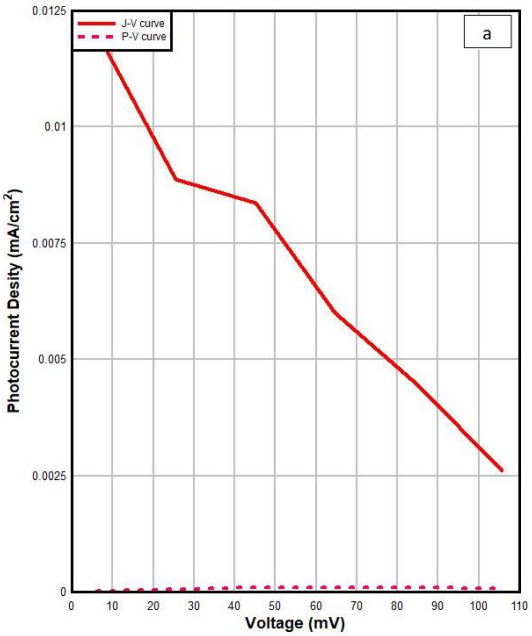

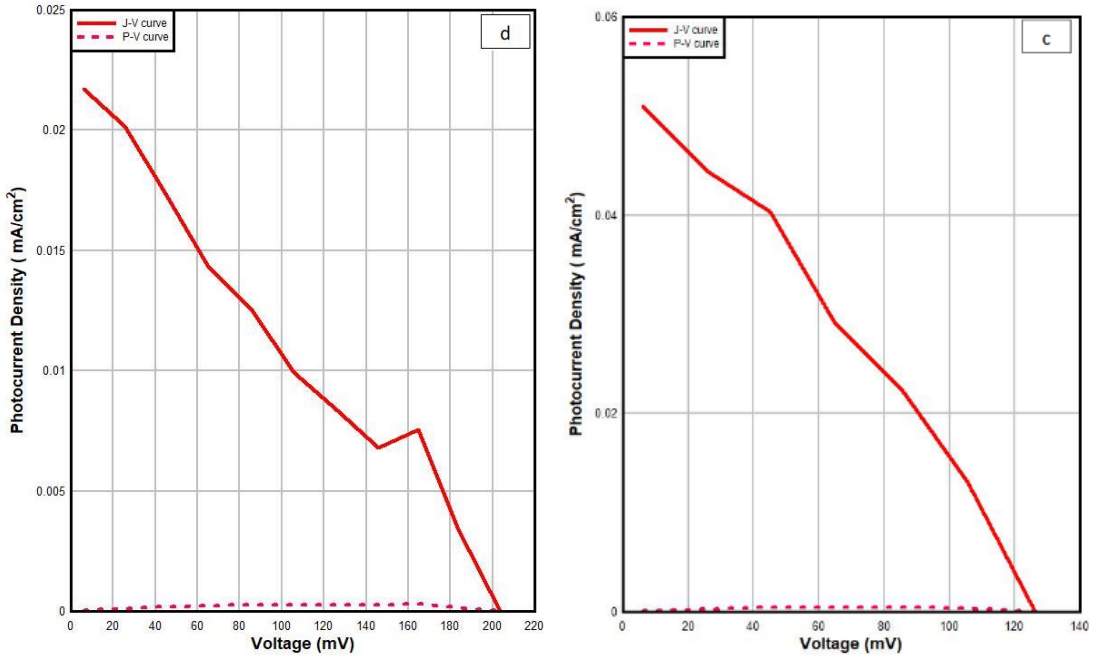

Figure 3-41: photocurrent-voltage curve of TiO_2 nanowire prepared at 3 hour (a) at 12 hour (b) at 24 hour (c) at 36 hour (d).

The figure 3-41 shows photocurrent voltage curve obtained by using titanium dioxide nanowire as a photoanode prepared with different time, V_{oc} of TiO_2 NW at prepared 12 hours is higher than other times. the photocurrent-voltage parameters such as open circuit voltage (V_{oc}), short circuit current density (J_{sc}), Voltage at max power point (V_{mpp}), current at max power point (I_{mpp}), fill factor (FF) and cell conversion efficiency (η) as well series

resistance (R_s)= and shunt resistance are estimated from the J-V curves a tabulated in Table 3-15.

Table 3-15.: photocurrent – voltage parameters of dye-sensitized NWs solar cell.

TiO_2 NWs prepared at different time	DSSC's	V_{oc} / V	J_{sc} / mA/cm^2	V_{mpp} / V	I_{mp} / mA	FF	η	R_s / Ω	R_{sh} / Ω
3 hour		0.142	0.012	0.064	0.008	0.227	0.0006	85271.11	666487.04
12 hour		0.262	0.064	0.164	0.024	0.234	0.0049	17981.98	128766.23
24 hour		0.244	0.032	0.224	0.032	0.918	0.0089	42876.61	241732.10
36 hour		0.203	0.020	0.161	0.008	0.317	0.0016	108015.7	369469.06

Chapter Four
Conclusion and Future Studies

Conclusions

First: Conclusions

The following items abstracted according to the results and discussion of the present study:-

1- XRD results confirmed prepare the nanomaterials (Tubes and Wires) at the different operation conditions and electrolytes by indicating the particular diffraction angle.
2- As general, the essential of Anatase phase formed for the nanotubes. In addition to that, Rutile crystal face also appeared in nanowires.
3- Raman technique emphasized the configuration of nanowires. At 638 cm^{-1} (Eg) which indicated to the vibration of stretching bond between the oxygen and the Titanium atoms. Moreover, the bending of vibration bond of O-Ti O appeared clear at 346 cm^{-1} (Eg). Furthermore, the DRS results showed the values of band gap energy of the nanowires and it close to 2.82 eV in spite of the change in the time preparation.
4- The B.E.T. results referred to the package of several parameters such as the surface area of nanowires in the range (8.84-18.49)m2/g, pore volume (1.70- 2.35) cm3/g, pore diameter (9.02-12.52)nm, and obey type three isotherm as well as meso-porous type.
5- For all samples, studied the topology and morphology to characterize of the surface electrode and the nanomaterials (TiO_2 nanowires) by the promising techniques in nanotechnology, that is, HFSEM, EDX with mapping as well as the TEM and AFM. The images and the parameters are enhanced nanometer scale and give a clear vision about the structure. In the nanotubes Titanium dioxide array in high order with dense and different thickness and

length. But, in nanowires, the length of wires are varied with random aggregation.

6- The influence of ultrasound wave also studied on the preparation process of TNT's. Moreover, the mechanism of TNT's showed according to the current density – time plot which depicts arise the nanotubes after the number of steps with proceeding time, as shown in chapter three.

7- The graphene nanoplates (GNP) counter electrode used with all the photoanodes to fabricate the solar cell. Silicon calibration cell used with a dye-sensitized solar cell to illustrate the full photoelectric parameters to find the conversion efficiency of solar energy. The values of the conversion efficiency are highest and consistent with other works elsewhere. But, the values of all parameters is lower in the nanowires solar cell because of the response to N3 dye enough in spite of taking more time in the immersion process.

Second: Future studies

We can summarize some of the useful works to achieve later:-

1- Preparation of the Titanium dioxide nanotubes as photoanode for the dye-sensitized solar cell using a new composition of the electrolytes.
2- Preparation TiO_2 nanowires directly on the FTO glass at different temperatures and times and estimate the conversion efficiency for the dye solar cell.
3- Synthesis of new composite with TiO_2 with MWCNT/ SWCNT and use it as photoanode by EPD method.
4- Preparation of the number of counter electrodes from the conductive polymer and check it with photoanode of the present study.
5- Extraction some of the new dyes from the plants and use it as dye sensitizer for the solar cell.
6- Build a new model to study how this solar cell work depending on the simulation program.

Chapter Five

References

References

[1] **A. Shukla, N. Dasgupta, S. Ranjan, S. Singh, and R. Chidambram,** "Nanotechnology towards prevention of anaemia and osteoporosis: from concept to market," *Biotechnology & Biotechnological Equipment,* vol. 31, pp. 863-879, 2017.

[2] **C. Selin,** "Expectations and the Emergence of Nanotechnology," *Science, Technology, & Human Values,* vol. 32, pp. 196-220, 2007.

[3] **C. Negin, S. Ali, and Q. Xie,** "Application of nanotechnology for enhancing oil recovery–A review," *Petroleum,* vol. 2, pp. 324-333, 2016.

[4] **N. C. Mueller, B. van der Bruggen, V. Keuter, P. Luis, T. Melin, W. Pronk, *et al.*,** "Nanofiltration and nanostructured membranes—Should they be considered nanotechnology or not?," *Journal of hazardous materials,* vol. 211, pp. 275-280, 2012.

[5] **A. Makarucha, N. Todorova, and I. Yarovsky,** "Nanomaterials in biological environment: a review of computer modelling studies," *European Biophysics Journal,* vol. 40, pp. 103-115, 2011.

[6] **N. A. Ochekpe, P. O. Olorunfemi, and N. C. Ngwuluka,** "Nanotechnology and drug delivery part 1: background and applications," *Tropical Journal of Pharmaceutical Research,* vol. 8, 2009.

[7] **S. Sahoo, S. Parveen, and J. Panda,** "The present and future of nanotechnology in human health care," *Nanomedicine: Nanotechnology, Biology and Medicine,* vol. 3, pp. 20-31, 2007.

[8] **M. Cushen, J. Kerry, M. Morris, M. Cruz-Romero, and E. Cummins,** "Nanotechnologies in the food industry–Recent

developments, risks and regulation," *Trends in Food Science & Technology,* vol. 24, pp. 30-46, 2012.

[9] **M. A. Cacciatore, D. A. Scheufele, and E. A. Corley,** "From enabling technology to applications: The evolution of risk perceptions about nanotechnology," *Public Understanding of Science,* vol. 20, pp. 385-404, 2011.

[10] **P. J. Borm, D. Robbins, S. Haubold, T. Kuhlbusch, H. Fissan, K. Donaldson, *et al.*,** "The potential risks of nanomaterials: a review carried out for ECETOC," *Particle and fibre toxicology,* vol. 3, p. 11, 2006.

[11] **V. Stone, B. Nowack, A. Baun, N. van den Brink, F. von der Kammer, M. Dusinska, *et al.*,** "Nanomaterials for environmental studies: classification, reference material issues, and strategies for physico-chemical characterisation," *Science of the total environment,* vol. 408, pp. 1745-1754, 2010.

[12] **D. D. Ganji and S. H. H. Kachapi,** *Application of nonlinear systems in nanomechanics and nanofluids: analytical methods and applications*: William Andrew, 2015.

[13] **M. Joshi, A. Bhattacharyya, and S. W. Ali,** "Characterization techniques for nanotechnology applications in textiles," 2008.

[14] **G. Gouadec and P. Colomban,** "Raman Spectroscopy of nanomaterials: How spectra relate to disorder, particle size and mechanical properties," *Progress in crystal growth and characterization of materials,* vol. 53, pp. 1-56, 2007.

[15] **R. Brause, H. Moeltgen, and K. Kleinermanns,** "Characterization of laser-ablated and chemically reduced silver colloids in aqueous solution by UV/VIS spectroscopy and STM/SEM microscopy," *Applied Physics B,* vol. 75, pp. 711-716, 2002.

[16] **K. Hyde, M. Rusa, and J. Hinestroza,** "Layer-by-layer deposition of polyelectrolyte nanolayers on natural fibres: cotton," *Nanotechnology*, vol. 16, p. S422, 2005.

[17] **M. A. Gatoo, S. Naseem, M. Y. Arfat, A. Mahmood Dar, K. Qasim, and S. Zubair,** "Physicochemical properties of nanomaterials: implication in associated toxic manifestations," *BioMed research international*, vol. 2014, 2014.

[18] **S. Naganathan, C. S. J. Singh, Y. W. Shen, P. E. Kiat, and S. Thiruchelvam,** "Nanotechnology in civil engineering-A review," in *Advanced Materials Research*, 2014, pp. 151-154.

[19] **M. Grätzel, "Photoelectrochemical cells,"** *nature*, vol. 414, p. 338, 2001.

[20] **H. Laroui, D. S. Wilson, G. Dalmasso, K. Salaita, N. Murthy, S. V. Sitaraman, *et al.*,** "Nanomedicine in GI," *American Journal of Physiology-Gastrointestinal and Liver Physiology*, vol. 300, pp. G371-G383, 2010.

[21] **B. D. Gates, Q. Xu, M. Stewart, D. Ryan, C. G. Willson, and G. M. Whitesides,** "New approaches to nanofabrication: molding, printing, and other techniques," *Chemical reviews*, vol. 105, pp. 1171-1196, 2005.

[22] **P. Roy, S. Berger, and P. Schmuki,** "TiO_2 nanotubes: synthesis and applications," *Angewandte Chemie International Edition*, vol. 50, pp. 2904-2939, 2011.

[23] **Y. Chen,** "Nanofabrication by electron beam lithography and its applications: a review," *Microelectronic Engineering*, vol. 135, pp. 57-72, 2015.

[24] **M. Cavallini, M. Facchini, M. Massi, and F. Biscarini,** "Bottom–up nanofabrication of materials for organic electronics," *Synthetic metals*, vol. 146, pp. 283-286, 2004.

[25] **O. Adamopoulos and T. Papadopoulos,** "Nanostructured bioceramics for maxillofacial applications," *Journal of Materials Science: Materials in Medicine*, vol. 18, pp. 1587-1597, 2007.

[26] **K. Choy, "Chemical vapour deposition of coatings,**" *Progress in materials science*, vol. 48, pp. 57-170, 2003.

[27] **A. H. Khan, S. Ghosh, B. Pradhan, A. Dalui, L. K. Shrestha, S. Acharya, *et al.*,** "Two-dimensional (2D) nanomaterials towards electrochemical nanoarchitectonics in energy-related applications," *Bulletin of the Chemical Society of Japan*, vol. 90, pp. 627-648, 2017.

[28] **C. Tan and H. Zhang,** "Wet-chemical synthesis and applications of non-layer structured two-dimensional nanomaterials," *Nature communications*, vol. 6, p. 7873, 2015.

[29] **S. A. M. Ealia and M. Saravanakumar,** "A review on the classification, characterisation, synthesis of nanoparticles and their application," in *IOP Conference Series: Materials Science and Engineering*, 2017, p. 032019.

[30] **S. Clarke and D. D. Vvedensky,** "Origin of Reflection High-Energy Electron-Diffraction Intensity Oscillations during Molecular-Beam Epitaxy: A Computational Modeling Approach," *Physical Review Letters*, vol. 60, p. 1209, 1988.

[31] **L. L. Chang and K. Ploog,** *Molecular beam epitaxy and heterostructures* vol. 87: Springer Science & Business Media, 2012.

[32] **T. K. Tseng, Y. S. Lin, Y. J. Chen, and H. Chu,** "A review of photocatalysts prepared by sol-gel method for VOCs removal,"

International journal of molecular sciences, vol. 11, pp. 2336-2361, 2010.

[33] **X. Chen and S. S. Mao,** "Titanium dioxide nanomaterials: synthesis, properties, modifications, and applications," *Chemical reviews,* vol. 107, pp. 2891-2959, 2007.

[34] **X. Chen and C. Burda,** "The electronic origin of the visible-light absorption properties of C-, N-and S-doped TiO_2 nanomaterials," *Journal of the American Chemical Society,* vol. 130, pp. 5018-5019, 2008.

[35] **H. Choi, E. Stathatos, and D. D. Dionysiou,** "Sol–gel preparation of mesoporous photocatalytic TiO_2 films and TiO_2/Al_2O_3 composite membranes for environmental applications," *Applied Catalysis B: Environmental,* vol. 63, pp. 60-67, 2006.

[36] **E. M. Saggioro, A. S. Oliveira, T. Pavesi, C. G. Maia, L. F. V. Ferreira, and J. C. Moreira,** "Use of titanium dioxide photocatalysis on the remediation of model textile wastewaters containing azo dyes," *Molecules,* vol. 16, pp. 10370-10386, 2011.

[37] **K. R. Reddy, K. Karthik, S. B. Prasad, S. K. Soni, H. M. Jeong, and A. V. Raghu,** "Enhanced photocatalytic activity of nanostructured titanium dioxide/polyaniline hybrid photocatalysts," *Polyhedron,* vol. 120, pp. 169-174, 2016.

[38] **Z. F. Yin, L. Wu, H. G. Yang, and Y. H. Su,** "Recent progress in biomedical applications of titanium dioxide," *Physical chemistry chemical physics,* vol. 15, pp. 4844-4858, 2013.

[39] **I. Iavicoli, V. Leso, L. Fontana, and A. Bergamaschi,** "Toxicological effects of titanium dioxide nanoparticles: a review of in vitro mammalian studies," *Eur Rev Med Pharmacol Sci,* vol. 15, pp. 481-508, 2011.

[40] **H. Chen, C. E. Nanayakkara, and V. H. Grassian,** "Titanium dioxide photocatalysis in atmospheric chemistry," *Chemical Reviews,* vol. 112, pp. 5919-5948, 2012.

[41] **M. Pelaez, N. T. Nolan, S. C. Pillai, M. K. Seery, P. Falaras, A. G. Kontos, *et al.,*** "A review on the visible light active titanium dioxide photocatalysts for environmental applications," *Applied Catalysis B: Environmental,* vol. 125, pp. 331-349, 2012.

[42] **A. Khataee and M. B. Kasiri,** "Photocatalytic degradation of organic dyes in the presence of nanostructured titanium dioxide: influence of the chemical structure of dyes," *Journal of Molecular Catalysis A: Chemical,* vol. 328, pp. 8-26, 2010.

[43] **J. Yan and B. R. Saunders,** "Third-generation solar cells: a review and comparison of polymer: fullerene, hybrid polymer and perovskite solar cells," *Rsc Advances,* vol. 4, pp. 43286-43314, 2014.

[44] **Q. Zhang and G. Cao,** "Nanostructured photoelectrodes for dye-sensitized solar cells," *Nano Today,* vol. 6, pp. 91-109, 2011.

[45] **N. Tétreault and M. Grätzel,** "Novel nanostructures for next generation dye-sensitized solar cells," *Energy & Environmental Science,* vol. 5, pp. 8506-8516, 2012.

[46] **A. Hagfeldt, G. Boschloo, L. Sun, L. Kloo, and H. Pettersson,** "Dye-sensitized solar cells," *Chemical reviews,* vol. 110, pp. 6595-6663, 2010.

[47] **J. Gong, J. Liang, and K. Sumathy,** "Review on dye-sensitized solar cells (DSSCs): fundamental concepts and novel materials," *Renewable and Sustainable Energy Reviews,* vol. 16, pp. 5848-5860, 2012.

[48] **J. Gong, K. Sumathy, Q. Qiao, and Z. Zhou,** "Review on dye-sensitized solar cells (DSSCs): advanced techniques and research

trends," *Renewable and Sustainable Energy Reviews,* vol. 68, pp. 234-246, 2017.

[49] **Y. Wang, D. Wu, L. M. Fu, X. C. Ai, D. Xu, and J. P. Zhang,** "Correlation between Energy and Spatial Distribution of Intragap Trap States in the TiO2 Photoanode of Dye-Sensitized Solar Cells," *ChemPhysChem,* vol. 16, pp. 2253-2259, 2015.

[50] **K. Ogiya, C. Lv, A. Suzuki, R. Sahnoun, M. Koyama, H. Tsuboi, *et al.*,** "Development of multiscale simulator for dye-sensitized TiO2 nanoporous electrode based on quantum chemical calculation," *Japanese Journal of Applied Physics,* vol. 47, p. 3010, 2008.

[51] **V. Sugathan, E. John, and K. Sudhakar,** "Recent improvements in dye sensitized solar cells: A review," *Renewable and Sustainable Energy Reviews,* vol. 52, pp. 54-64, 2015.

[52] **S. Shalini, S. Prasanna, T. K. Mallick, and S. Senthilarasu,** "Review on natural dye sensitized solar cells: operation, materials and methods," *Renewable and Sustainable Energy Reviews,* vol. 51, pp. 1306-1325, 2015.

[53] **G. Richhariya, A. Kumar, P. Tekasakul, and B. Gupta,** "Natural dyes for dye sensitized solar cell: A review," *Renewable and Sustainable Energy Reviews,* vol. 69, pp. 705-718, 2017.

[54] **C. Sima, C. Grigoriu, and S. Antohe,** "Comparison of the dye-sensitized solar cells performances based on transparent conductive ITO and FTO," *Thin Solid Films,* vol. 519, pp. 595-597, 2010.

[55] **S. Mahalingam and H. Abdullah,** "Electron transport study of indium oxide as photoanode in DSSCs: A review," *Renewable and Sustainable Energy Reviews,* vol. 63, pp. 245-255, 2016.

[56] **J. N. Clifford, E. Martínez-Ferrero, A. Viterisi, and E. Palomares,** "Sensitizer molecular structure-device efficiency relationship in dye

sensitized solar cells," *Chemical Society Reviews,* vol. 40, pp. 1635-1646, 2011.

[57] **S. Kim, J. K. Lee, S. O. Kang, J. Ko, J.-H. Yum, S. Fantacci, *et al.*,** "Molecular engineering of organic sensitizers for solar cell applications," *Journal of the American Chemical Society,* vol. 128, pp. 16701-16707, 2006.

[58] **L. Andrade, J. Sousa, H. A. Ribeiro, and A. Mendes,** "Phenomenological modeling of dye-sensitized solar cells under transient conditions," *Solar Energy,* vol. 85, pp. 781-793, 2011.

[59] **M. A. Al-Alwani, A. B. Mohamad, N. A. Ludin, A. A. H. Kadhum, and K. Sopian,** "Dye-sensitised solar cells: Development, structure, operation principles, electron kinetics, characterisation, synthesis materials and natural photosensitisers," *Renewable and Sustainable Energy Reviews,* vol. 65, pp. 183-213, 2016.

[60] **O. Adedokun, K. Titilope, and A. O. Awodugba,** "Review on Natural Dye-Sensitized Solar Cells (DSSCs)," *International Journal of Engineering Technologies,* vol. 2, pp. 34-41, 2016.

[61] **A. Kay and M. Grätzel,** "Low cost photovoltaic modules based on dye sensitized nanocrystalline titanium dioxide and carbon powder," *Solar Energy Materials and Solar Cells,* vol. 44, pp. 99-117, 1996.

[62] **T. Wan, S. Ramakrishna, and Y. Liu,** "Recent progress in electrospinning TiO2 nanostructured photo-anode of dye-sensitized solar cells," *Journal of Applied Polymer Science,* vol. 135, p. 45649, 2018.

[63] **A. Jena, S. P. Mohanty, P. Kumar, J. Naduvath, V. Gondane, P. Lekha, *et al.*,** "Dye sensitized solar cells: a review," *Transactions of the Indian Ceramic Society,* vol. 71, pp. 1-16, 2012.

[64] **S. Uchida, R. Chiba, M. Tomiha, N. Masaki, and M. Shirai,** "Hydrothermal synthesis of titania nanotube and its application for dye-sensitized solar cell," in *Studies in surface science and catalysis*. vol. 146, ed: Elsevier, 2003, pp. 791-794.

[65] **G. K. Mor, O. K. Varghese, M. Paulose, K. Shankar, and C. A. Grimes,** "A review on highly ordered, vertically oriented TiO_2 nanotube arrays: Fabrication,
material properties, and solar energy applications," *Solar Energy Materials and Solar Cells*, vol. 90, pp. 2011-2075, 2006.

[66] **L. Que, Z. Lan, W. Wu, J. Wu, J. Lin, and M. Huang,** "High-efficiency dye-sensitized solar cells based on ultra-long single crystalline titanium dioxide nanowires," *Journal of Power Sources*, vol. 266, pp. 440-447, 2014.

[67] **M. A. Othman, N. F. Amat, B. H. Ahmad, and J. Rajan,** "Electrical conductivity characteristic of TiO_2 nanowires from hydrothermal method," in *Journal of Physics: Conference Series*, 2014, p. 012027.

[68] **K. Rokesh, S. Anandan, and K. Jothivenkatachalam,** "Polymer electrolytes in dye sensitized solar cells," *Materials Focus*, vol. 4, pp. 262-271, 2015.

[69] **M. R. Narayan,** "Dye sensitized solar cells based on natural photosensitizers," *Renewable and Sustainable Energy Reviews*, vol. 16, pp. 208-215, 2012.

[70] **J. Wu, Z. Lan, S. Hao, P. Li, J. Lin, M. Huang, *et al.*,** "Progress on the electrolytes for dye-sensitized solar cells," *Pure and Applied Chemistry*, vol. 80, pp. 2241-2258, 2008.

[71] **M. Ye, X. Wen, M. Wang, J. Iocozzia, N. Zhang, C. Lin, *et al.*,** "Recent advances in dye-sensitized solar cells: from photoanodes,

sensitizers and electrolytes to counter electrodes," *Materials Today*, vol. 18, pp. 155-162, 2015.

[72] **U. Mehmood, S.-u. Rahman, K. Harrabi, I. A. Hussein, and B. Reddy,** "Recent advances in dye sensitized solar cells," *Advances in Materials Science and Engineering*, vol. 2014, 2014.

[73] **R. Cruz, D. A. P. Tanaka, and A. Mendes,** "Reduced graphene oxide films as transparent counter-electrodes for dye-sensitized solar cells," *Solar Energy*, vol. 86, pp. 716-724, 2012.

[74] **W. Hong, Y. Xu, G. Lu, C. Li, and G. Shi,** "Transparent graphene/PEDOT–PSS composite films as counter electrodes of dye-sensitized solar cells," *Electrochemistry Communications*, vol. 10, pp. 1555-1558, 2008.

[75] **Q. Li, J. Wu, Q. Tang, Z. Lan, P. Li, J. Lin, *et al.*,** "Application of microporous polyaniline counter electrode for dye-sensitized solar cells," *Electrochemistry Communications*, vol. 10, pp. 1299-1302, 2008.

[76] **W. J. Lee, E. Ramasamy, D. Y. Lee, and J. S. Song,** "Efficient dye-sensitized solar cells with catalytic multiwall carbon nanotube counter electrodes," *ACS applied materials & interfaces*, vol. 1, pp. 1145-1149, 2009.

[77] **S. Hao, J. Wu, Y. Huang, and J. Lin,** "Natural dyes as photosensitizers for dye-sensitized solar cell," *Solar energy*, vol. 80, pp. 209-214, 2006.

[78] **S. Shalini, R. Balasundaraprabhu, T. S. Kumar, N. Prabavathy, S. Senthilarasu, and S. Prasanna,** "Status and outlook of sensitizers/dyes used in dye sensitized solar cells (DSSC): a review," *International Journal of Energy Research*, vol. 40, pp. 1303-1320, 2016.

[79] **L. Giribabu, R. K. Kanaparthi, and V. Velkannan,** "Molecular engineering of sensitizers for dye-sensitized solar cell applications," *The Chemical Record*, vol. 12, pp. 306-328, 2012.

[80] **A. Fattori,** "Electrochemical and spectroelectrochemical studies of dyes used in dye-sensitized solar cells," University of Bath, 2010.

[81] **N. Sekar and V. Y. Gehlot,** "Metal complex dyes for dye-sensitized solar cells: Recent developments," *Resonance*, vol. 15, pp. 819-831, 2010.

[82] **B. B. Çırak, S. M. Karadeniz, T. Kılınç, B. Caglar, A. E. Ekinci, H. Yelgin, *et al.*,** "Synthesis, surface properties, crystal structure and dye sensitized solar cell performance of TiO_2 nanotube arrays anodized under different voltages," *Vacuum*, vol. 144, pp. 183-189, 2017.

[83] **N. Nyein, W. K. Tan, G. Kawamura, A. Matsuda, and Z. Lockman,** "Formation of anodic TiO_2 nanotube arrays in NaOH added fluoride-ethylene glycol electrolyte for dye-sensitized solar cells," in *AIP Conference Proceedings*, 2017, p. 020006.

[84] **J. Hu, P. Liu, M. Chen, S. Li, and Y. Yang,** "Synthesis and First-principle Calculation of TiO_2 Rutile Nanowire Electrodes for Dye-sensitized Solar Cells," *Int. J. Electrochem. Sci*, vol. 12, pp. 9725-9735, 2017.

[85] **S. Jin, E. Shin, and J. Hong,** "TiO_2 nanowire networks prepared by titanium corrosion and their application to bendable dye-sensitized solar cells," *Nanomaterials*, vol. 7, p. 315, 2017.

[86] **Á. Kukovecz, K. Kordás, J. Kiss, and Z. Kónya,** "Atomic scale characterization and surface chemistry of metal modified titanate nanotubes and nanowires," *Surface Science Reports*, vol. 71, pp. 473-546, 2016.

[87] **F. Mohammadpour, M. Altomare, S. So, K. Lee, M. Mokhtar, A. Alshehri, *et al.*,** "High-temperature annealing of TiO_2 nanotube membranes for efficient dye-sensitized solar cells," *Semiconductor Science and Technology*, vol. 31, p. 014010, 2015.

[88] **G. Liu, K. Du, and K. Wang,** "Surface wettability of TiO_2 nanotube arrays prepared by electrochemical anodization," *Applied Surface Science*, vol. 388, pp. 313-320, 2016.

[89] **L. Qin, Q. Chen, R. Lan, R. Jiang, X. Quan, B. Xu, *et al.*,** "Effect of anodization parameters on morphology and photocatalysis properties of TiO_2 nanotube arrays," *Journal of Materials Science & Technology*, vol. 31, pp. 1059-1064, 2015.

[90] **P. Pichat,** "Are TiO_2 nanotubes worth using in photocatalytic purification of air and water?," *Molecules*, vol. 19, pp. 15075-15087, 2014.

[91] **I. Kustiningsih and W. W. P. Slamet,** "Synthesis of Titania Nanotubes and Titania Nanowires by Combination Sonication-hydrothermal Treatment and their Photocatalytic Activity for Hydrogen Production," *International Journal of Technology*, vol. 5, pp. 133-141, 2014.

[92] **Y.-Z. Zeng, Y.-C. Liu, Y.-F. Lu, and J.-C. Chung,** "Study on the Preparation of Nanosized Titanium Dioxide with Tubular Structure by Hydrothermal Method and Their Photocatalytic Activity," *International Journal of Chemical Engineering and Applications*, vol. 5, p. 234, 2014.

[93] **A. Ranjitha, N. Muthukumarasamy, M. Thambidurai, D. Velauthapillai, S. Agilan, and R. Balasundaraprabhu,** "Effect of reaction time on the formation of TiO2 nanotubes prepared by hydrothermal method," *Optik*, vol. 126, pp. 2491-2494, 2015.

[94] **A.-F. Kanta, M. Poelman, and A. Decroly,** "Electrochemical characterisation of TiO2 nanotube array photoanodes for dye-sensitized solar cell application," *Solar Energy Materials and Solar Cells*, vol. 133, pp. 76-81, 2015.

[95] **R. Camposeco, S. Castillo, I. Mejia-Centeno, J. Navarrete, and R. Gómez,** "Effect of the Ti/Na molar ratio on the acidity and the structure of TiO_2 nanostructures: nanotubes, nanofibers and nanowires," *Materials Characterization*, vol. 90, pp. 113-120, 2014.

[96] **I. Roman, R. D. Trusca, M.-L. Soare, C. Fratila, E. Krasicka-Cydzik, M.-S. Stan, *et al.*,** "Titanium dioxide nanotube films: Preparation, characterization and electrochemical biosensitivity towards alkaline phosphatase," *Materials Science and Engineering: C*, vol. 37, pp. 374-382, 2014.

[97] **M. Nischk, P. Mazierski, M. Gazda, and A. Zaleska,** "Ordered TiO_2 nanotubes: The effect of preparation parameters on the photocatalytic activity in air purification process," *Applied Catalysis B: Environmental*, vol. 144, pp. 674-685, 2014.

[98] **V. Galstyan, E. Comini, G. Faglia, and G. Sberveglieri,** "TiO_2 nanotubes: recent advances in synthesis and gas sensing properties," *Sensors*, vol. 13, pp. 14813-14838, 2013.

[99] **T. H. T. Vu, H. T. Au, L. T. Tran, T. M. T. Nguyen, T. T. T. Tran, M. T. Pham, *et al.*,** "Synthesis of titanium dioxide nanotubes via one-step dynamic hydrothermal process," *Journal of Materials Science*, vol. 49, pp. 5617-5625, 2014.

[100] **W. Sharmoukh and N. K. Allam,** "TiO_2 nanotube-based dye-sensitized solar cell using new photosensitizer with enhanced open-circuit voltage and fill factor," *ACS applied materials & interfaces*, vol. 4, pp. 4413-4418, 2012.

[101] **J. H. Kim, X. H. Zhang, J. D. Kim, H. M. Park, S. B. Lee, J. W. Yi, *et al.*,** "Synthesis and characterization of anatase TiO_2 nanotubes with controllable crystal size by a simple MWCNT template method," *Journal of Solid State Chemistry*, vol. 196, pp. 435-440, 2012.

[102] **K.-C. Huang and S.-H. Chien,** "Improved visible-light-driven photocatalytic activity of rutile/titania-nanotube composites prepared by microwave-assisted hydrothermal process," *Applied Catalysis B: Environmental*, vol. 140, pp. 283-288, 2013.

[103] **A. Lambertia, A. Saccoa, D. Hidalgoa, S. Biancoa, D. Manfredia, M. Quaglioa, *et al.*,** "TiO_2 Nanotube Array as E cient Transparent Photoanode in Dye-Sensitized Solar Cell with High Electron Lifetime."

[104] **X. Jiao, X. Wang, X. Li, H. Chen, G. Wang, J. Li, *et al.*,** "Electron transport in dye-sensitized solar cells based on TiO_2 nanowires," *SCIENCE CHINA Physics, Mechanics & Astronomy*, vol. 57, pp. 892-897, 2014.

[105] **N. F. Atta, H. M. Amin, M. W. Khalil, and A. Galal,** "Nanotube arrays as photoanodes for dye sensitized solar cells using metal phthalocyanine dyes," *Int J Electrochem Sci*, vol. 6, pp. 3316-3332, 2011.

[106] **H. Jha, P. Roy, R. Hahn, I. Paramasivam, and P. Schmuki,** "Fast formation of aligned high-aspect ratio TiO_2 nanotube bundles that lead to increased open circuit voltage when used in dye sensitized solar cells," *Electrochemistry communications*, vol. 13, pp. 302-305, 2011.

[107] **J. Huang, Y. Cao, Z. Deng, and H. Tong,** "Formation of titanate nanostructures under different NaOH concentration and their application in wastewater treatment," *Journal of Solid State Chemistry*, vol. 184, pp. 712-719, 2011.

[108] **A. Kumar, A. R. Madaria, and C. Zhou,** "Growth of aligned single-crystalline rutile TiO_2 nanowires on arbitrary substrates and their application in dye-sensitized solar cells," *The Journal of Physical Chemistry C,* vol. 114, pp. 7787-7792, 2010.

[109] **J. Wang and Z. Lin,** "Dye-sensitized TiO_2 nanotube solar cells with markedly enhanced performance via rational surface engineering," *Chemistry of Materials,* vol. 22, pp. 579-584, 2009.

[110] **E. Şennik, Z. Çolak, N. Kılınç, and Z. Z. Öztürk,** "Synthesis of highly-ordered TiO_2 nanotubes for a hydrogen sensor," *International Journal of Hydrogen Energy,* vol. 35, pp. 4420-4427, 2010.

[111] **N. Viriya-empikul, T. Charinpanitkul, N. Sano, A. Soottitantawat, T. Kikuchi, K. Faungnawakij, *et al.*,** "Effect of preparation variables on morphology and anatase–brookite phase transition in sonication assisted hydrothermal reaction for synthesis of titanate nanostructures," *Materials Chemistry and Physics,* vol. 118, pp. 254-258, 2009.

[112] **S. Bhardwaj, T. Rana, P. Laha, A. Barman, and S. Biswas,** "Study of titanium dioxide nanotube array for the application in dye-sensitized solar cells," 2014.

[113] **Y. Alivov, M. Pandikunta, S. Nikishin, and Z. Fan,** "The anodization voltage influence on the properties of TiO_2 nanotubes grown by electrochemical oxidation," *Nanotechnology,* vol. 20, p. 225602, 2009.

[114] **H. Park, W.-R. Kim, H.-T. Jeong, J.-J. Lee, H.-G. Kim, and W.-Y. Choi,** "Fabrication of dye-sensitized solar cells by transplanting highly ordered TiO_2 nanotube arrays," *Solar energy materials and solar cells,* vol. 95, pp. 184-189, 2011.

[115] **T.-S. Kang, A. P. Smith, B. E. Taylor, and M. F. Durstock,** "Fabrication of highly-ordered TiO_2 nanotube arrays and their use in dye-sensitized solar cells," *Nano letters,* vol. 9, pp. 601-606, 2009.

[116] **S. Sreekantan, Z. Lockman, R. Hazan, M. Tasbihi, L. K. Tong, and A. R. Mohamed,** "Influence of electrolyte pH on TiO_2 nanotube formation by Ti anodization," *Journal of Alloys and Compounds*, vol. 485, pp. 478-483, 2009.

[117] **K. Asagoe, S. Ngamsinlapasathian, Y. Suzuki, and S. Yoshikawa,** "Addition of TiO_2 nanowires in different polymorphs for dye-sensitized solar cells," *Central European Journal of Chemistry*, vol. 5, pp. 605-619, 2007.

[118] **H.-K. Seo, G.-S. Kim, S. Ansari, Y.-S. Kim, H.-S. Shin, K.-H. Shim, *et al.*,** "A study on the structure/phase transformation of titanate nanotubes synthesized at various hydrothermal temperatures," *Solar Energy Materials and Solar Cells*, vol. 92, pp. 1533-1539, 2008.

[119] **D. Wang, F. Zhou, Y. Liu, and W. Liu,** "Synthesis and characterization of anatase TiO2 nanotubes with uniform diameter from titanium powder," *Materials Letters*, vol. 62, pp. 1819-1822, 2008.

[120] **K. Shankar, G. K. Mor, H. E. Prakasam, S. Yoriya, M. Paulose, O. K. Varghese, *et al.*,** "Highly-ordered TiO_2 nanotube arrays up to 220 μm in length: use in water photoelectrolysis and dye-sensitized solar cells," *Nanotechnology*, vol. 18, p. 065707, 2007.

[121] **K. Zhu, N. R. Neale, A. Miedaner, and A. J. Frank,** "Enhanced charge-collection efficiencies and light scattering in dye-sensitized solar cells using oriented TiO_2 nanotubes arrays," *Nano letters*, vol. 7, pp. 69-74, 2007.

[122] **Y. Suzuki, S. Ngamsinlapasathian, R. Yoshida, and S. Yoshikawa,** "Partially nanowire-structured TiO_2 electrode for dye-sensitized solar cells," *Central European Journal of Chemistry*, vol. 4, pp. 476-488, 2006.

[123] **R. Yoshida, Y. Suzuki, and S. Yoshikawa,** "Syntheses of TiO_2 (B) nanowires and TiO_2 anatase nanowires by hydrothermal and post-heat treatments," *Journal of solid state Chemistry,* vol. 178, pp. 2179-2185, 2005.

[124] **Y. Zhang, G. Li, Y. Jin, Y. Zhang, J. Zhang, and L. Zhang,** "Hydrothermal synthesis and photoluminescence of TiO_2 nanowires," *Chemical Physics Letters,* vol. 365, pp. 300-304, 2002.

[125] **P. Pookmanee and S. Phanichphant,** "Titanium dioxide powder prepared by a sol-gel method," *Journal of Ceramic Processing Research,* vol. 10, pp. 167-170, 2009.

[126] **R. Mohammadinejad, S. Pourseyedi, A. Baghizadeh, S. Ranjbar, and G. Mansoori,** "Synthesis of silver nanoparticles using Silybum marianum seed extract," *International Journal of Nanoscience and Nanotechnology,* vol. 9, pp. 221-226, 2013.

[127] R. Abazari, A. R. Mahjoub, and S. Sanati, "A facile and efficient preparation of anatase titania nanoparticles in micelle nanoreactors: morphology, structure, and
their high photocatalytic activity under UV light illumination," *RSC Advances,* vol. 4, pp. 56406-56414, 2014.

[128] **S. Bai, J. Hu, D. Li, R. Luo, A. Chen, and C. C. Liu,** "Quantum-sized ZnO nanoparticles: synthesis, characterization and sensing properties for NO2," *Journal of Materials Chemistry,* vol. 21, pp. 12288-12294, 2011.

[129] **F. Boulc'h, M.-C. Schouler, P. Donnadieu, J.-M. Chaix, and E. Djurado,** "Domain size distribution of Y-TZP nano-particles using XRD and HRTEM," *Image Analysis & Stereology,* vol. 20, pp. 157-161, 2011.

[130] **P. Qiang, Z. Chen, P. Yang, X. Cai, S. Tan, P. Liu, *et al.*,** "TiO_2 nanowires for potential facile integration of solar cells and electrochromic devices," *Nanotechnology*, vol. 24, p. 435403, 2013.

[131] **B. Tan and Y. Wu,** "Dye-sensitized solar cells based on anatase TiO_2 nanoparticle/nanowire composites," *The Journal of Physical Chemistry B*, vol. 110, pp. 15932-15938, 2006.

[132] **T. Ohsaka, F. Izumi, and Y. Fujiki,** "Raman spectrum of anatase, TiO_2," *Journal of Raman spectroscopy*, vol. 7, pp. 321-324, 1978.

[133] **M. M. Khan, S. A. Ansari, D. Pradhan, M. O. Ansari, J. Lee, and M. H. Cho,** "Band gap engineered TiO_2 nanoparticles for visible light induced photoelectrochemical and photocatalytic studies," *Journal of Materials Chemistry A*, vol. 2, pp. 637-644, 2014.

[134] **J. Tauc, R. Grigorovici, and A. Vancu,** "Optical properties and electronic structure of amorphous germanium," *physica status solidi (b)*, vol. 15, pp. 627-637, 1966.

[135] **M. A. Hossain, J. Park, J. Y. Ahn, C. Park, Y. Kim, S. H. Kim, *et al.*,** "Investigation of TiO2 nanotubes/nanoparticles stacking sequences to improve power conversion efficiency of dye-sensitized solar cells," *Electrochimica Acta*, vol. 173, pp. 665-671, 2015.

[136] **A. Subramanian and H.-W. Wang,** "Effects of boron doping in TiO_2 nanotubes and the performance of dye-sensitized solar cells," *Applied Surface Science*, vol. 258, pp. 6479-6484, 2012.

[137] **L. Yu, X. Ren, Z. Yang, Y. Han, and Z. Li,** "The preparation and assembly of CdS x Se 1− x alloyed quantum dots on TiO_2 nanowire arrays for quantum dot-sensitized solar cells," *Journal of Materials Science: Materials in Electronics*, vol. 27, pp. 7150-7160, 2016.

[138] **D. Regonini, C. R. Bowen, A. Jaroenworaluck, and R. Stevens,** "A review of growth mechanism, structure and crystallinity of anodized

TiO_2 nanotubes," *Materials Science and Engineering: R: Reports,* vol. 74, pp. 377-406, 2013.

[139] **J. Hernández-López, A. Conde, J. De Damborenea, and M. Arenas,** "TiO_2 nanotubes with tunable morphologies," *RSC Advances,* vol. 4, pp. 62576-62585, 2014.

[140] **R. Jose, A. Kumar, V. Thavasi, K. Fujihara, S. Uchida, and S. Ramakrishna,** "Relationship between the molecular orbital structure of the dyes and photocurrent density in the dye-sensitized solar cells," *Applied Physics Letters,* vol. 93, p. 023125, 2008.

[141] **K. Fan, J. Yu, and W. Ho,** "Improving photoanodes to obtain highly efficient dye-sensitized solar cells: a brief review," *Materials Horizons,* vol. 4, pp. 319-344, 2017.

[142] **W.-R. Kim, H. Park, and W.-Y. Choi,** "Conical islands of TiO_2 nanotube arrays in the photoelectrode of dye-sensitized solar cells," *Nanoscale research letters,* vol. 10, p. 63, 2015.

الخلاصة

حضرت الانابيب النانوية لثنائي أوكسيد التيتانيوم و اسلاك النانوية بطرق مختلفة الطريقة الحرارية وعملية الانودة ومن مواد بادئة مختلفة حيث استخدم ثنائي أوكسيد التيتانوم P_{25} كمادة بادئة لتحضير اسلاك النانو في حين استخدمت سبيكة التيتانيوم لتحضير انابيب النانو ورسبت على الزجاج الموصل FTO بطريقة الترسيب الكهربائي بأستخدام تقنية ثلاثية الاقطاب . شخصتُ المواد المحضرة بتقنيات منها تقنية المجهر الالكتروني الماسح وحيود الاشعة السينية ومطيافية رامان ودراسة المساحة السطحية ومعرفة توزيع الحجم المسامي لجسيمات النانوية وتم استخدامها كأقطاب ضوئية انودية للخلايا المتحسسة الصبغية.

القطب المساعد حضر باستخدام صفائح كرافين نانوية بعد ترسيبها على الزجاج الموصل FTO باستخدام التقنية ثلاثية الاقطاب أيضا واستخدمت صبغة الروثونيوم N3 والالكتروليت المستخدم هو يوديد الليثيوم واليودين وبعض المضافات العضوية ومنها رباعي بيوتل بيريدين في الاسيتو نترايل لتحسين استقراية الالكتروليت وكفاءة تحويل الخلية المتحسسة للصبغة .

صُنعتْ عشرة خلايا متحسسة صبغية من نوع الخلايا الشمسية المتحسسة للصبغة مؤلفة من 10 اقطاب ضوئية وتم حساب كفاءة الخلايا الشمسية المحضرة من خلال تشخيص منحني التيار والفولتية وقياس عامل الملئ حيث كانت افضل كفاءة تحويل 1.238 للقطب الضوئي ثنائي أوكسيد التيتانيوم انابيب النانوية اما بالنسبة ل ثنائي أوكسيد التيتانيوم الاسلاك النانوية بلغت اعلى كفاءة تحويل 0.0089 .

جمهورية العراق
وزارة التعليم العالي والبحث العلمي
جامعة القادسية – كلية العلوم
قسم الكيمياء

تقييم أداء الاسلاك والانابيب النانويةلاوكسيد التيتانيوم كأنودات ضوئية للخلايا الشمسية الصبغية

رسالة مقدمة الى مجلس كلية العلوم / جامعة القادسية كجزء من متطلبات نيل شهادة الماجستير في الكيمياء / الكيمياء الفيزياوية

من قبل

نورا حسين حران
بكالوريوس كيمياء(2011)

تحت اشراف

أ.د قحطان عدنان يوسف

1440 هـ

2019 م